7-7-2009

Extreme Chirped/ Stretched Pulsed Amplification and Laser DIVB

Peter Delfyett
University of Central Florida

Resan Bojan
University of Central Florida

Kim Kyungbum
University of Central Florida

US007558302B1

(12) **United States Patent**
Delfyett et al.

(10) **Patent No.: US 7,558,302 B1**
(45) **Date of Patent: Jul. 7, 2009**

(54) **EXTREME CHIRPED/STRETCHED PULSED AMPLIFICATION AND LASER**

(75) Inventors: **Peter Delfyett**, Orlando, FL (US); **Kyungbum Kim**, Cotati, CA (US); **Bojan Resan**, Santa Clara, CA (US)

(73) Assignee: **University of Central Florida Research Foundation, Inc.**, Orlando, FL (US)

(*) Notice: Subject to any disclaimer, the term of this patent is extended or adjusted under 35 U.S.C. 154(b) by 14 days.

(21) Appl. No.: **11/725,209**

(22) Filed: **Mar. 16, 2007**

Related U.S. Application Data

(62) Division of application No. 11/445,565, filed on Jun. 2, 2006, which is a division of application No. 10/828,965, filed on Apr. 21, 2004, now Pat. No. 7,095,772.

(60) Provisional application No. 60/472,383, filed on May 21, 2003.

(51) **Int. Cl.**

H01S 3/00	(2006.01)
H01S 3/10	(2006.01)
H01S 3/04	(2006.01)
H01S 3/08	(2006.01)
H04B 10/12	(2006.01)

(52) **U.S. Cl.** **372/25**; 372/6; 372/42.01; 372/102; 372/109; 359/337.5; 359/344

(58) **Field of Classification Search** 372/6, 372/25, 43.01, 102, 109; 359/337.5, 344
See application file for complete search history.

(56) **References Cited**

U.S. PATENT DOCUMENTS

3,609,001	A *	9/1971	Weber	359/240
5,572,355	A	11/1996	Cotton et al.	359/333
5,633,885	A	5/1997	Galvanauskas et al.	372/25
5,696,782	A	12/1997	Harter et al.	372/25
5,701,319	A	12/1997	Fermann	372/18
5,818,630	A	10/1998	Fermann et al.	359/341
5,847,863	A	12/1998	Galvanauskas et al.	359/341
5,862,287	A	1/1999	Stock et al.	385/123
5,880,877	A	3/1999	Fermann et al.	359/341
6,014,249	A	1/2000	Fermann et al.	359/341
6,154,310	A	11/2000	Galvanauskas et al.	359/328
6,181,463	B1	1/2001	Galvanauskas et al.	359/330
6,198,568	B1	3/2001	Galvanauskas et al.	359/332

(Continued)

OTHER PUBLICATIONS

Applicant's Admission re Galvanauskas on p. 9 of the Jan. 18, 2008 Reply in U.S. Appl. No. 11/445,565.*

Primary Examiner—Kenneth A Parker
Assistant Examiner—Hrayr A Sayadian
(74) *Attorney, Agent, or Firm*—Brian S. Steinberger; Phyllis K. Wood; Law Offices of Brian S. Steinberger, P.A.

(57) **ABSTRACT**

Methods, devices and systems for generating ultrashort optical linear chirped pulses with very high power by amplifying the pulses so that their temporal duration is longer than the storage time of the amplifying medium. The additional gain factor is related to the ratio of the storage time to the stretched pulse. A preferred embodiment connects a mode locked laser source that generates optical pulses whose duration is stretched with a chirped fiber Bragg grating. Embodiments include methods, devices and systems causing an extreme chirped pulse amplifier (XCPA) effect in an oscillator.

1 Claim, 48 Drawing Sheets

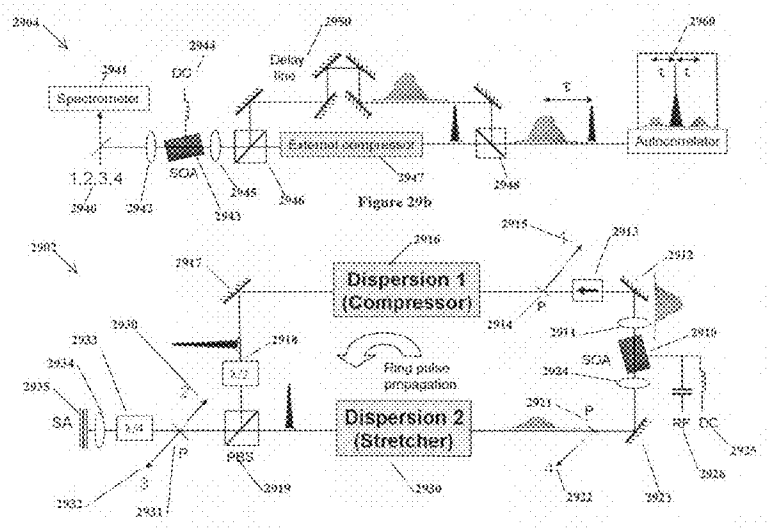

U.S. PATENT DOCUMENTS

6,208,458	B1	3/2001	Galvanauskas et al.	359/345
6,249,630	B1	6/2001	Stock et al.	385/123
6,275,512	B1	8/2001	Fermann	372/6
6,334,011	B1	12/2001	Galvanauskas et al.	385/22
6,345,058	B1	2/2002	Hartemann et al.	372/2
6,363,090	B1	3/2002	Wintner et al.	372/21
6,456,417	B1 *	9/2002	Maywar et al.	359/245
6,549,547	B2	4/2003	Galvanauskas et al.	372/25
6,590,910	B2	7/2003	Lin	372/18
6,603,600	B2	8/2003	Pang	359/348
2001/0053008	A1 *	12/2001	Ueno	359/158

* cited by examiner

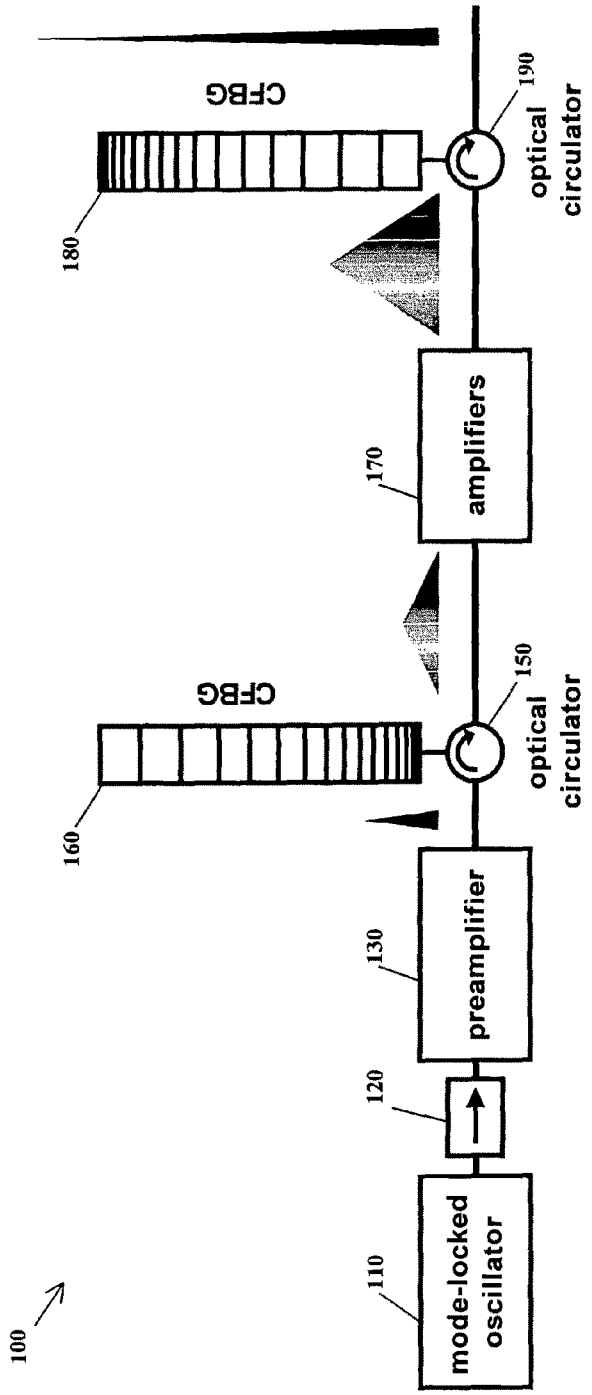

Figure 1a

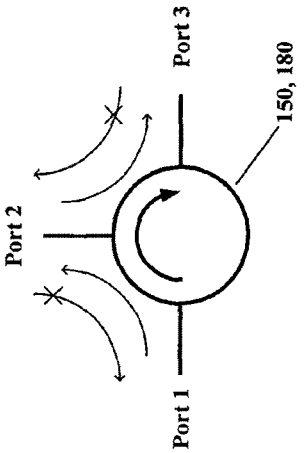

Figure 1b

Function	Selected Device	Advantage
Master Oscillator	Mode-locked Semiconductor Laser	Compactness Simple Electrical Pumping
Stretcher and Compressor	Chirped Fiber Bragg Grating	Compactness Large Dispersion Dispersion Manipulation Inherent Beam Shaping
Power Amplifiers	Semiconductor Optical Amplifiers	Compactness Simple Electrical Pumping

Figure 2

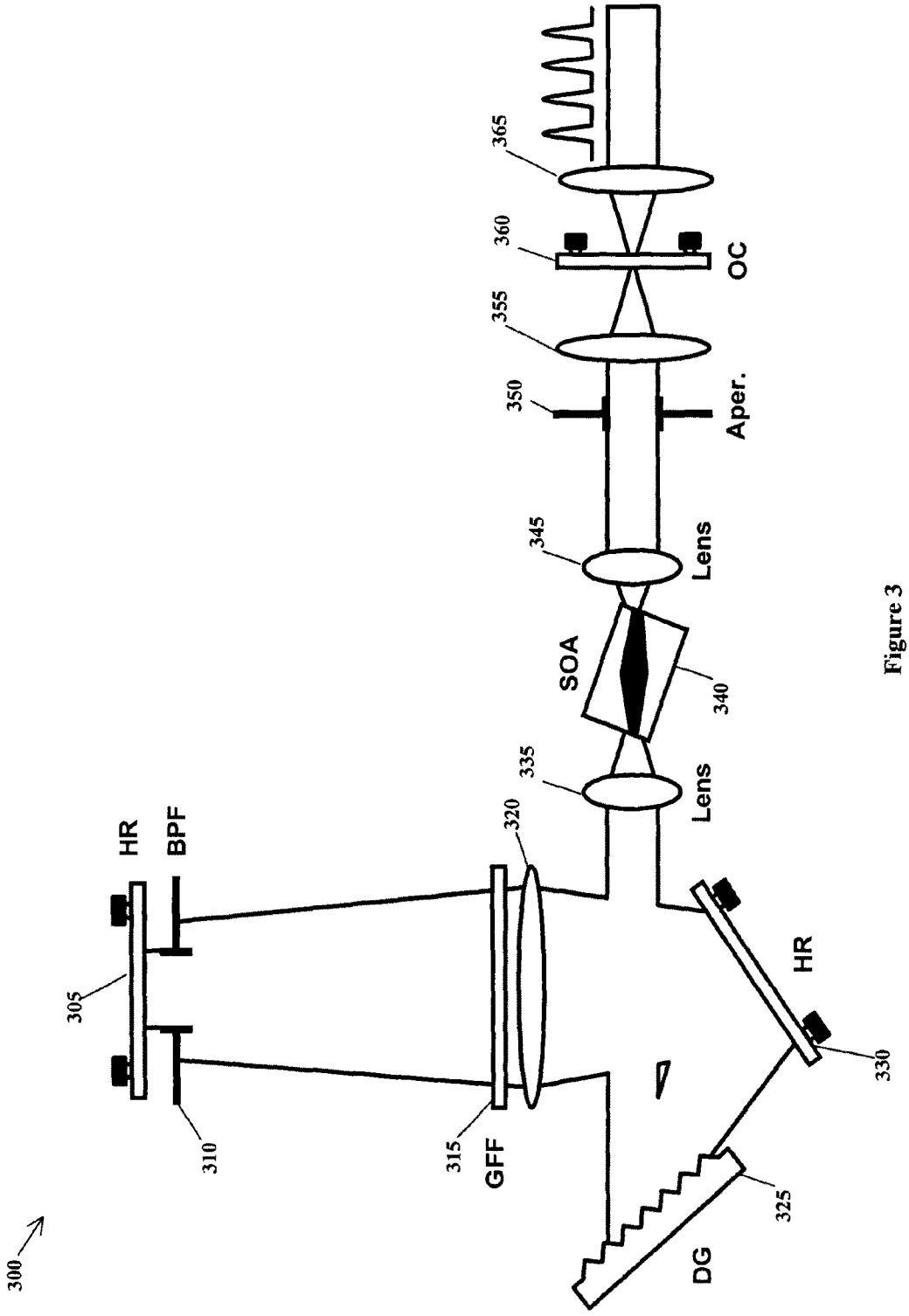
300
305
HR
BPF
310
315
GFF
320
335
Lens
SOA
340
345
Lens
350
Aper.
355
360
OC
365
HR
330
325
DG

Figure 3

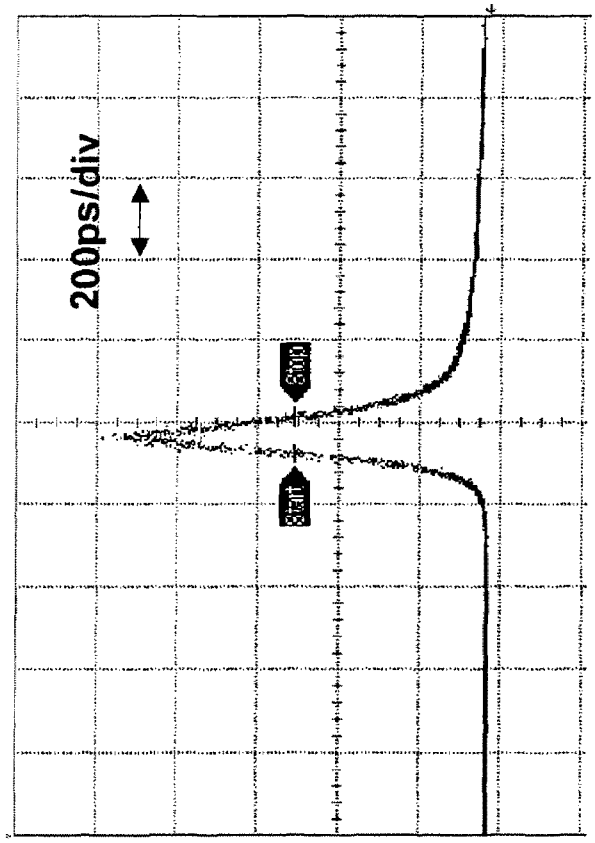

Figure 4b

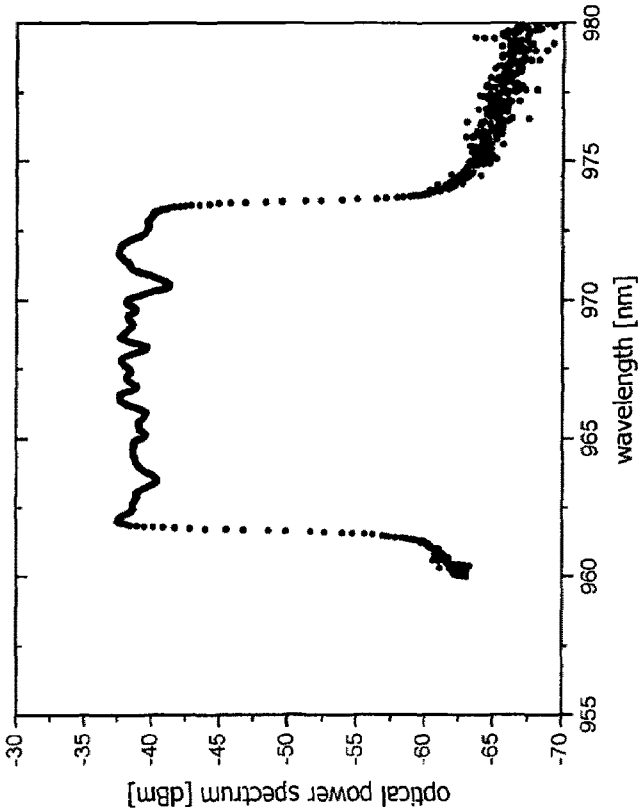

Figure 4a

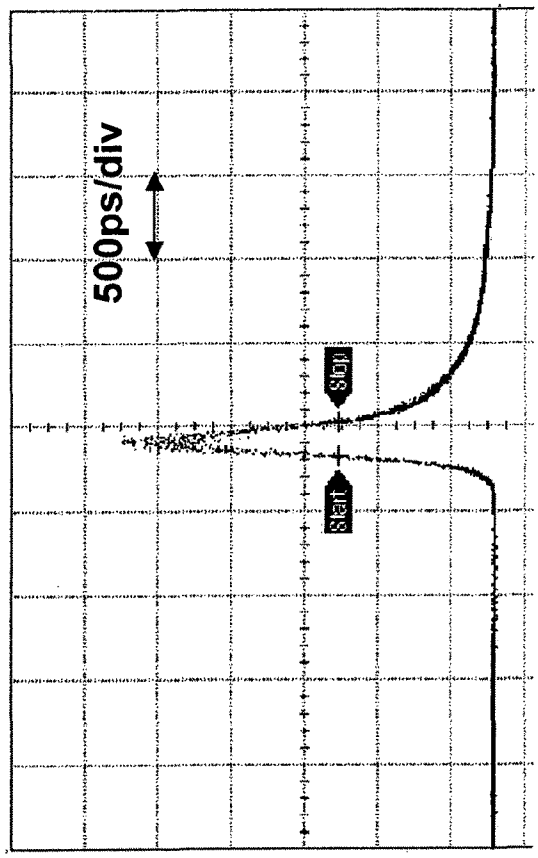

Figure 5b

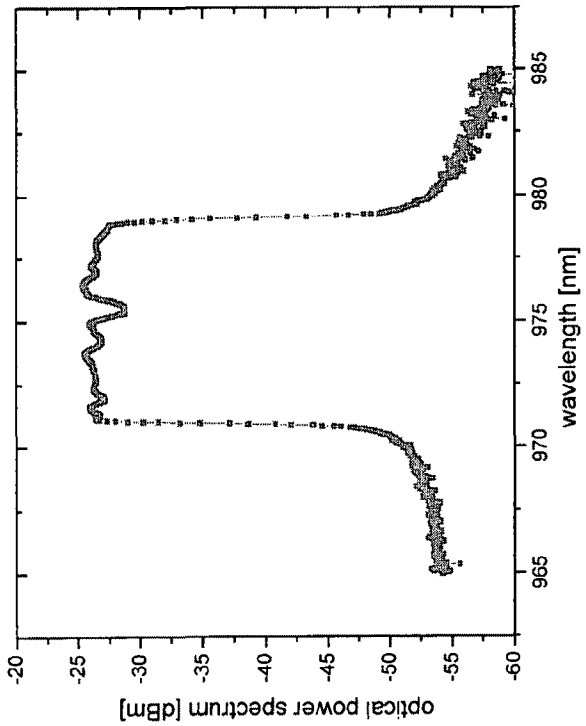

Figure 5a

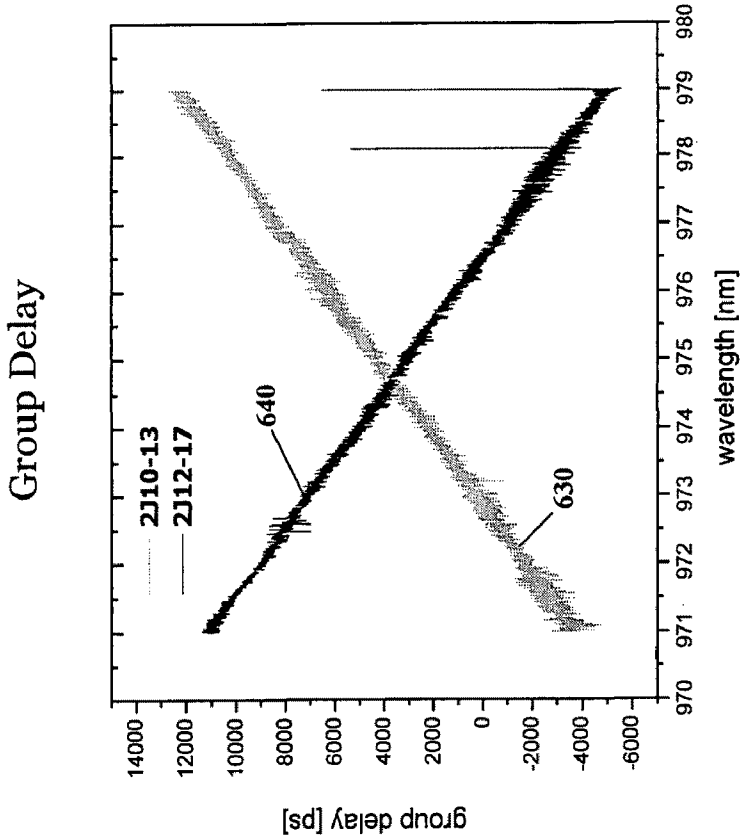

Figure 6b

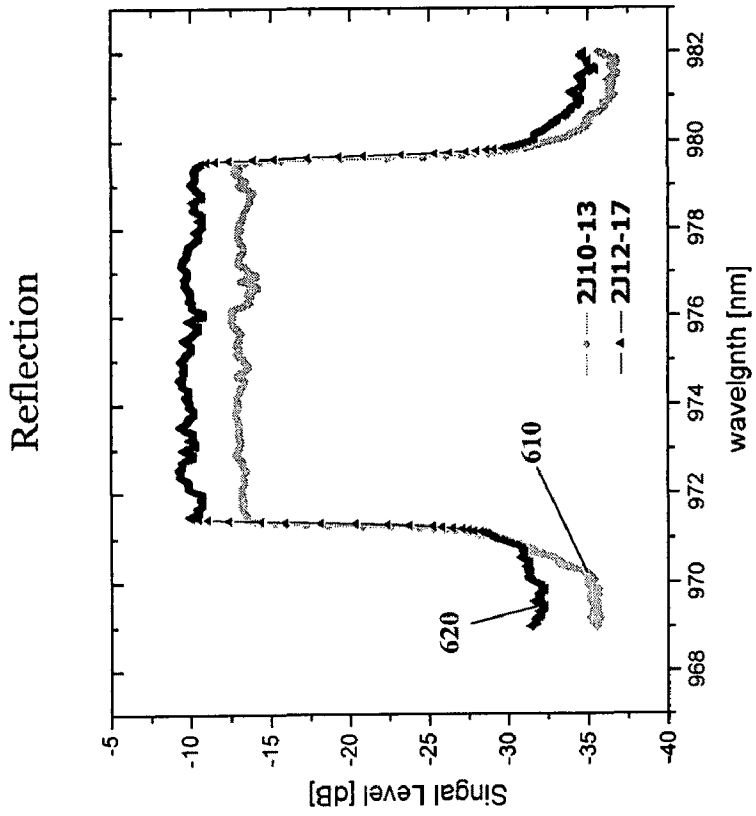

Figure 6a

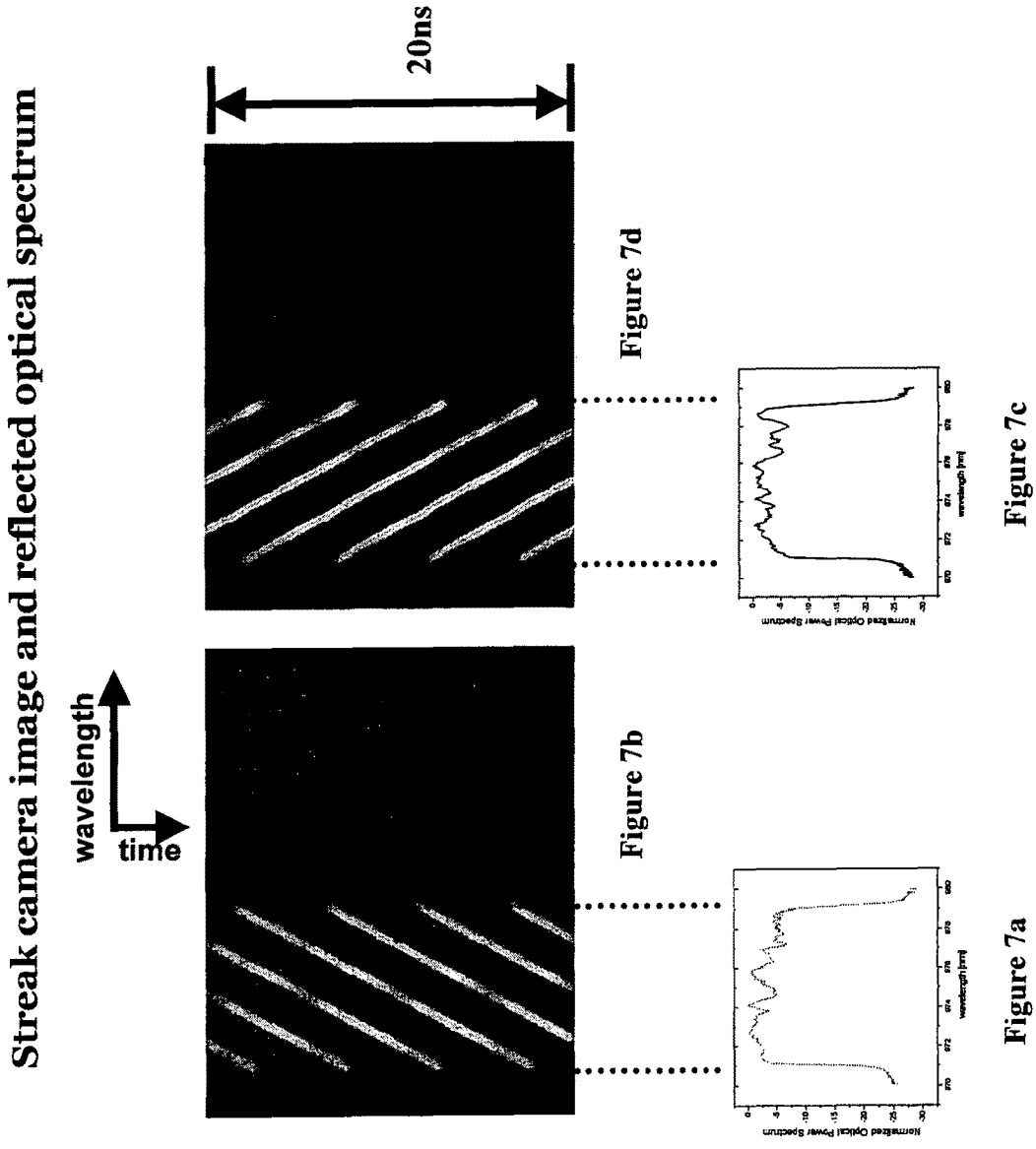
Streak camera image and reflected optical spectrum
20ns
wavelength
time
Figure 7d
Figure 7b
Figure 7c
Figure 7a

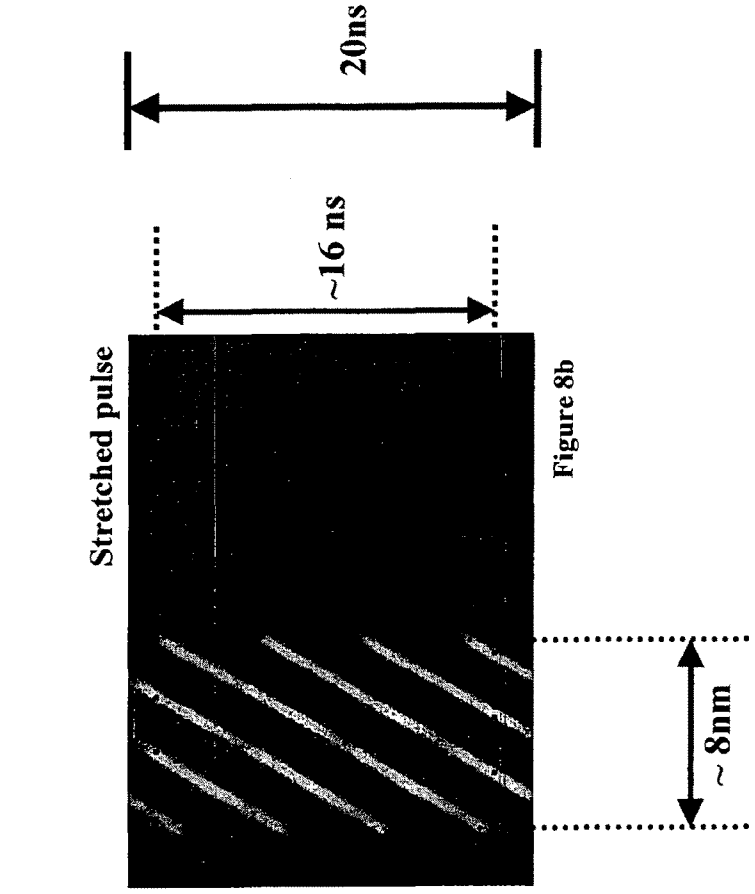

Figure 8b

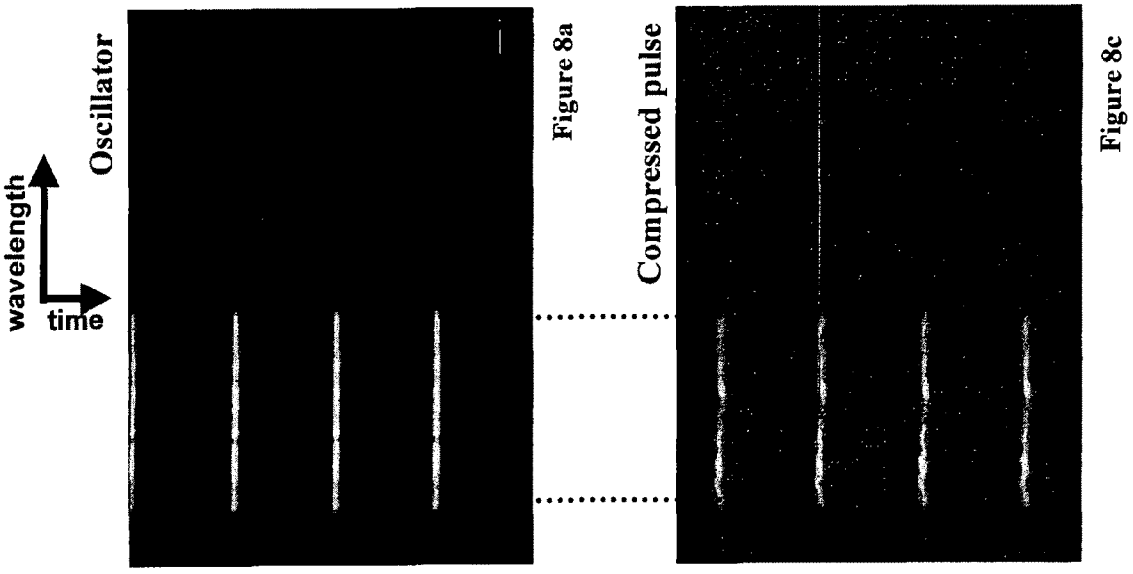

Figure 8a

Figure 8c

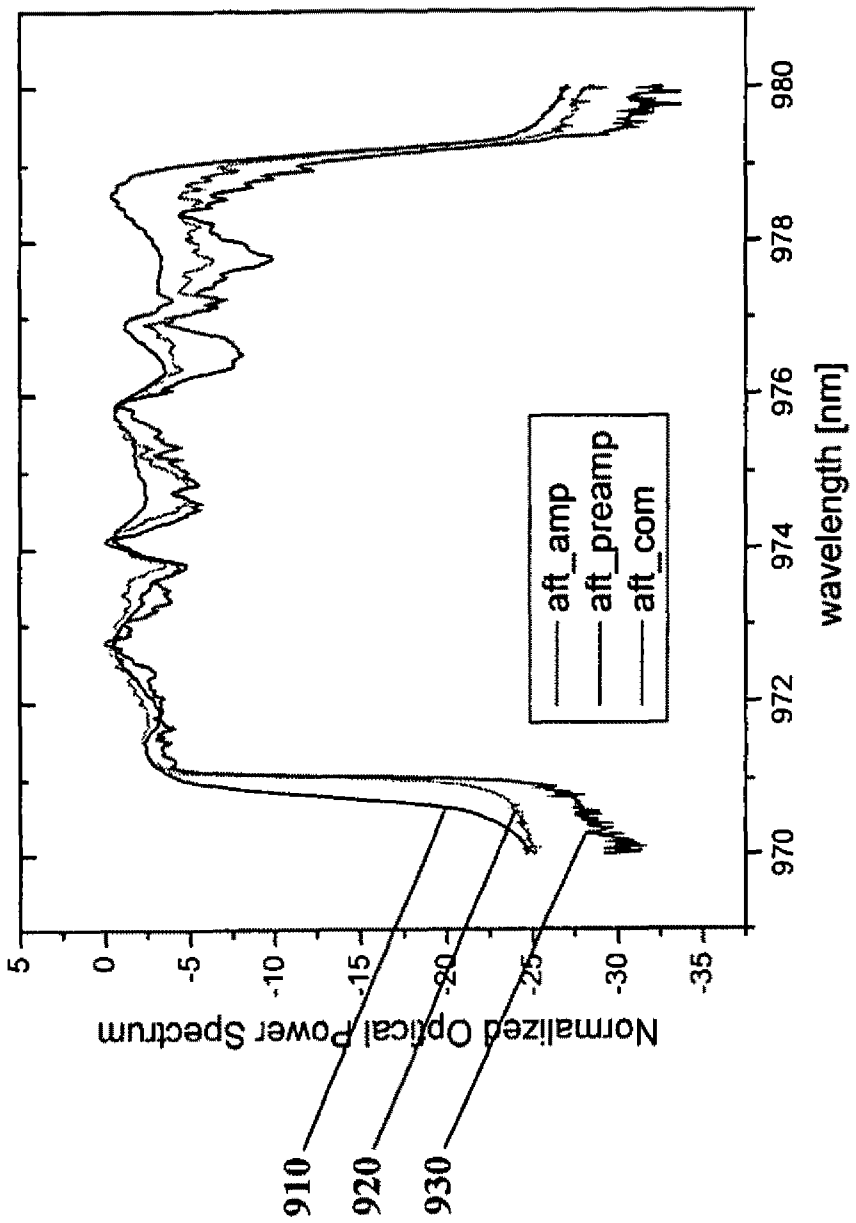
Normalized Optical Power Spectrum
wavelength [nm]
aft_amp
aft_preamp
aft_com
910
920
930

Figure 9

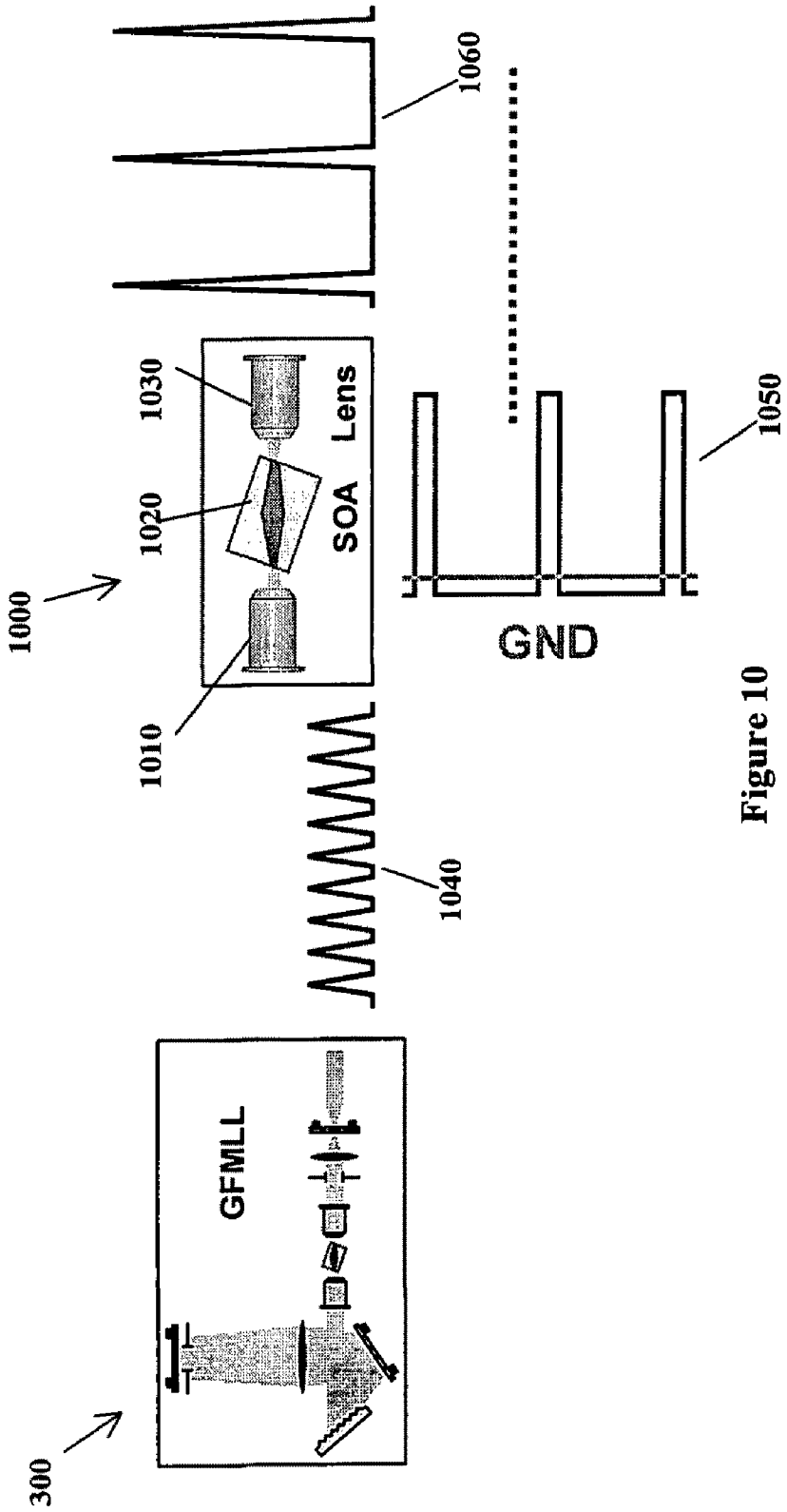

Figure 10

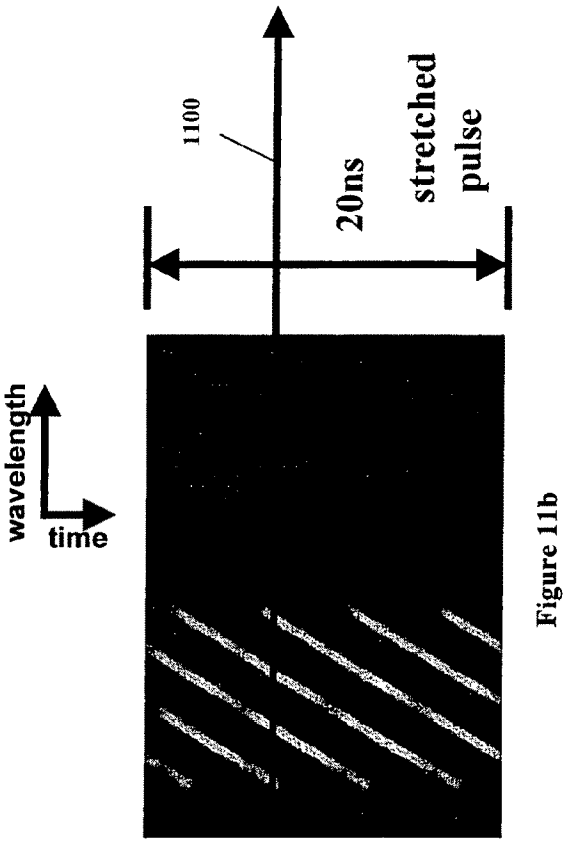

Figure 11b

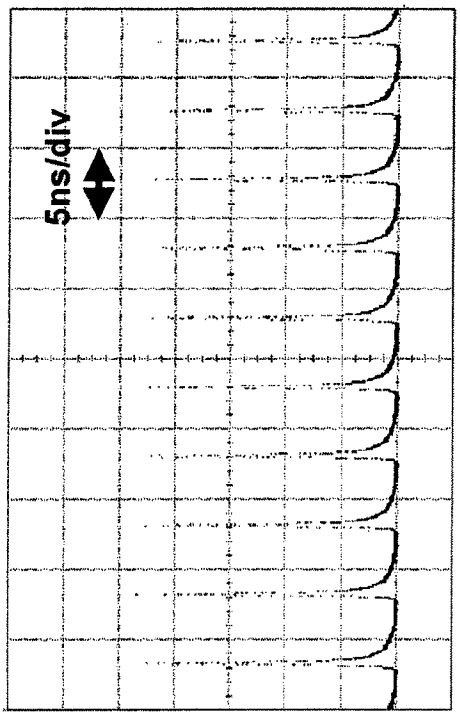

Figure 11a

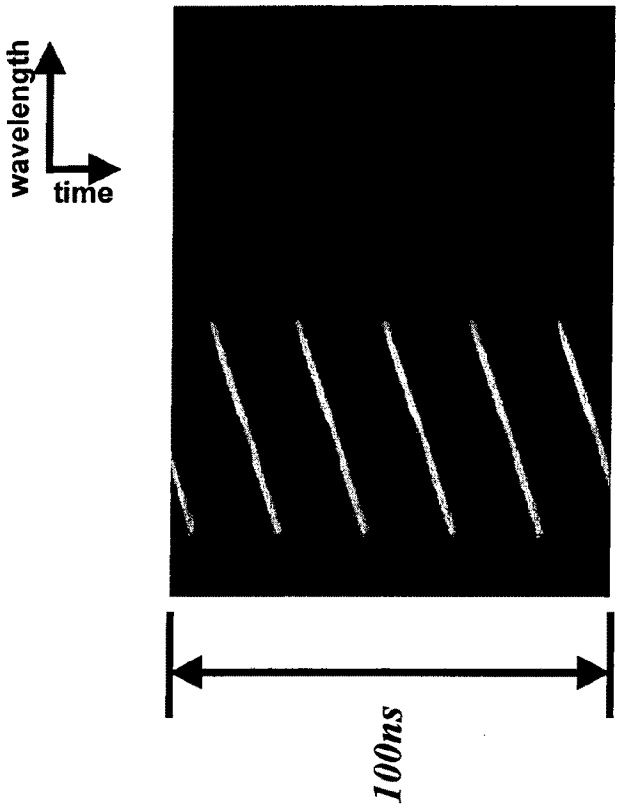

Figure 12b

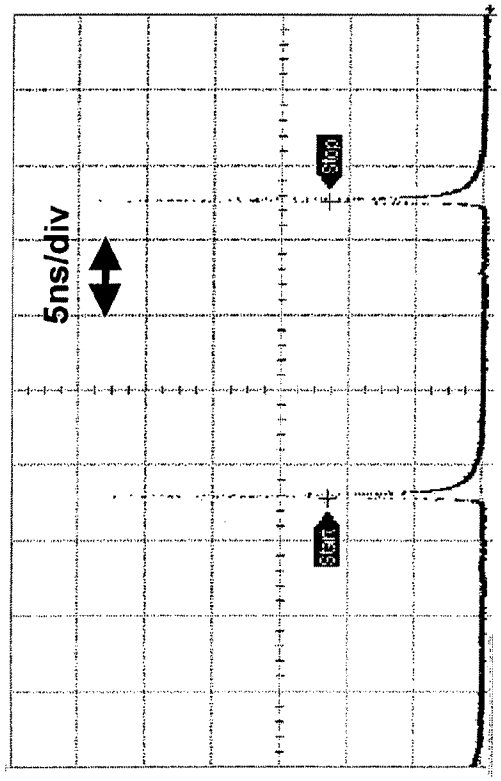

Figure 12a

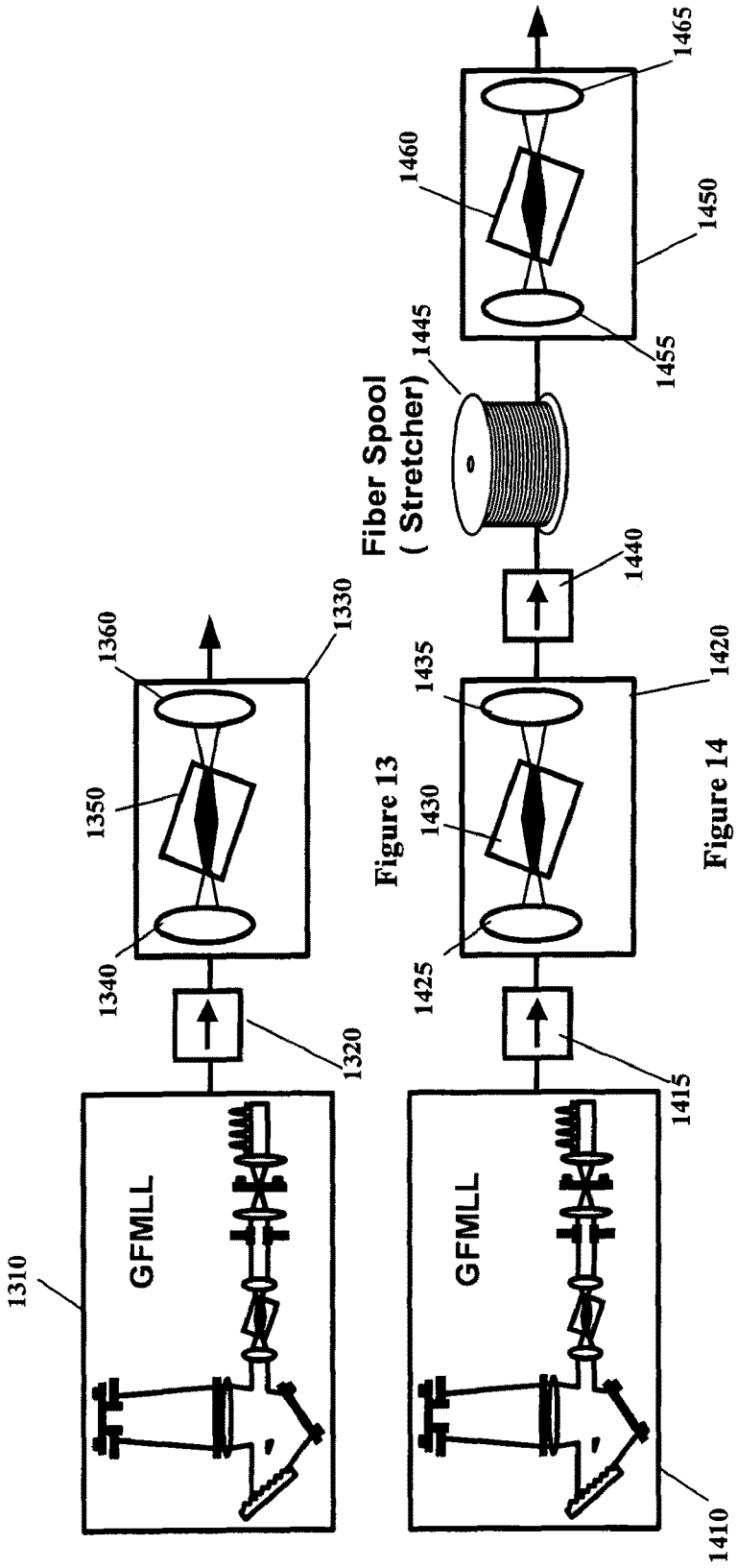

Figure 13

Figure 14

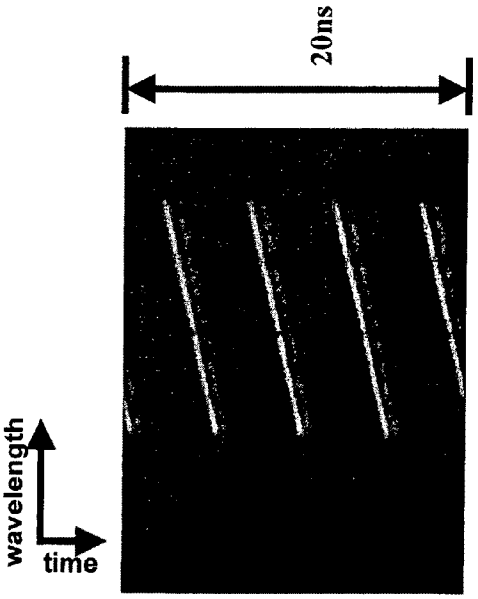

Figure 15d

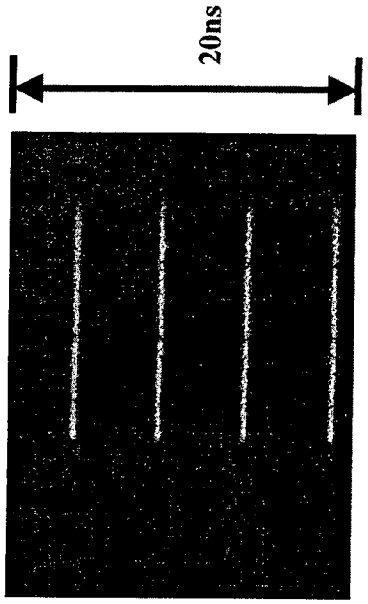

Figure 15c

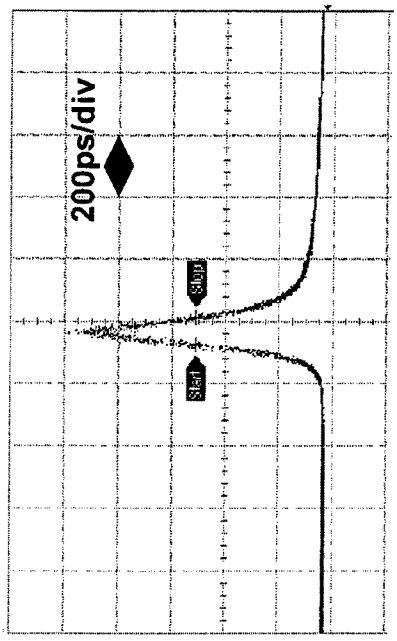

Figure 15b

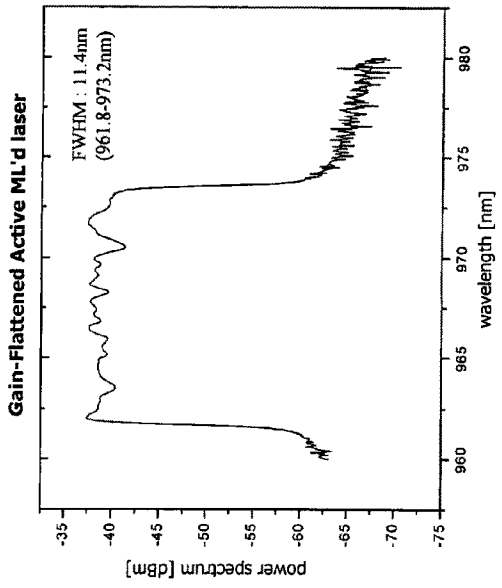

Figure 15a

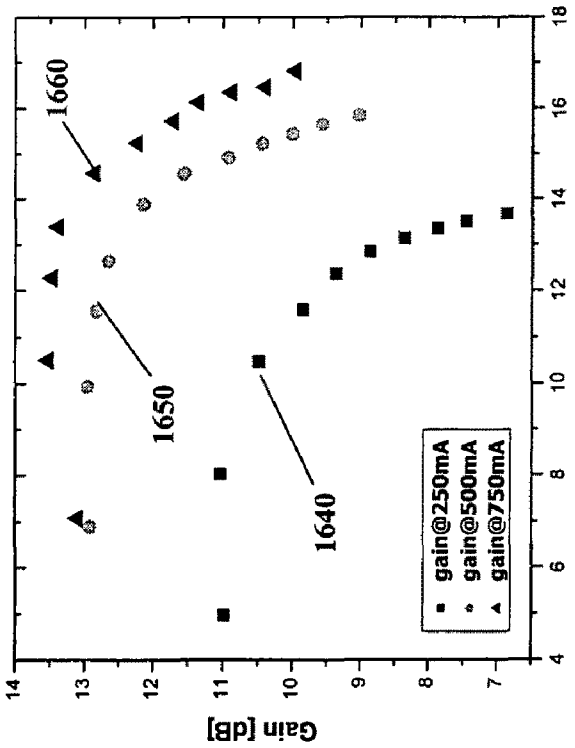

Figure 16b

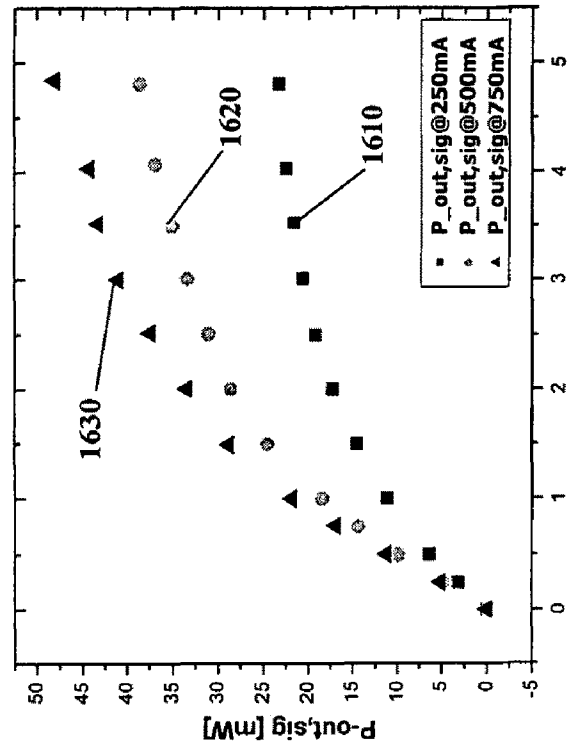

Figure 16a

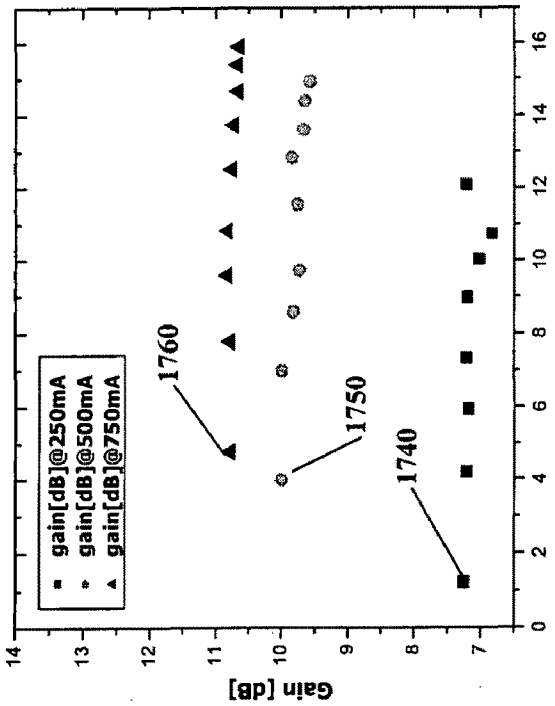

Figure 17b

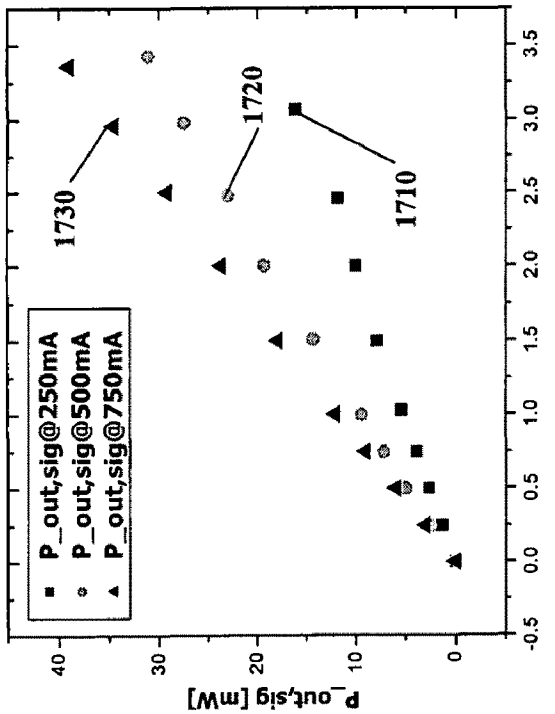

Figure 17a

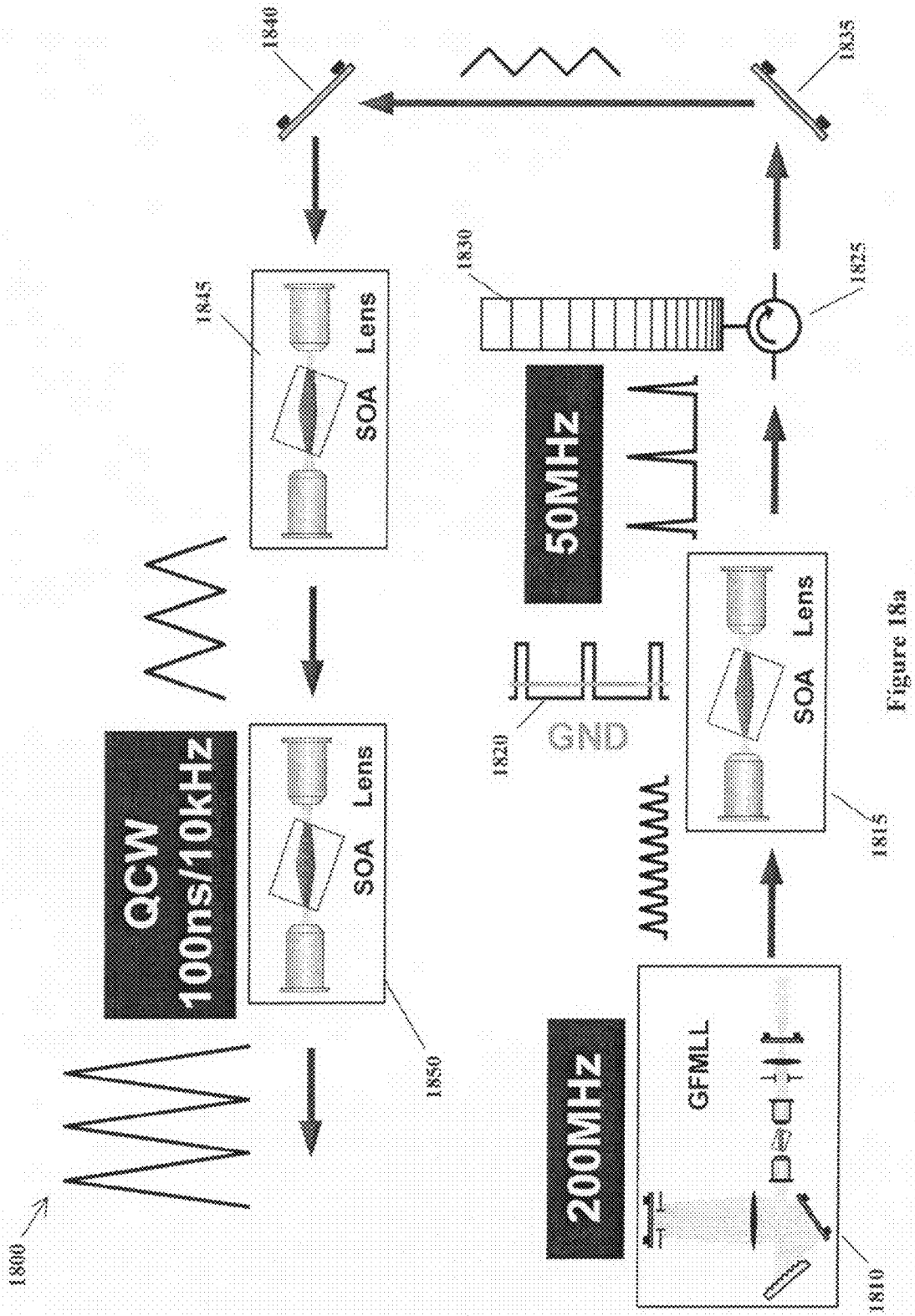
1800
1810
GFMLL
200MHz
1815
SOA Lens
1820
GND
50MHz
1825
1830
1835
1840
1845
SOA Lens
QCW
100ns/10kHz
1850
SOA Lens

Figure 18a

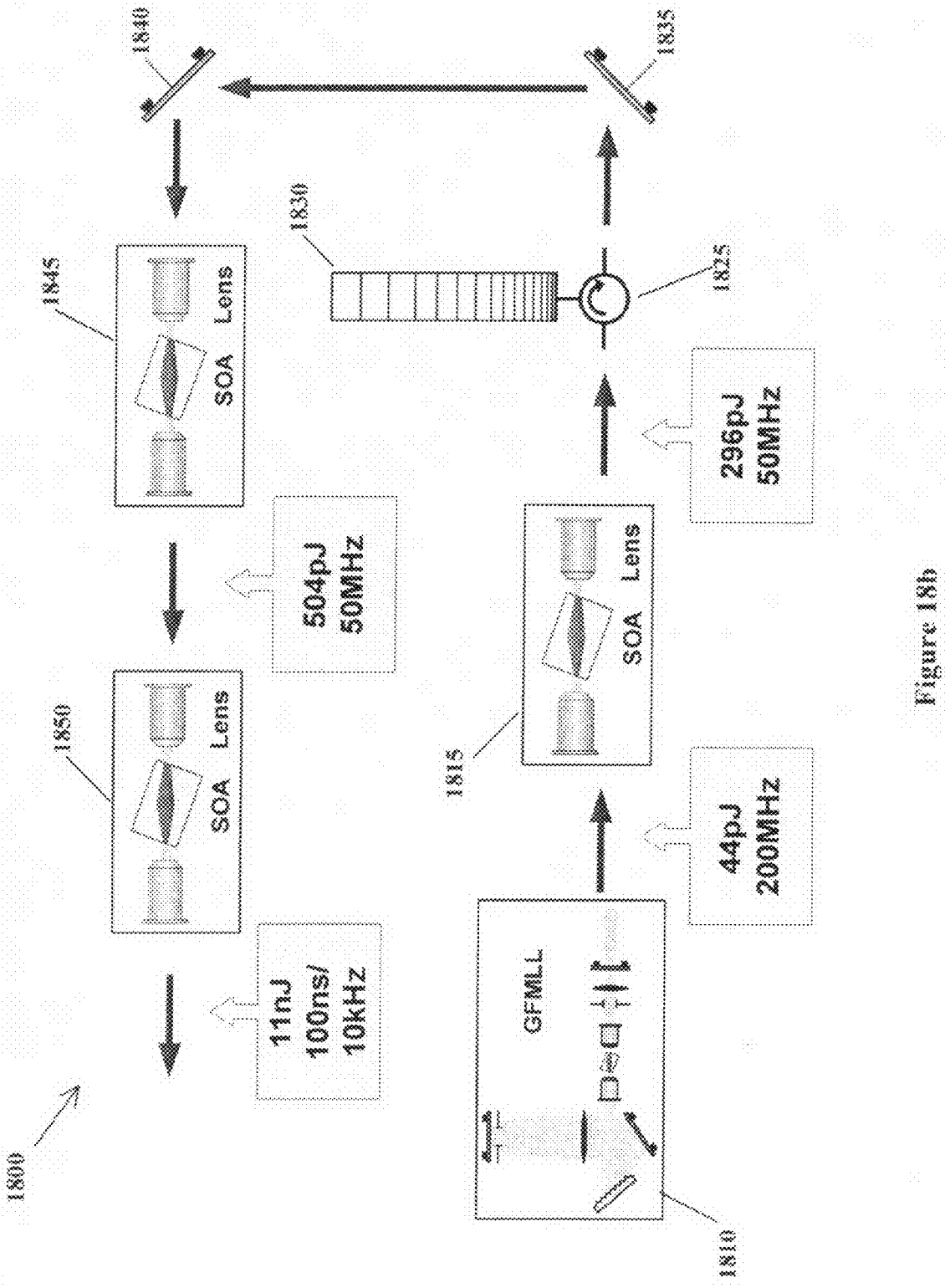
1800
1810
GFMLL
1815
SOA
Lens
1825
1830
1835
1840
1845
1850
44pJ
200MHz
296pJ
50MHz
504pJ
50MHz
11nJ
100ns/
10kHz

Figure 18b

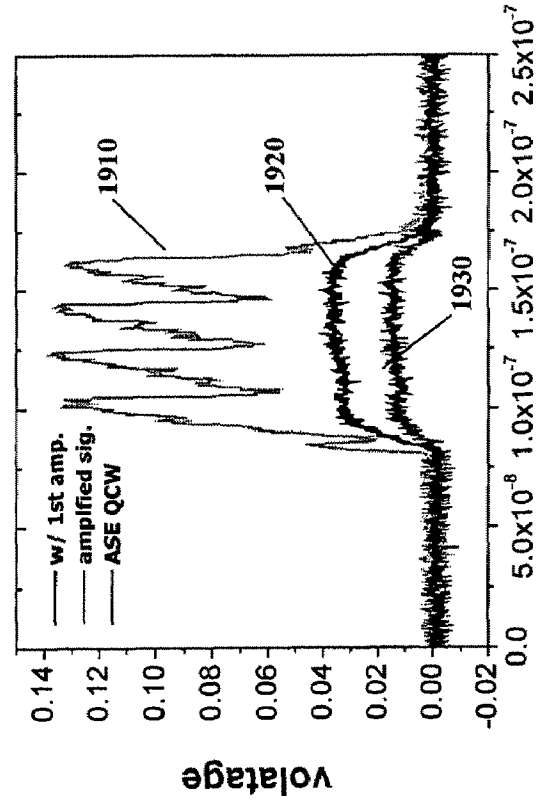

Figure 19b

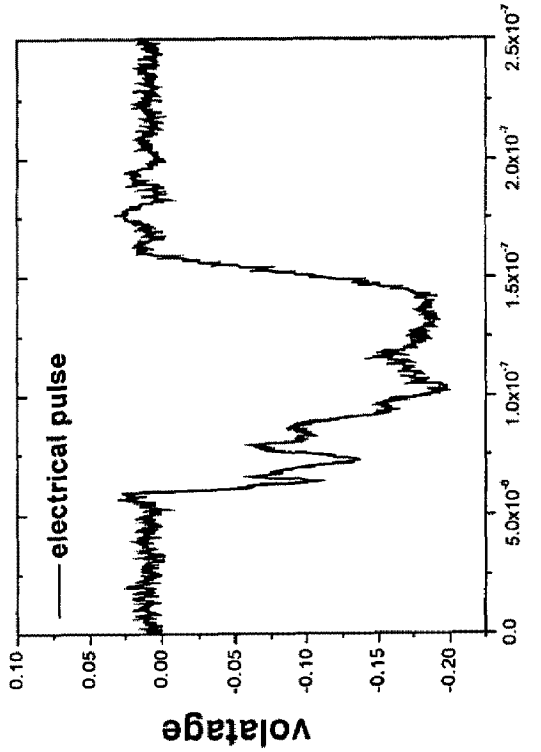

Figure 19a

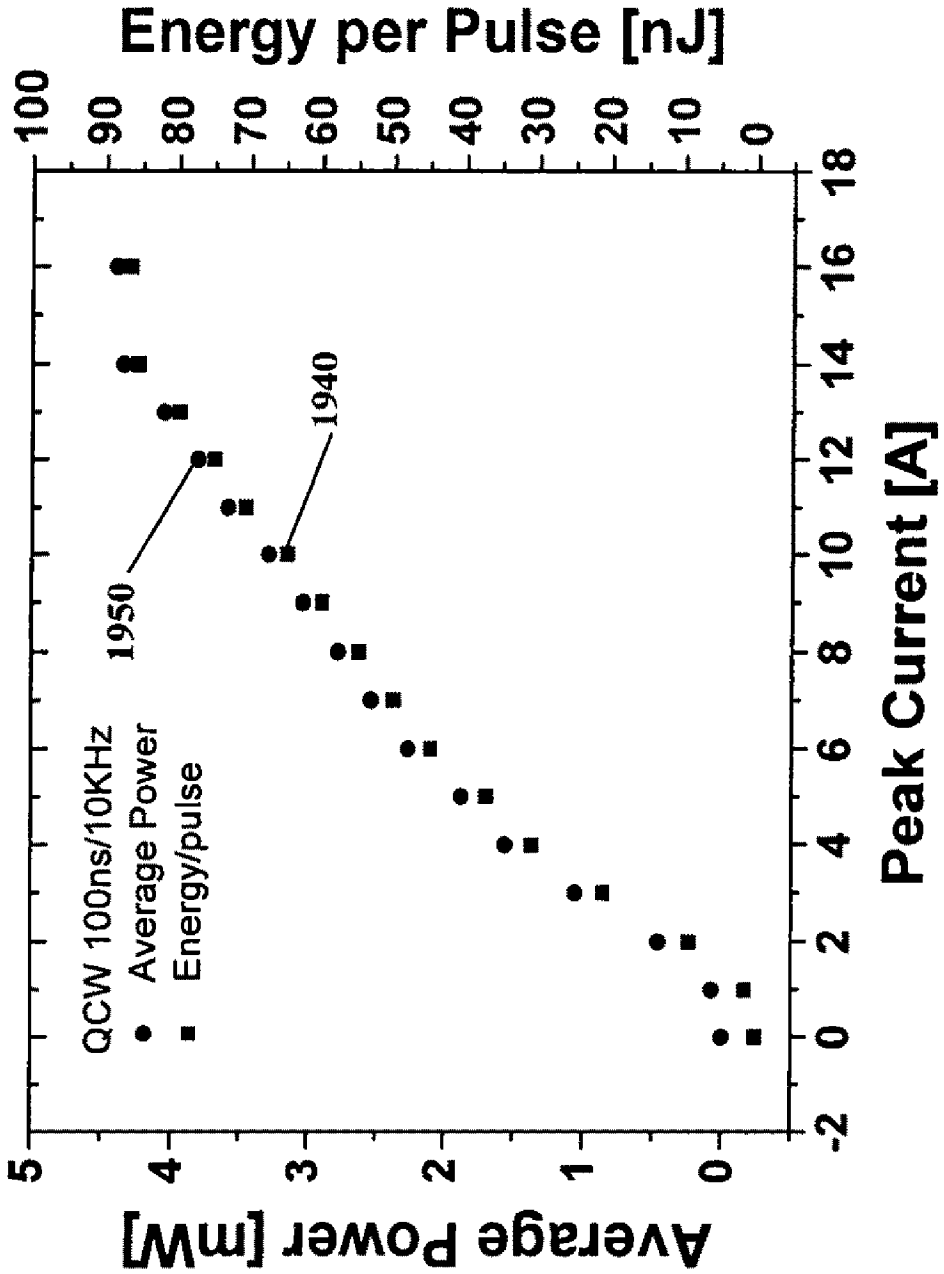
Energy per Pulse [nJ]
100
90
80
70
60
50
40
30
20
10
0
18
16
14
12
10
8
6
4
2
0
-2
Peak Current [A]
1950
1940
QCW 100ns/10KHz
Average Power
Energy/pulse
5
4
3
2
1
0
Average Power [mW]

Figure 19c

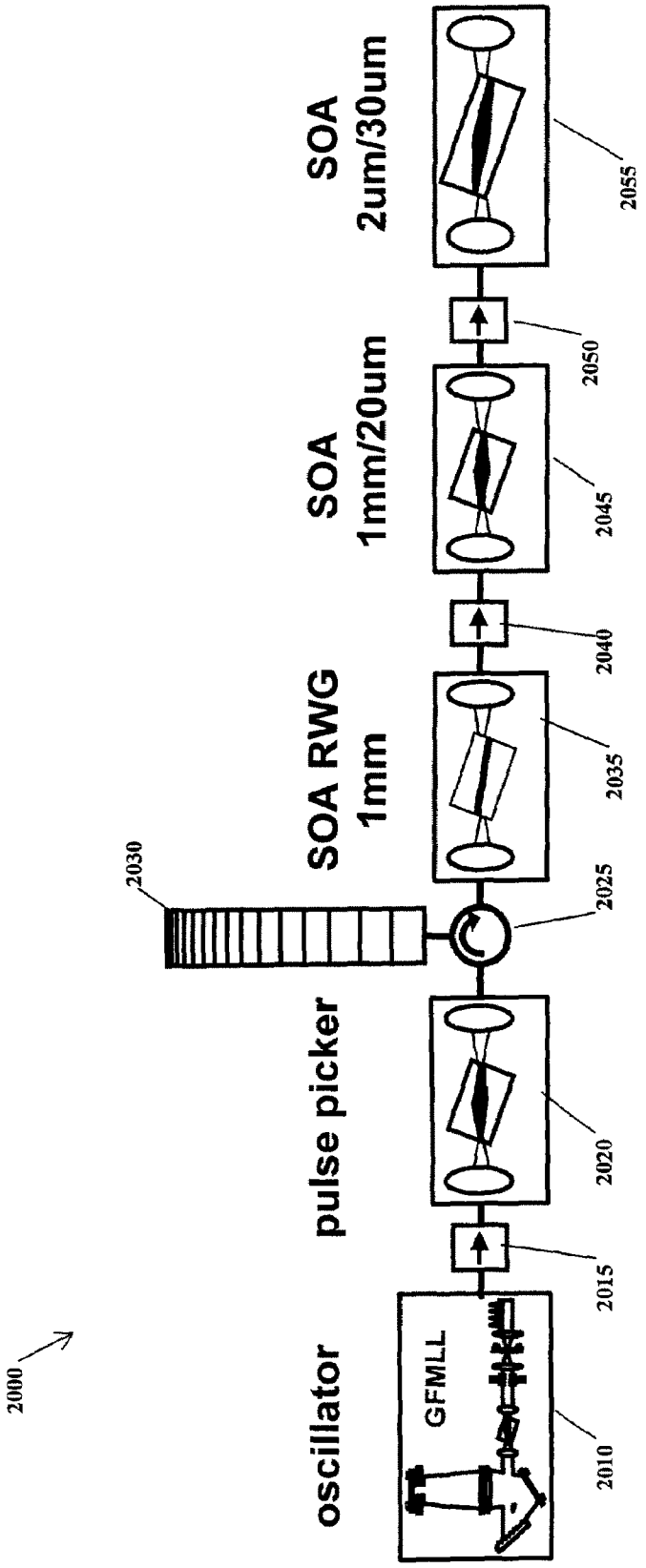
2000
oscillator
GFMLL
2010
2015
pulse picker
2020
2025
2030
SOA RWG
1mm
2035
2040
SOA
1mm/20um
2045
2050
SOA
2um/30um
2055

Figure 20a

	operating condition	average power	energy per pulse	gain/loss
oscillator	200MHz	~7mW	35pJ	
pulse picker	50MHz 250mA+44m V	12mW	240pJ	8.34dB
stretcher		1.6mW	32pJ	-8.75dB
preamplifier	125mA DC	16.3mW	326pJ	10.1dB
1st amplifier	500mA DC	162mW	3.24nJ	9.97dB
2nd amplifier	16A peak 100ns/10kHz	3.8mW	76nJ	13.7dB
total gain ~ 33.3 dB				

Figure 20b

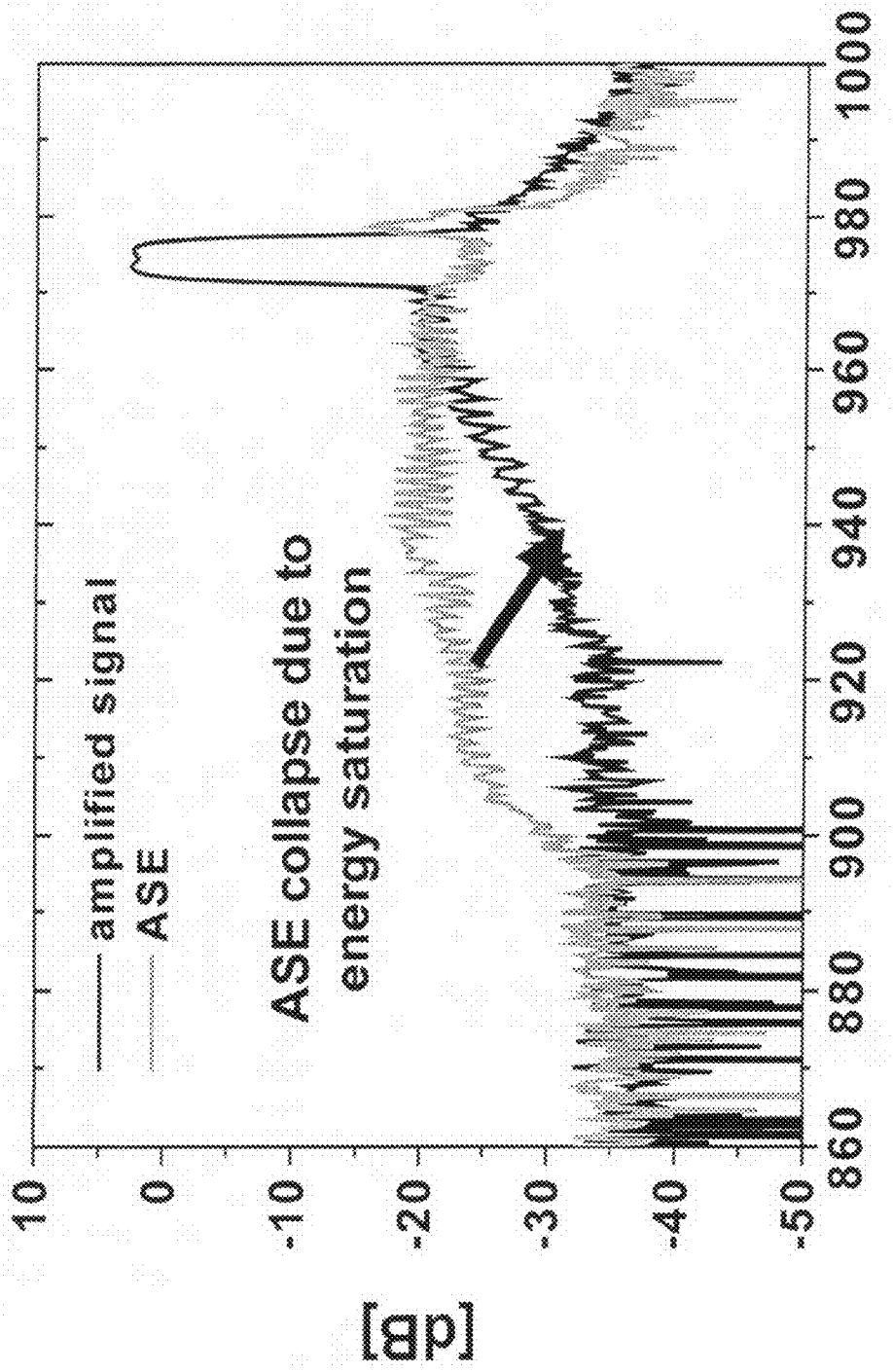
amplified signal
ASE
ASE collapse due to
energy saturation
[dB]
10
0
-10
-20
-30
-40
-50
860
880
900
920
940
960
980
1000
Wavelength [nm]

Figure 20c

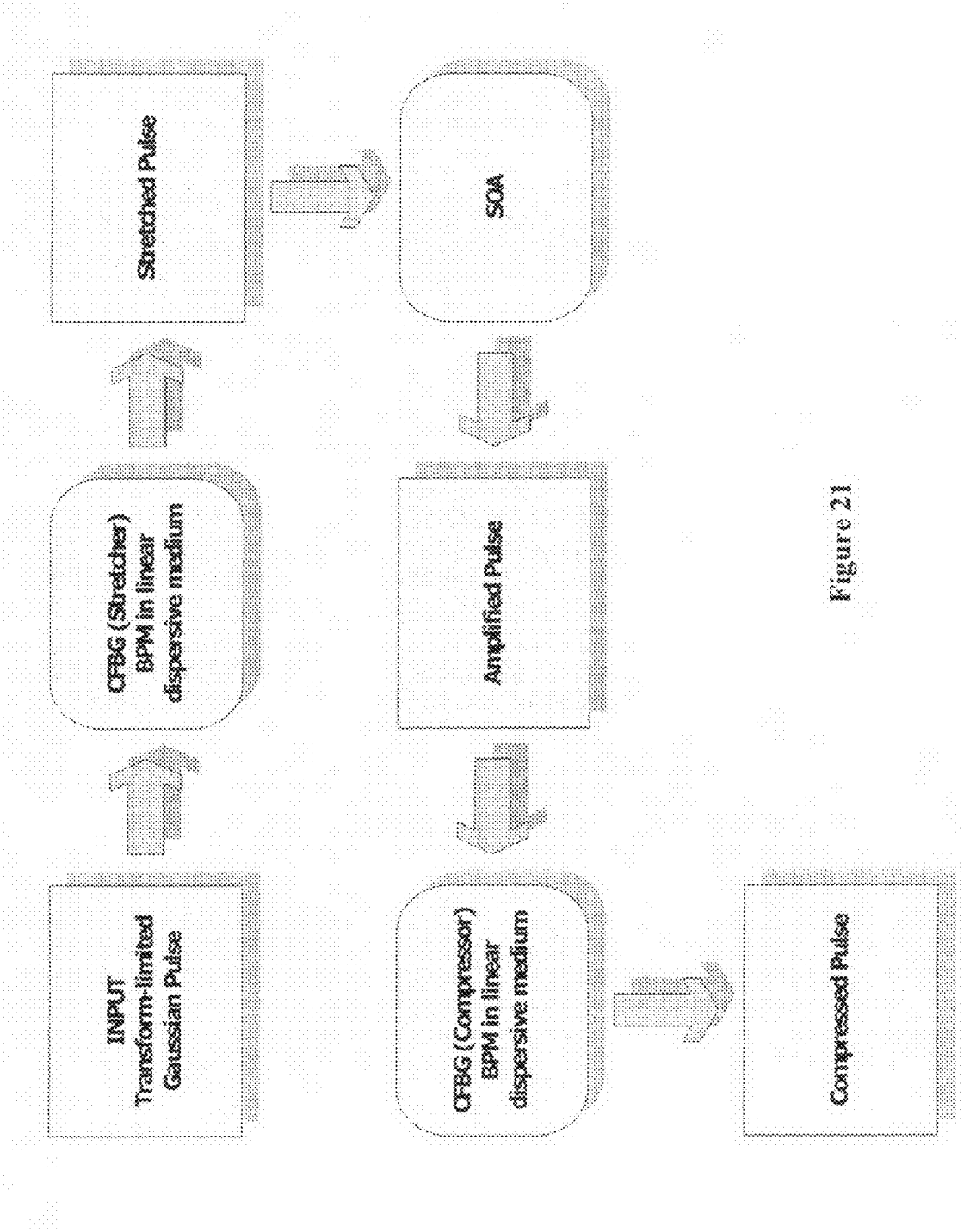
INPUT
Transform-limited
Gaussian Pulse
CFBG (Stretcher)
BPM in linear
dispersive medium
Stretched Pulse
SOA
Amplified Pulse
CFBG (Compressor)
BPM in linear
dispersive medium
Compressed Pulse

Figure 21

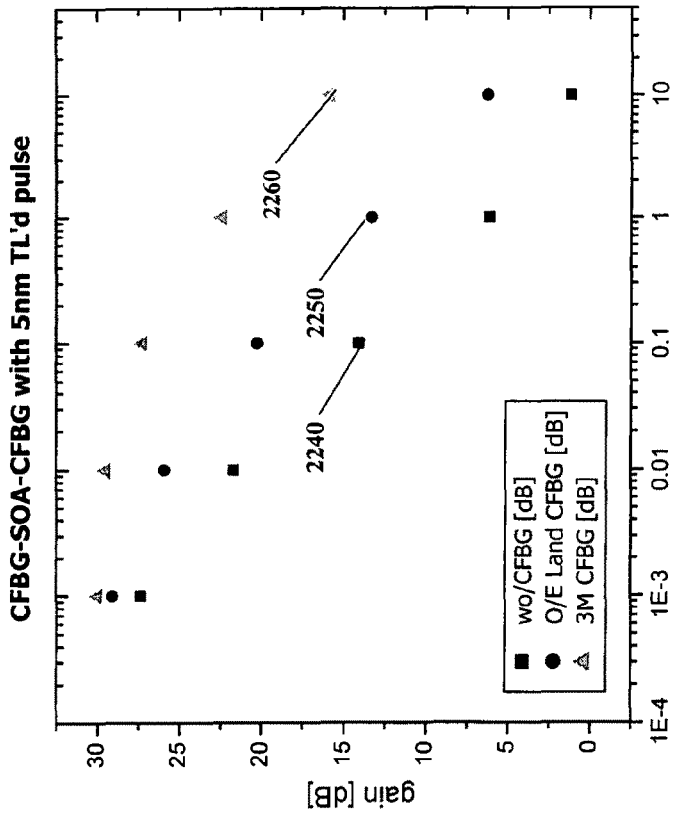

Figure 22b

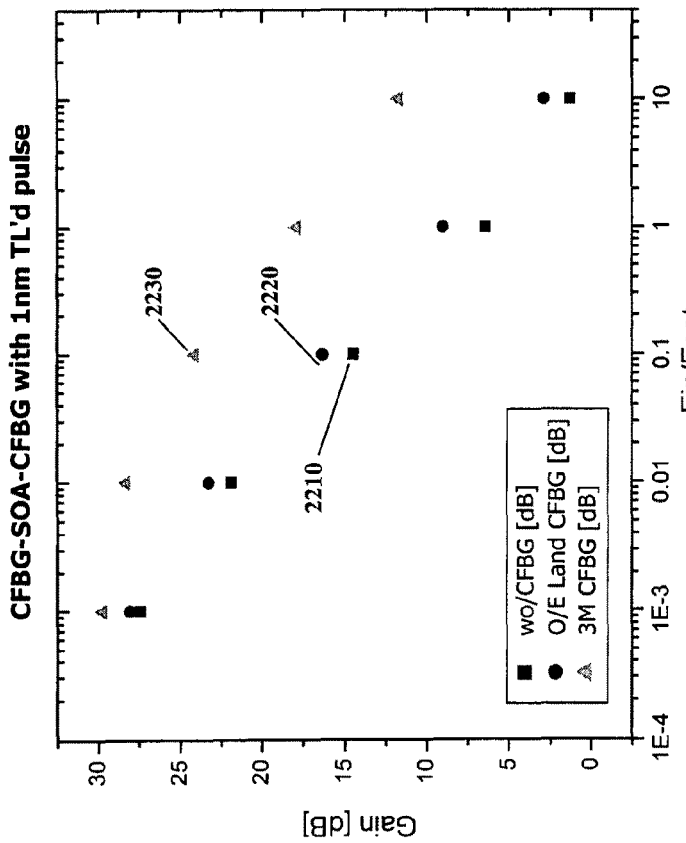

Figure 22a

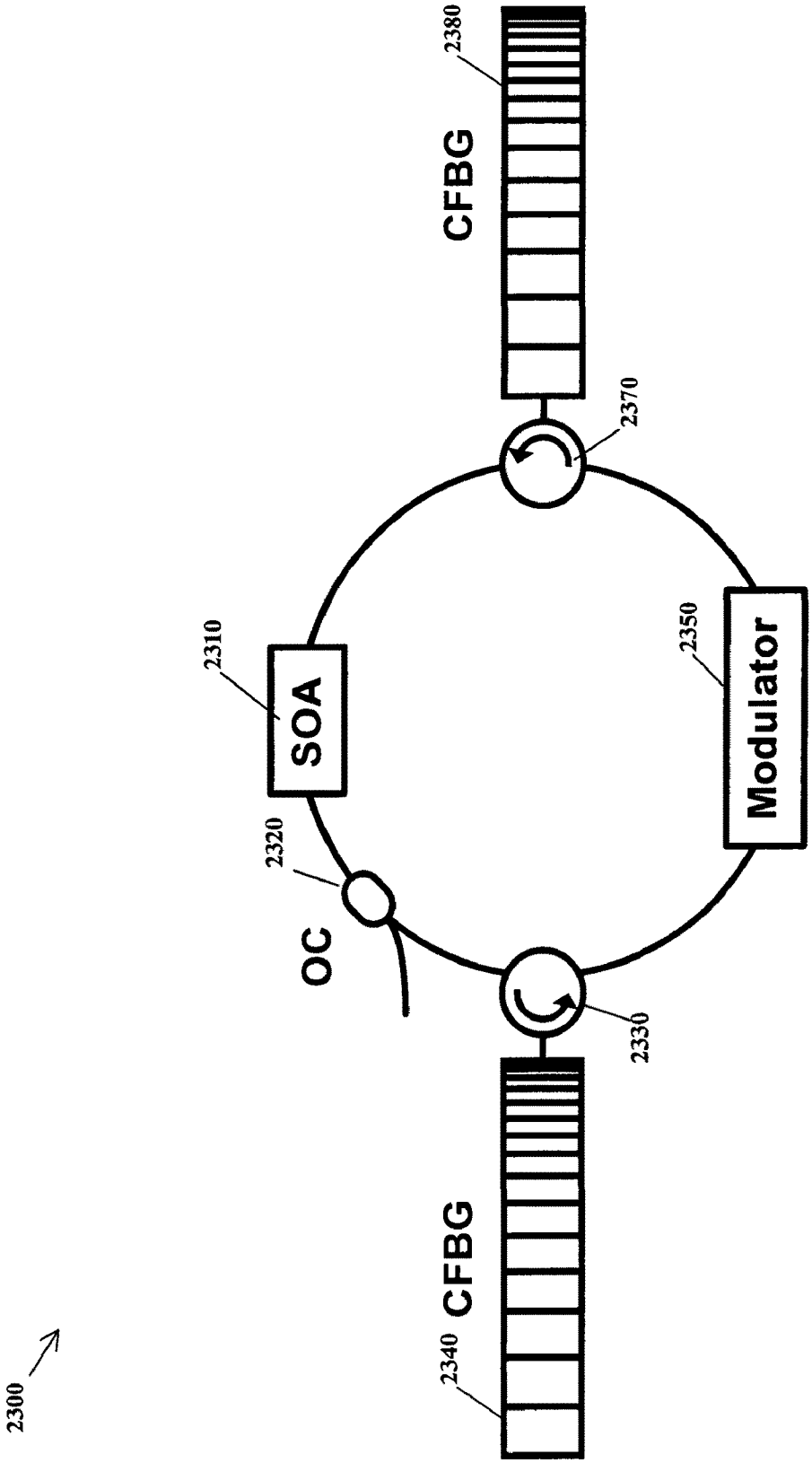
2300
2310
SOA
2320
OC
2330
2340
CFBG
2350
Modulator
2370
2380
CFBG

Figure 23

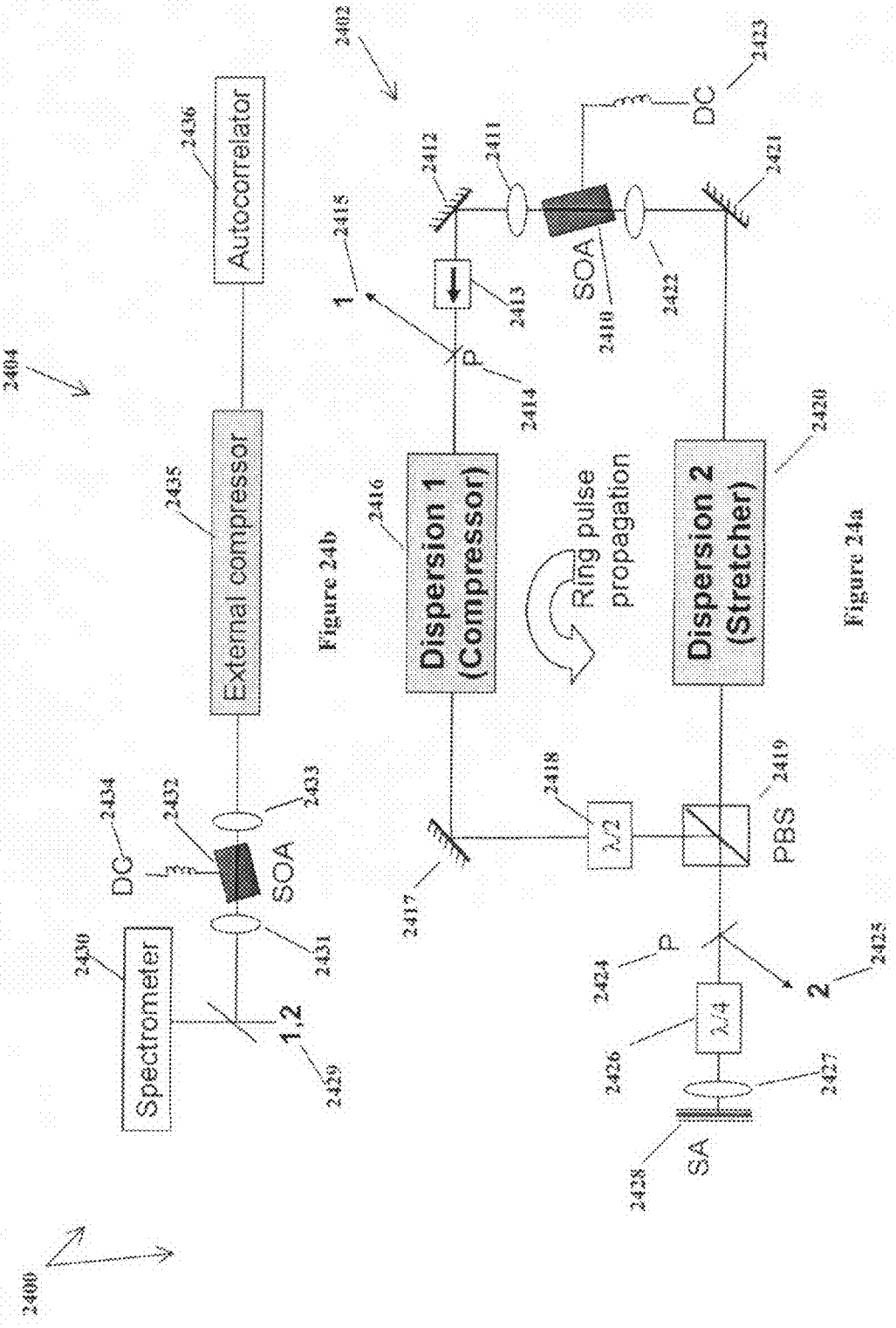

Figure 24b

Figure 24a

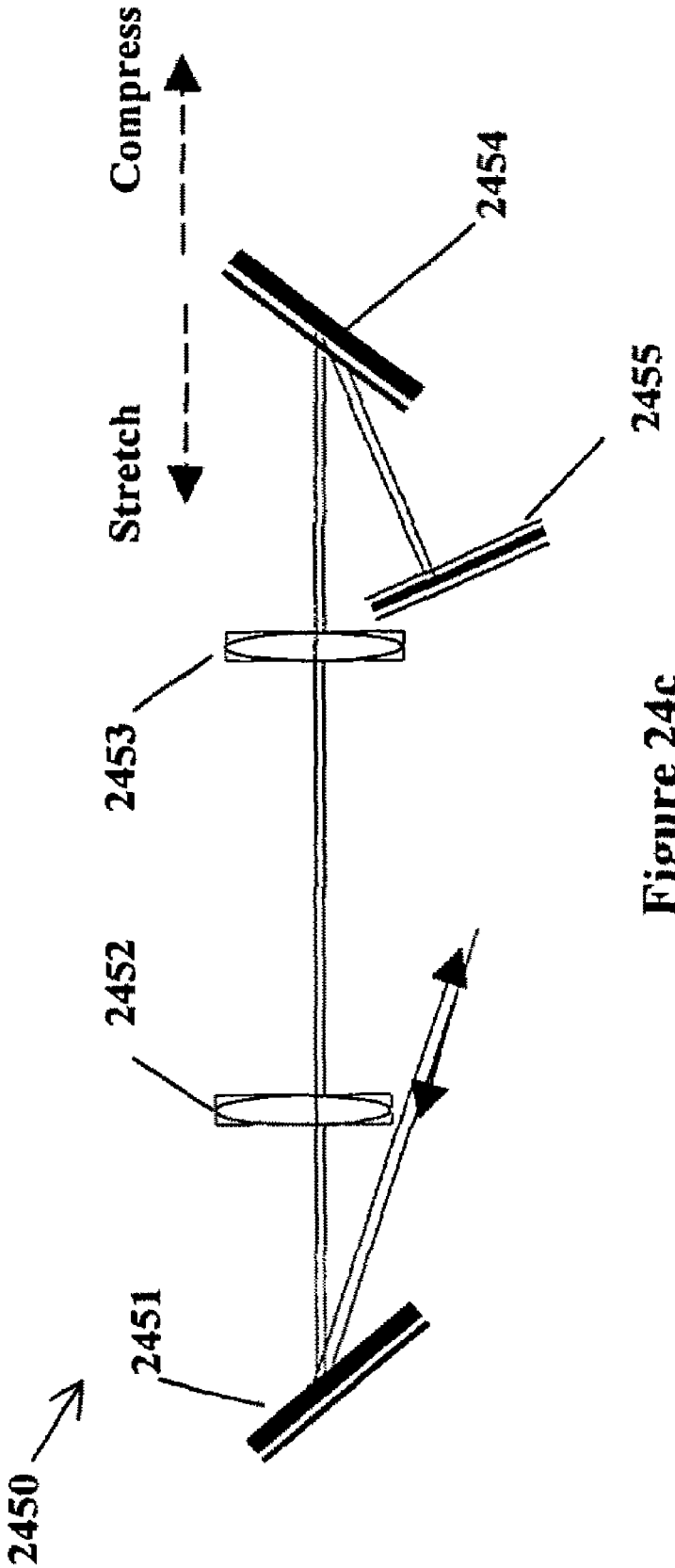

Figure 24c

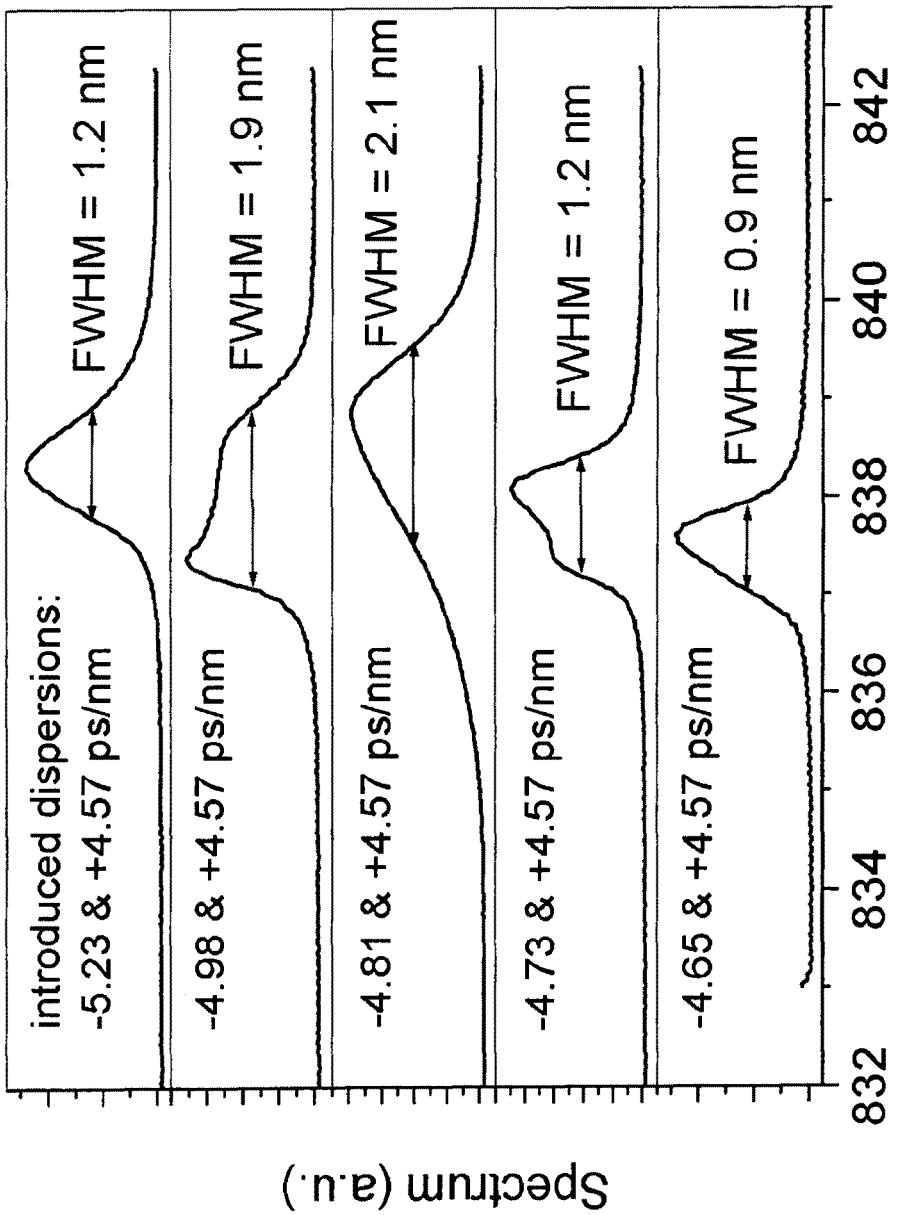
introduced dispersions:
-5.23 & +4.57 ps/nm
FWHM = 1.2 nm
-4.98 & +4.57 ps/nm
FWHM = 1.9 nm
-4.81 & +4.57 ps/nm
FWHM = 2.1 nm
-4.73 & +4.57 ps/nm
FWHM = 1.2 nm
-4.65 & +4.57 ps/nm
FWHM = 0.9 nm
832
834
836
838
840
842
Wavelength (nm)
Spectrum (a.u.)

Figure 25

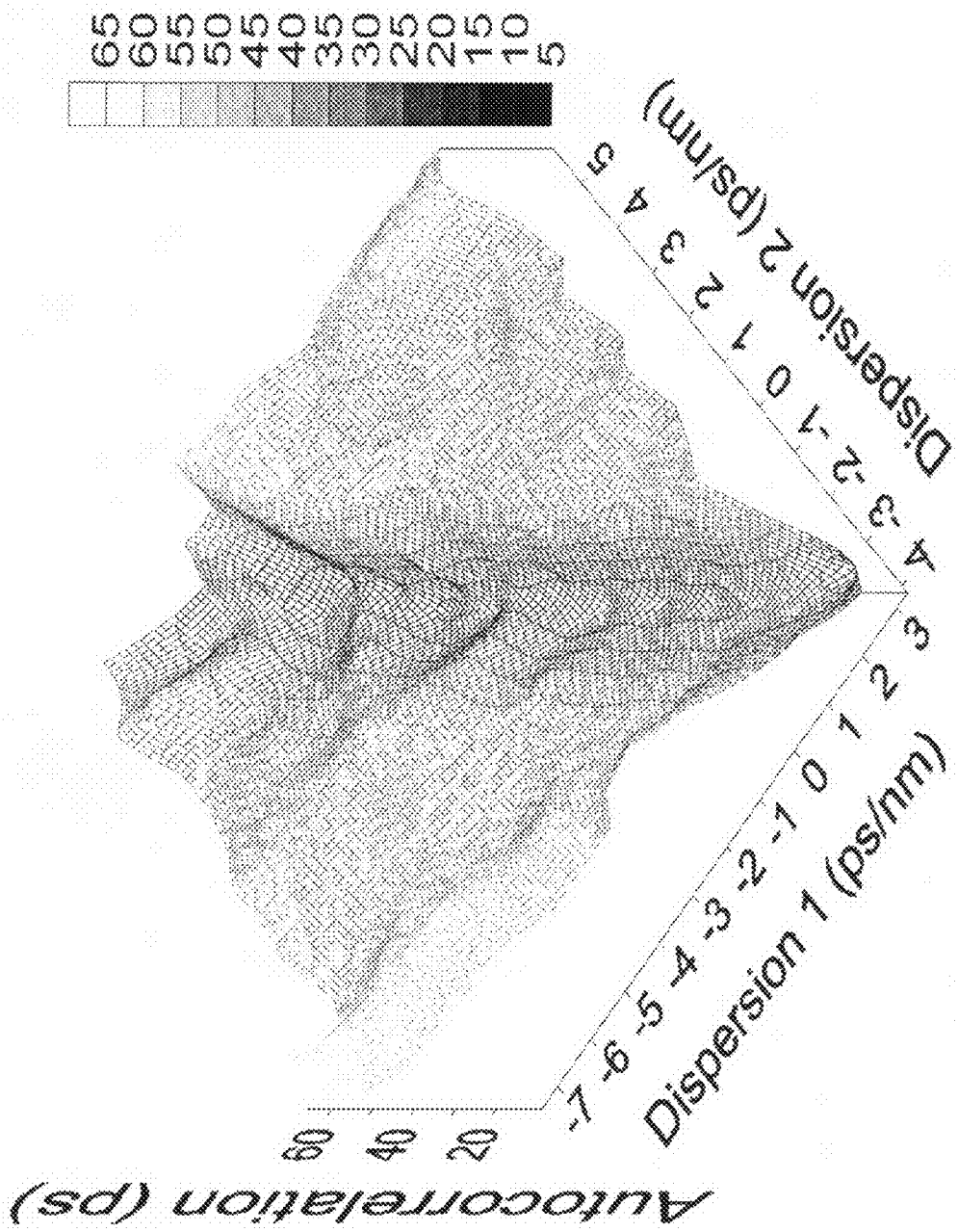
65
60
55
50
45
40
35
30
25
20
15
10
5
Autocorrelation (ps)
Dispersion 1 (ps/nm)
Dispersion 2 (ps/nm)

Figure 26

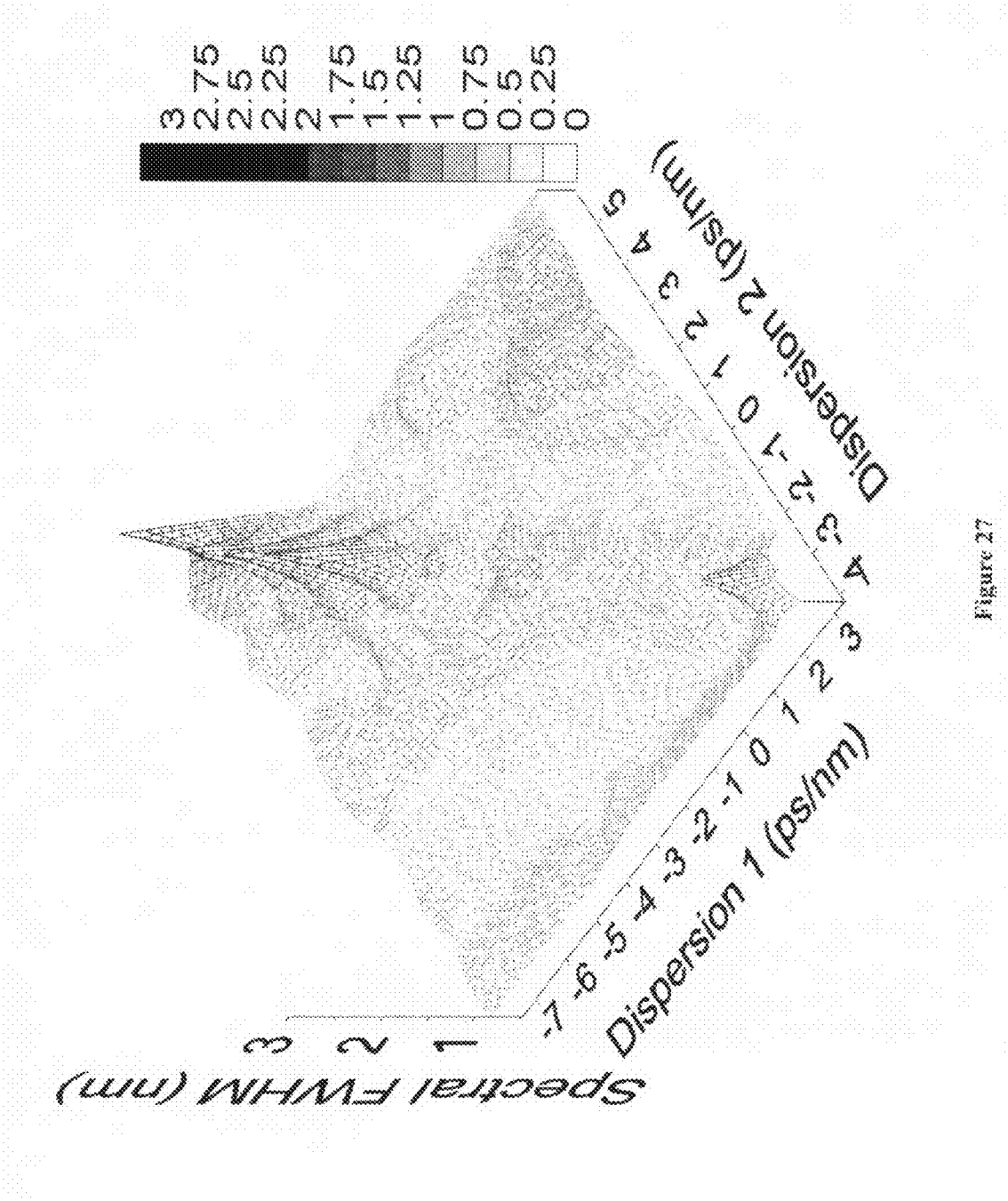
3.75
3.25
2.75
2.25
1.75
1.25
0.75
0.25
0
Spectral FWHM (nm)
Dispersion 1 (ps/nm)
Dispersion 2 (ps/nm)

Figure 27

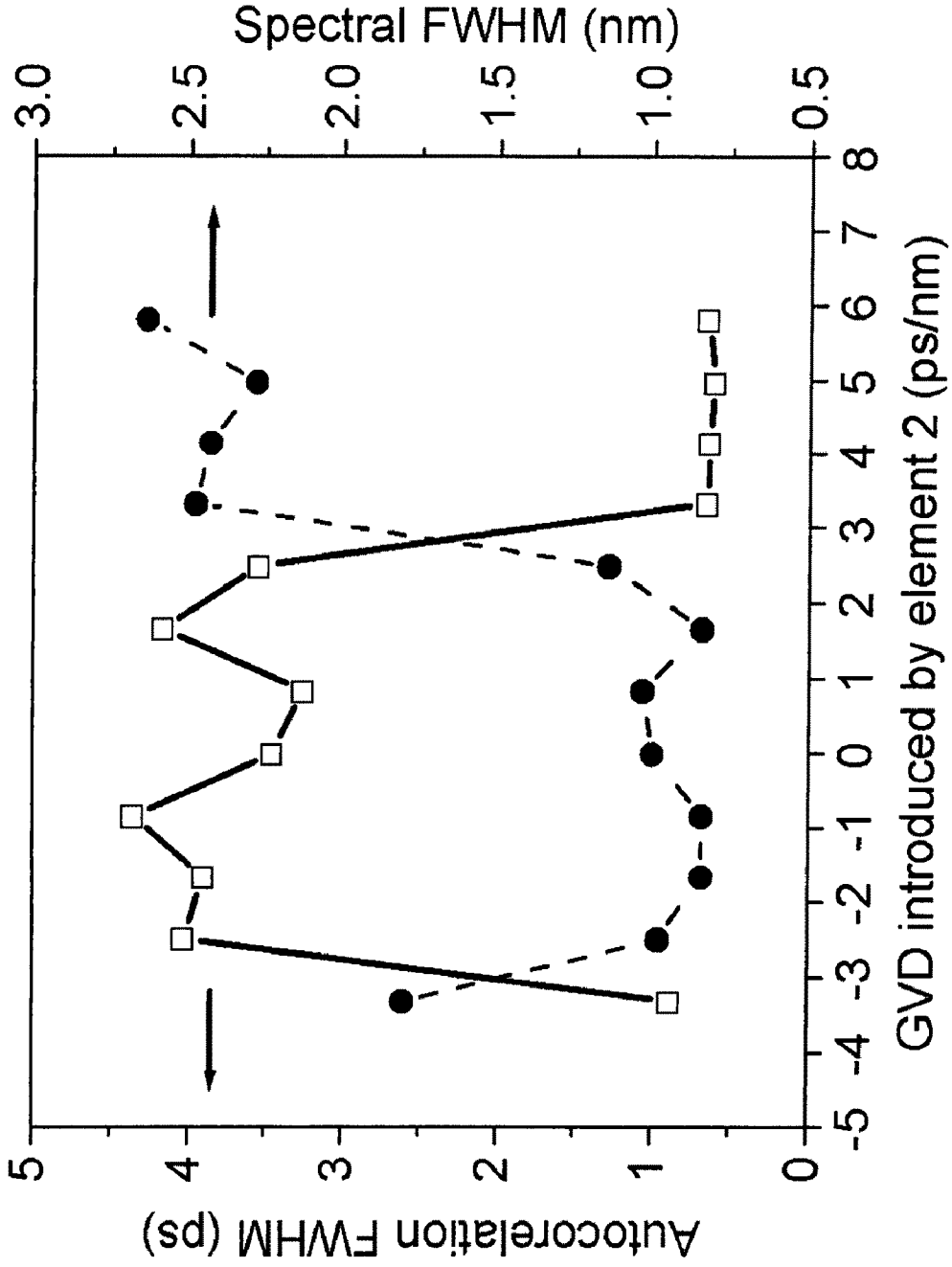
Spectral FWHM (nm)
3.0
2.5
2.0
1.5
1.0
0.5
Autocorrelation FWHM (ps)
5
4
3
2
1
0
-5 -4 -3 -2 -1 0 1 2 3 4 5 6 7 8
GVD introduced by element 2 (ps/nm)

Figure 28

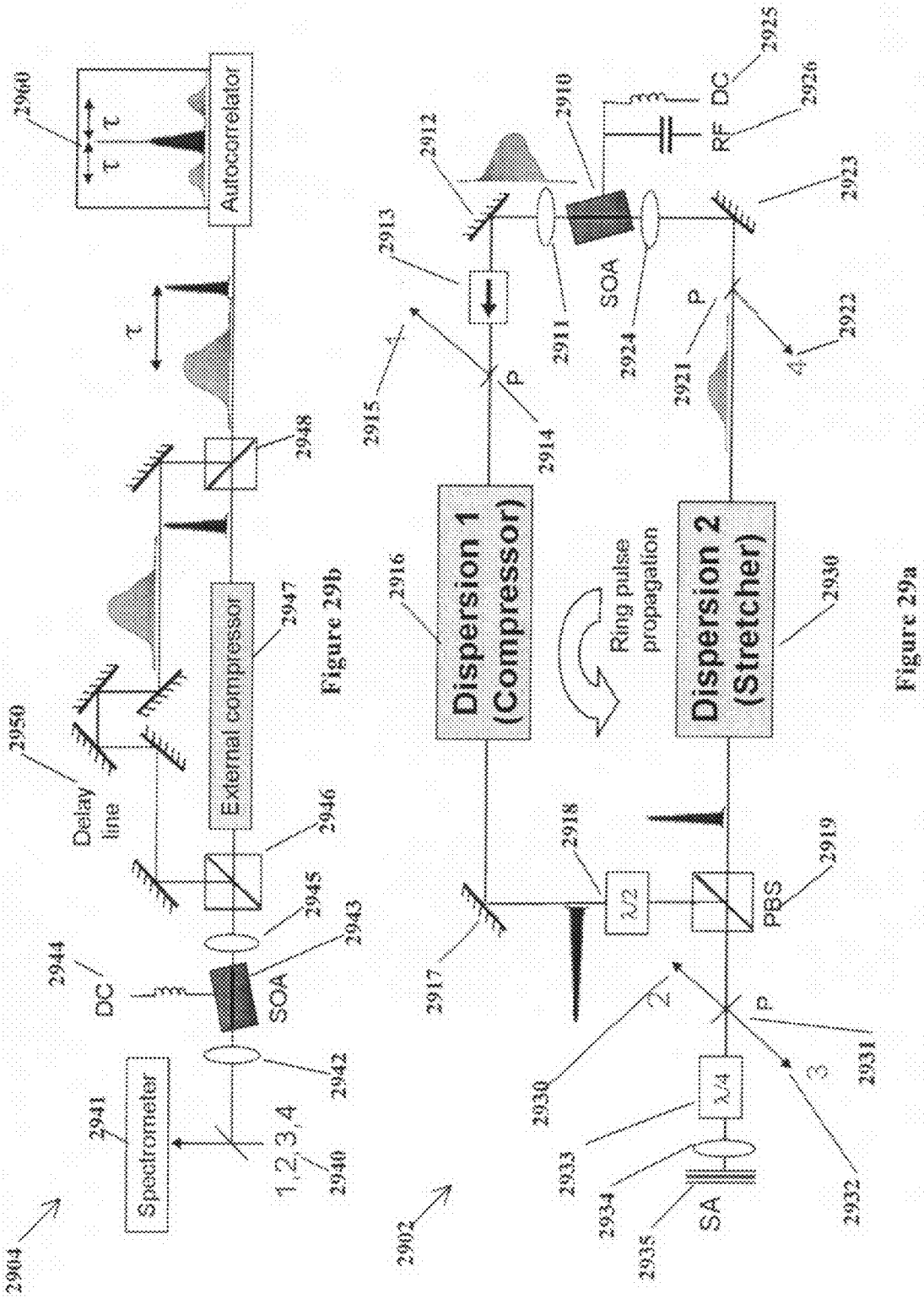

Figure 29a

Figure 29b

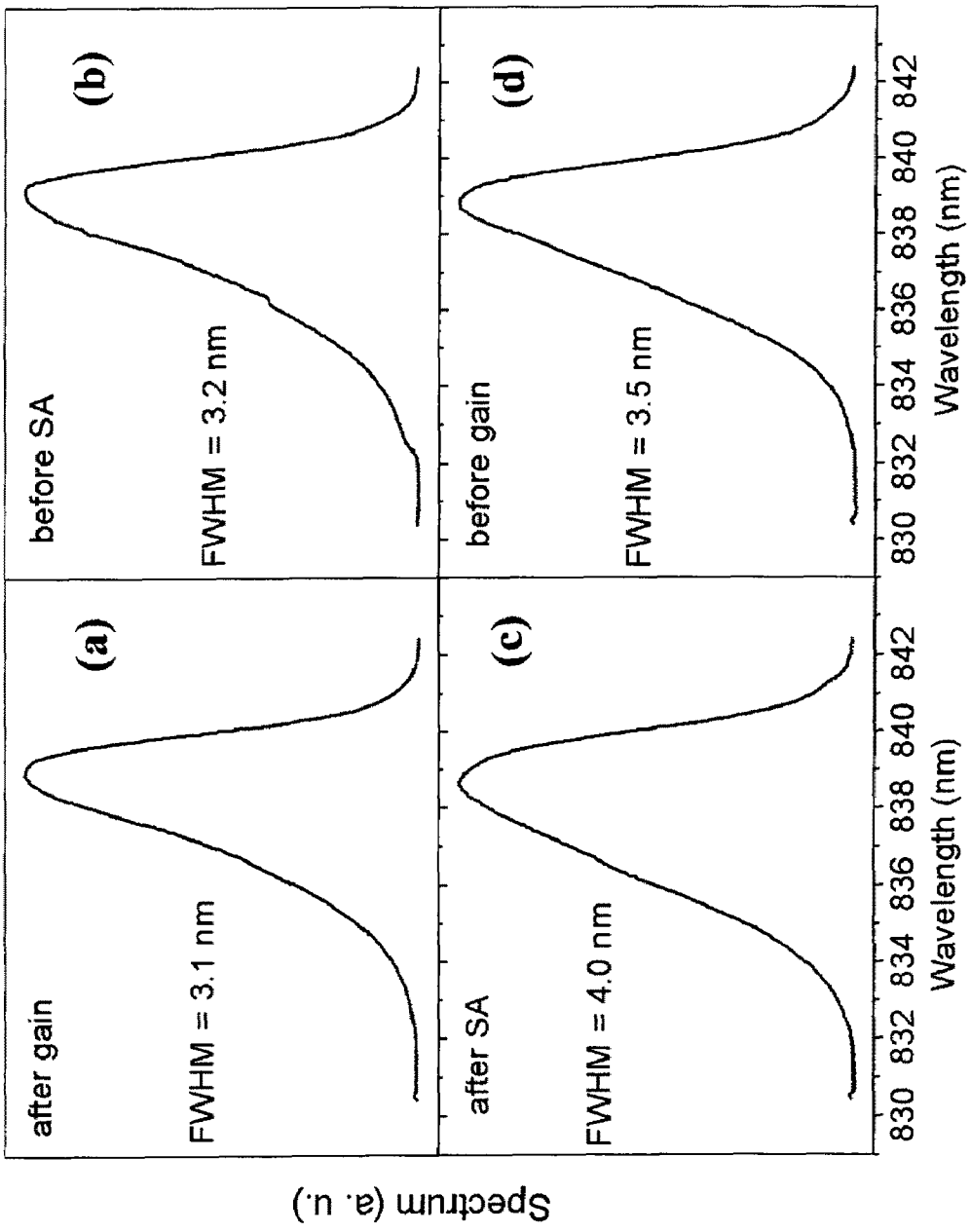
(a)
after gain
FWHM = 3.1 nm
(b)
before SA
FWHM = 3.2 nm
(c)
after SA
FWHM = 4.0 nm
(d)
before gain
FWHM = 3.5 nm
Spectrum (a. u.)
830 832 834 836 838 840 842
Wavelength (nm)
830 832 834 836 838 840 842
Wavelength (nm)

Figure 30

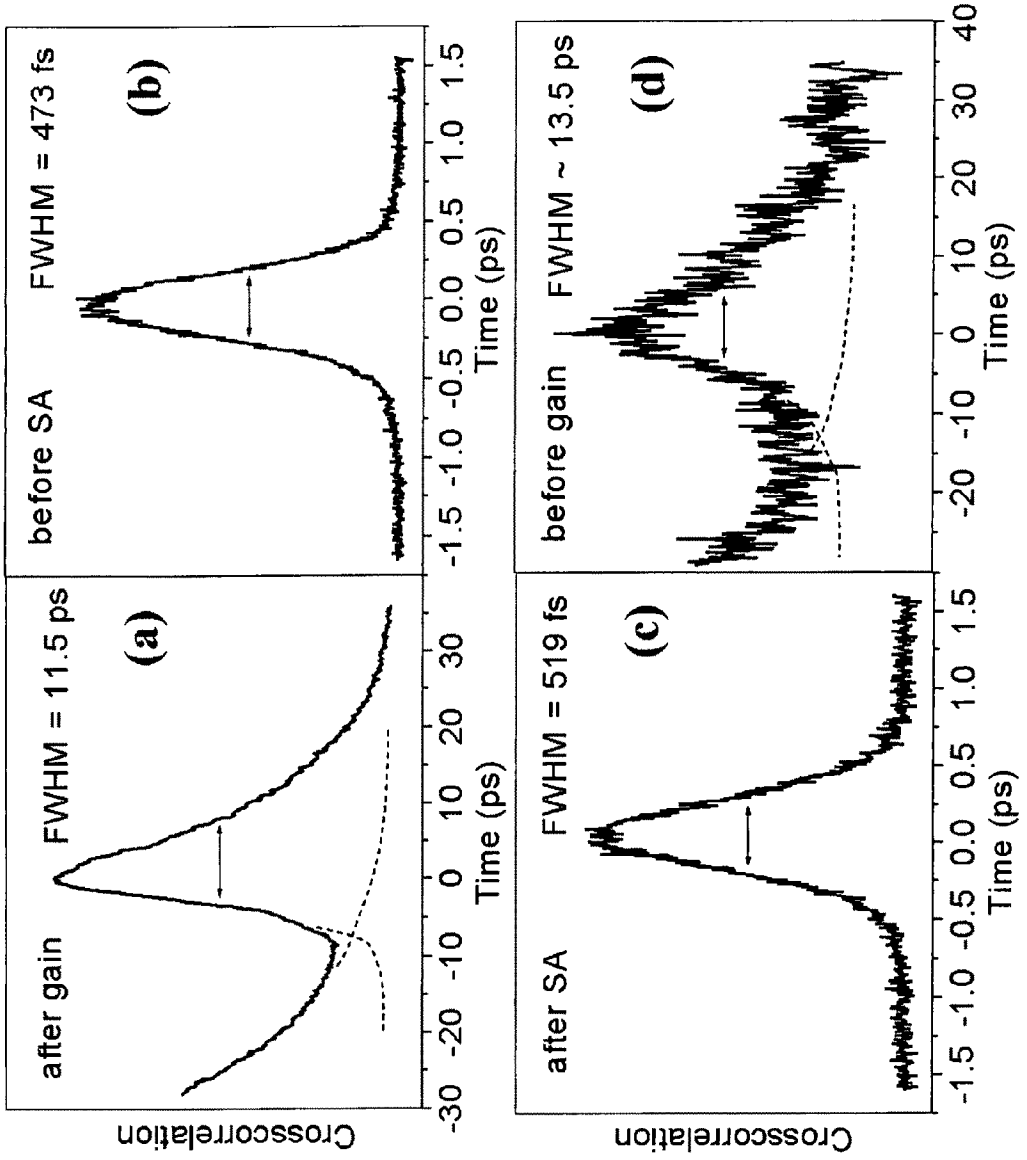
after gain
FWHM = 11.5 ps
(a)
before SA
FWHM = 473 fs
(b)
after SA
FWHM = 519 fs
(c)
before gain
FWHM ~ 13.5 ps
(d)
Crosscorrelation
Time (ps)
-30 -20 -10 0 10 20 30
-1.5 -1.0 -0.5 0.0 0.5 1.0 1.5
-40 -30 -20 -10 0 10 20 30 40

Figure 31

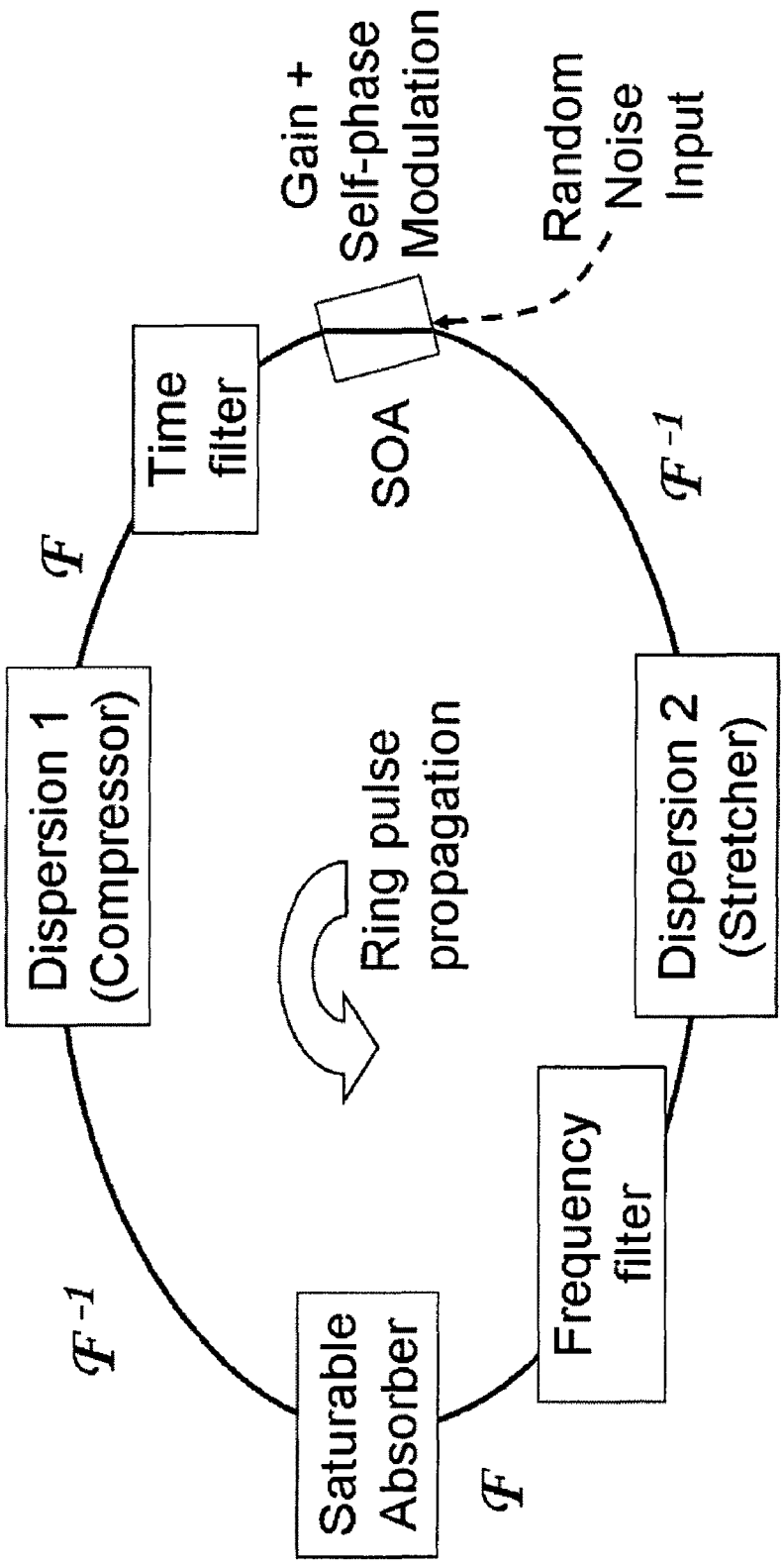
Gain + Self-phase Modulation
Random Noise Input
Time filter
SOA
$\mathcal{F}^{-1}$
$\mathcal{F}$
Dispersion 1 (Compressor)
Ring pulse propagation
Dispersion 2 (Stretcher)
Frequency filter
$\mathcal{F}^{-1}$
Saturable Absorber
$\mathcal{F}$

Figure 32

Quantity	Value
SOA small signal gain exponential coefficient	96 cm^{-1}
SOA saturation energy	20.14 pJ
SA unsaturated reflectivity	2.2 %
SA saturation energy	0.31 pJ
Integrating SPM coefficient	0.35 pJ^{-1}
Introduced GVD (by dispersion element 2)	4.1 ps/nm

Figure 33

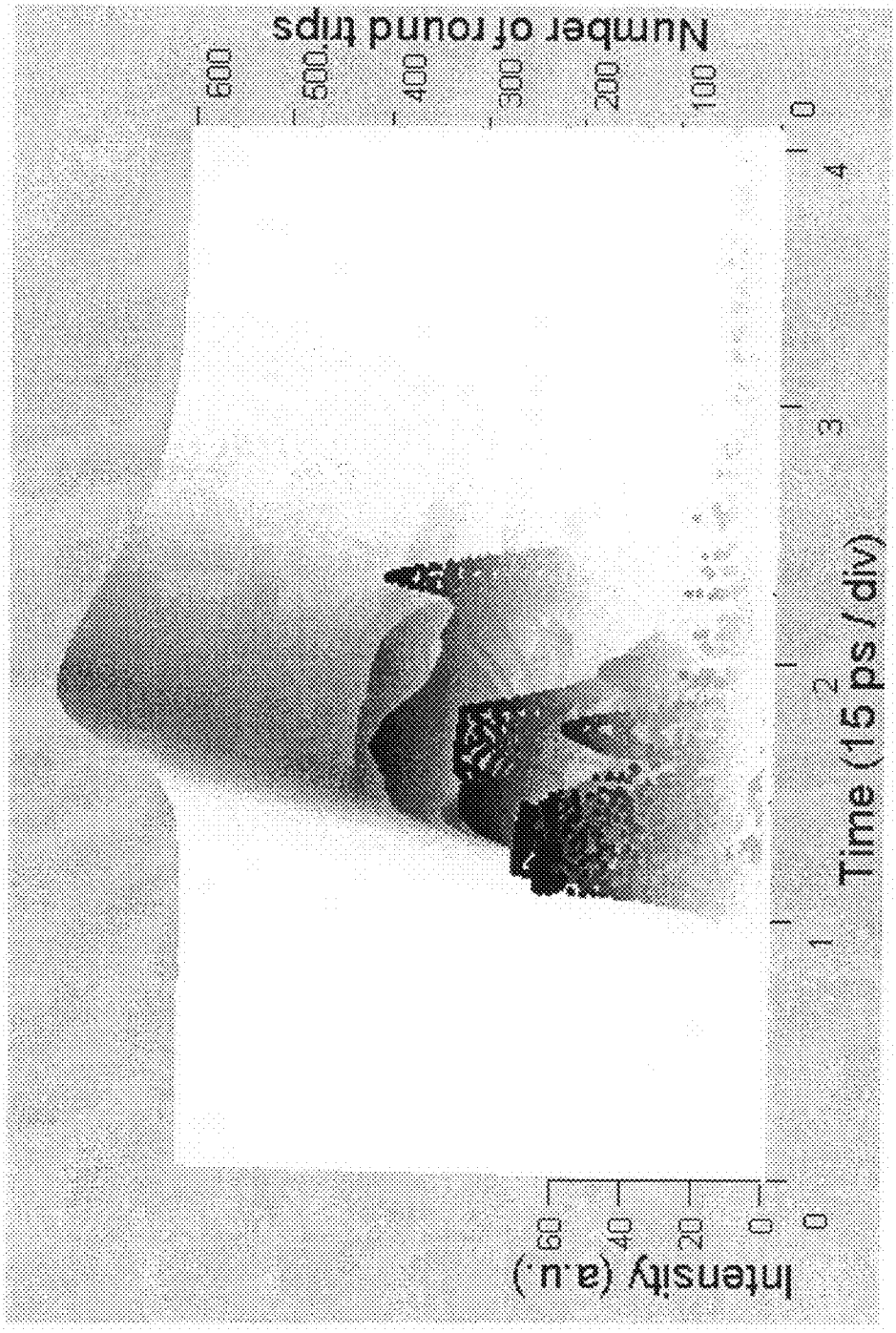
Intensity (a.u.)
0
20
40
60
Time (15 ps / div)
1
2
3
4
Number of round trips
0
100
200
300
400
500
600

Figure 34

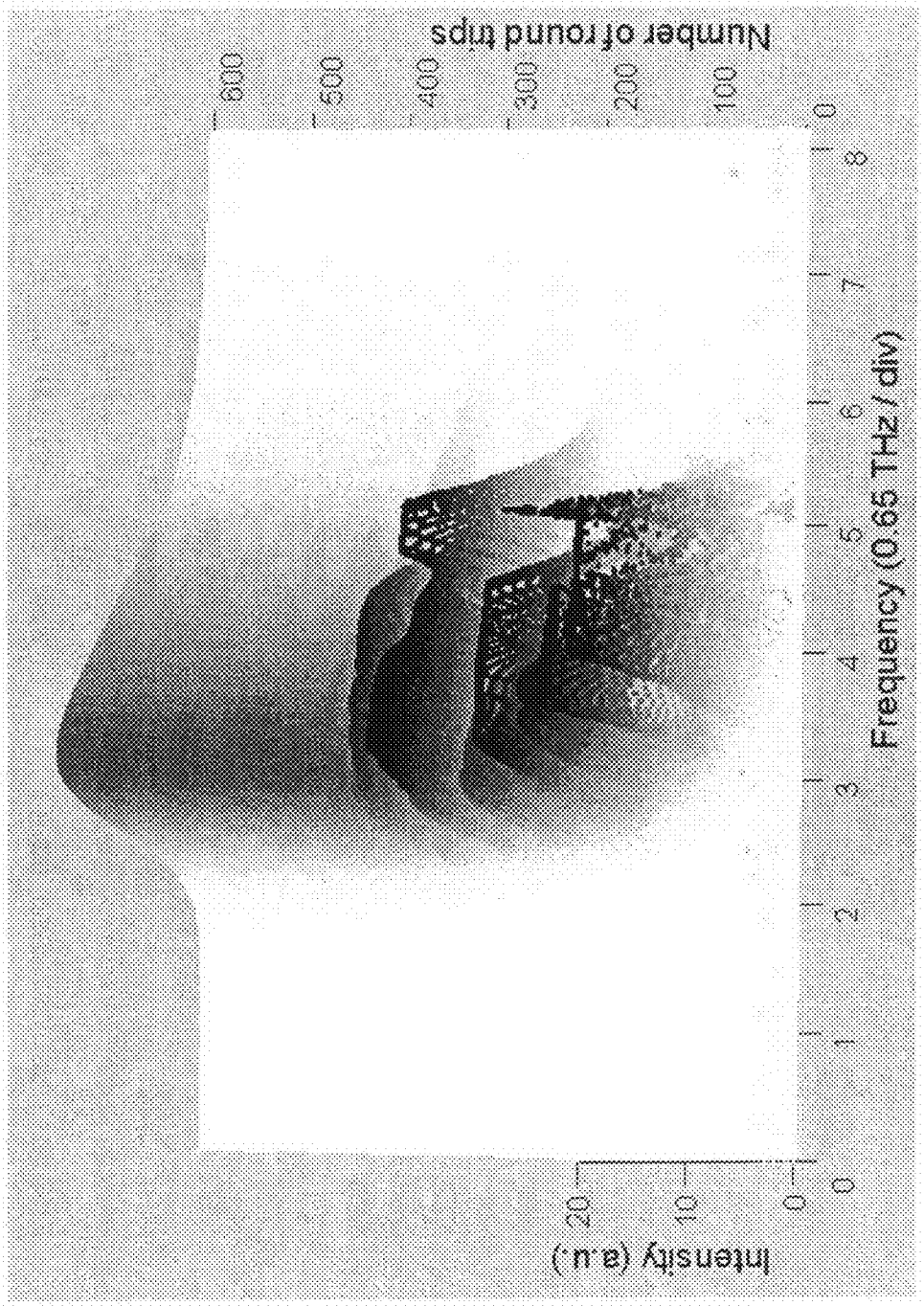
Number of round trips
600
500
400
300
200
100
0
Frequency (0.65 THz / div)
1
2
3
4
5
6
7
8
Intensity (a.u.)
20
10
0

Figure 35

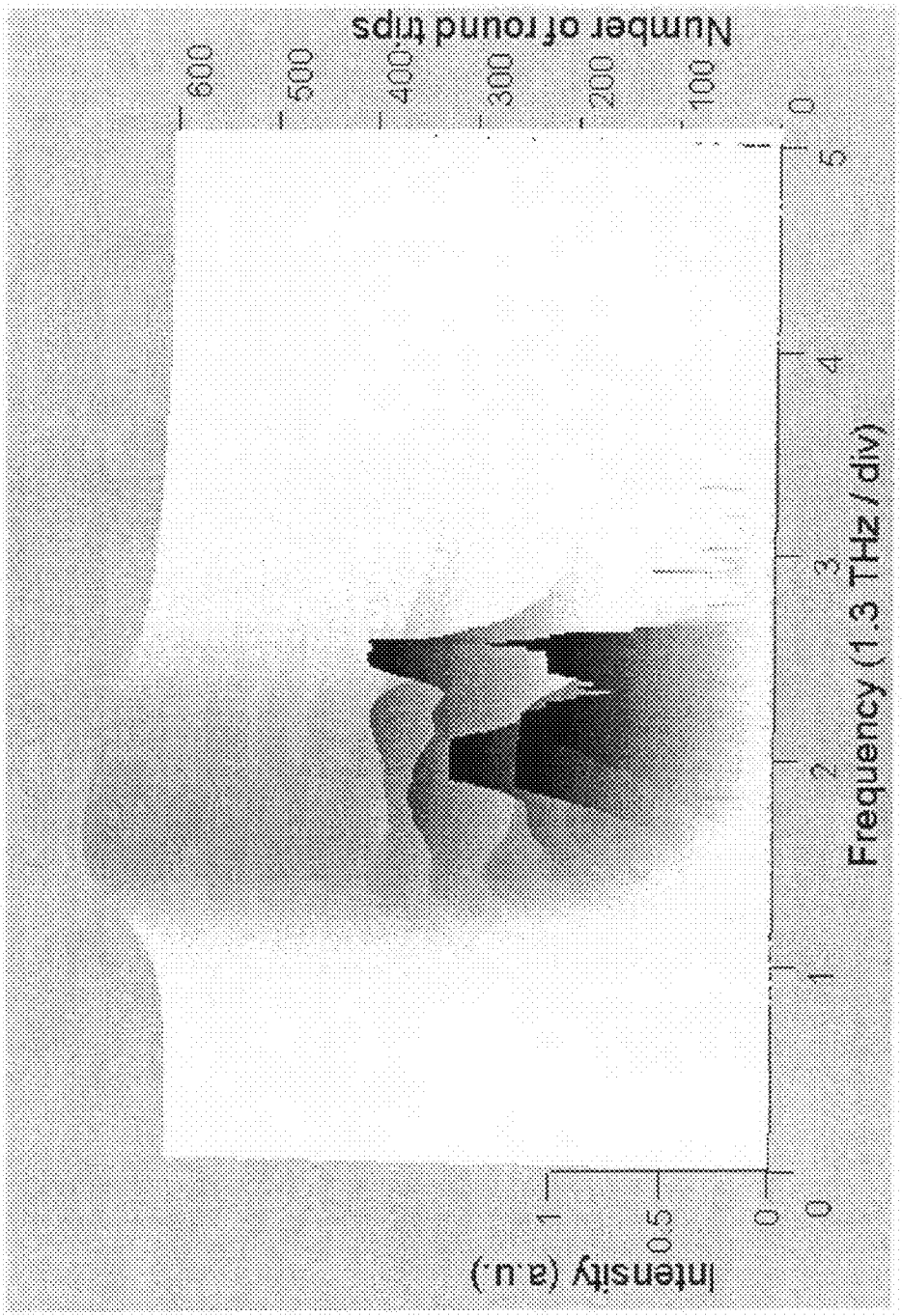
Intensity (a.u.)
0
0.5
1
Frequency (1.3 THz / div)
1
2
3
4
5
Number of round trips
0
100
200
300
400
500
600

Figure 36

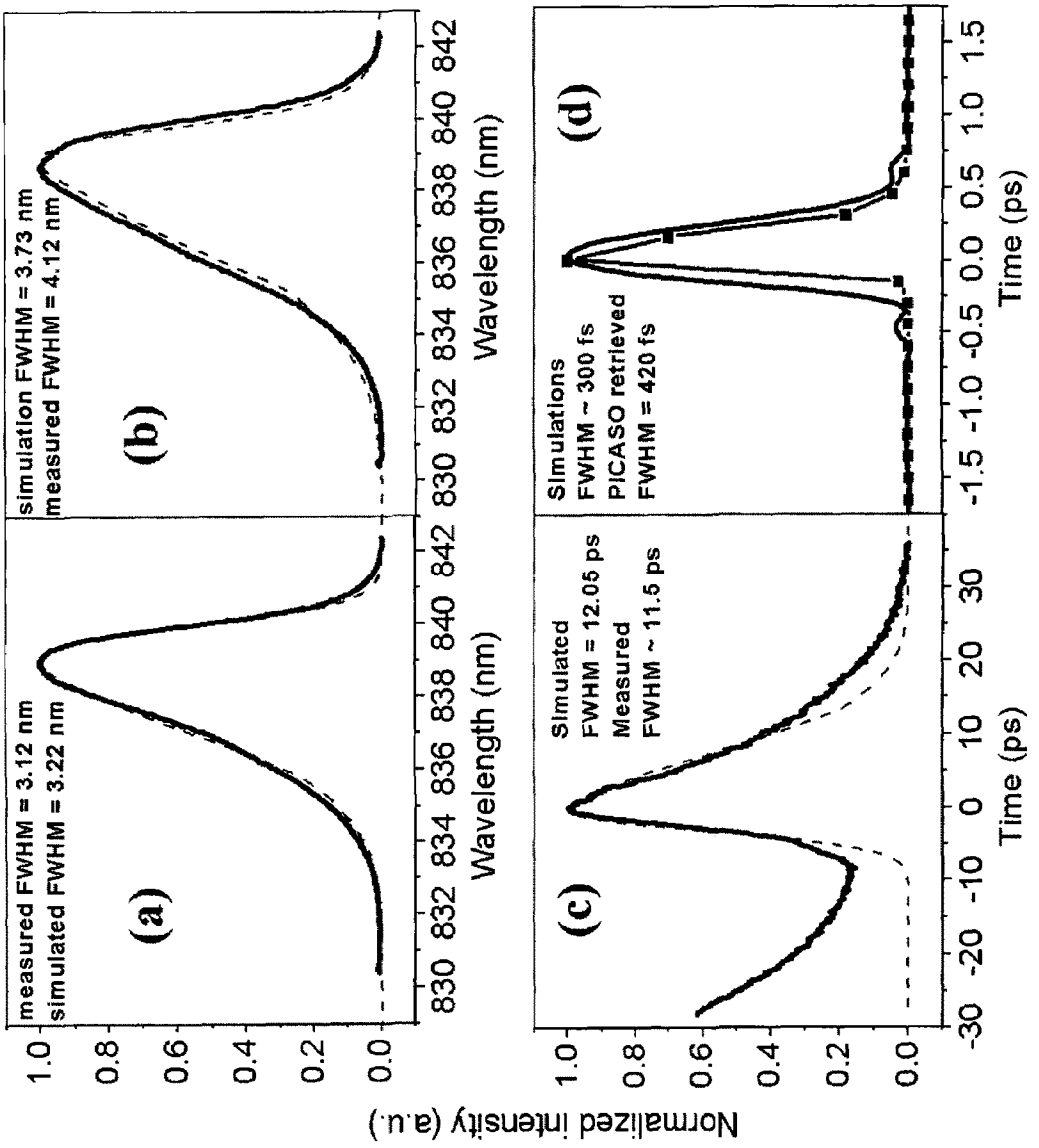
measured FWHM = 3.12 nm
simulated FWHM = 3.22 nm
(a)
simulation FWHM = 3.73 nm
measured FWHM = 4.12 nm
(b)
Simulated
FWHM = 12.05 ps
Measured
FWHM ~ 11.5 ps
(c)
Simulations
FWHM ~ 300 fs
PICASO retrieved
FWHM = 420 fs
(d)
Normalized intensity (a.u.)
Wavelength (nm)
Time (ps)

Figure 37

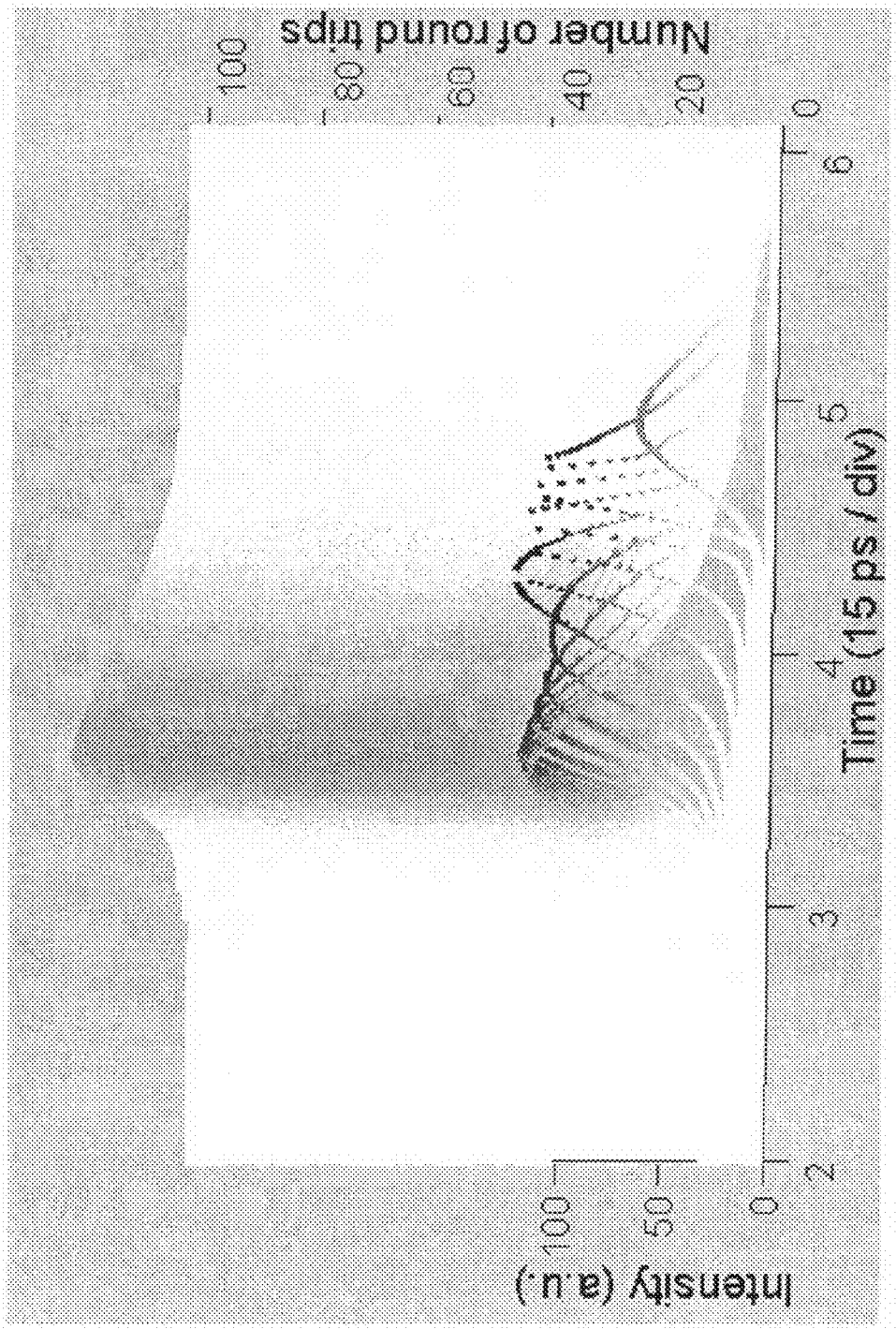
Number of round trips
100
80
60
40
20
0
Time (15 ps / div)
2
3
4
5
6
Intensity (a.u.)
100
50
0

Figure 38

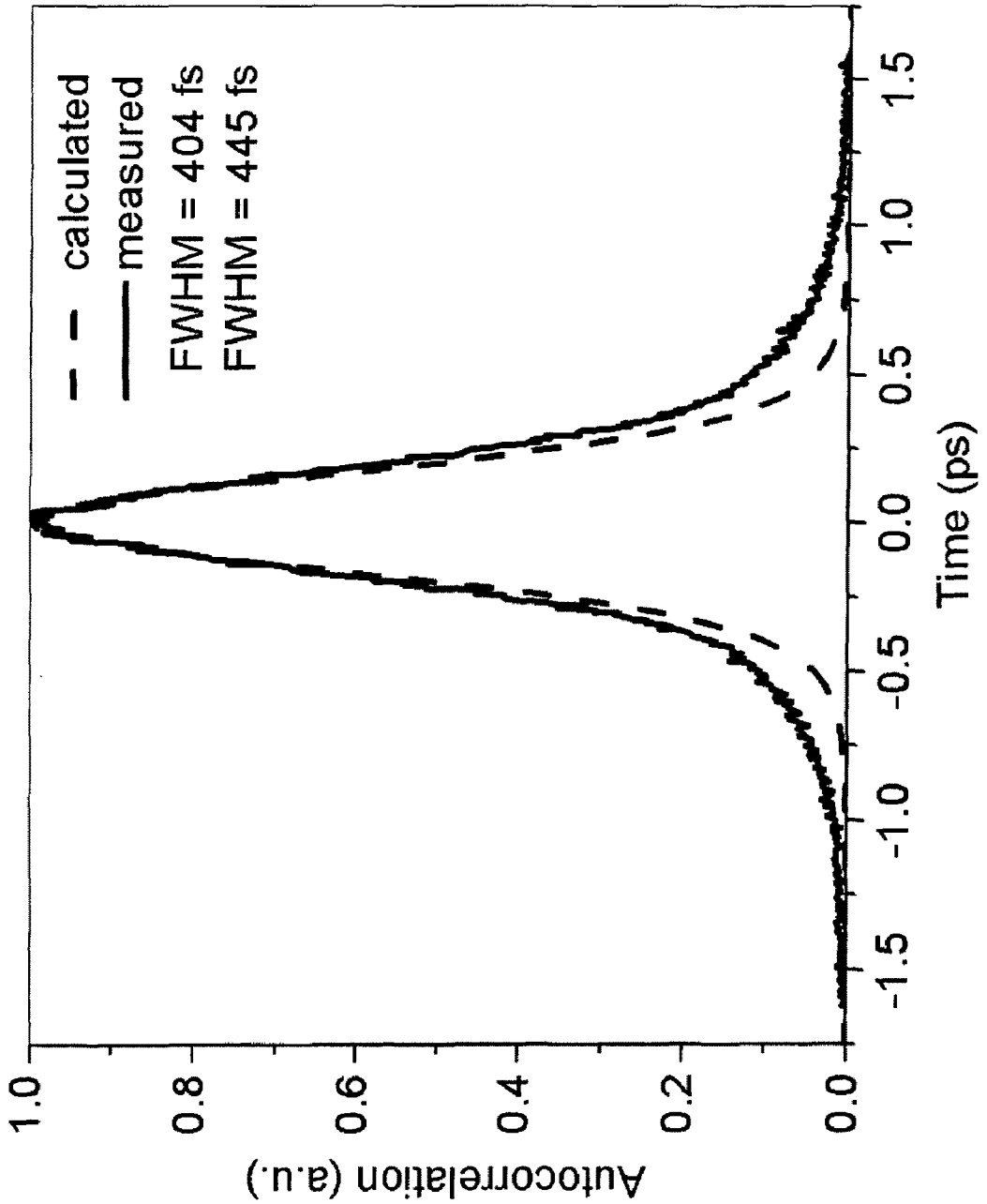
calculated
measured
FWHM = 404 fs
FWHM = 445 fs
Autocorrelation (a.u.)
Time (ps)
1.0
0.8
0.6
0.4
0.2
0.0
-1.5
-1.0
-0.5
0.0
0.5
1.0
1.5

Figure 39

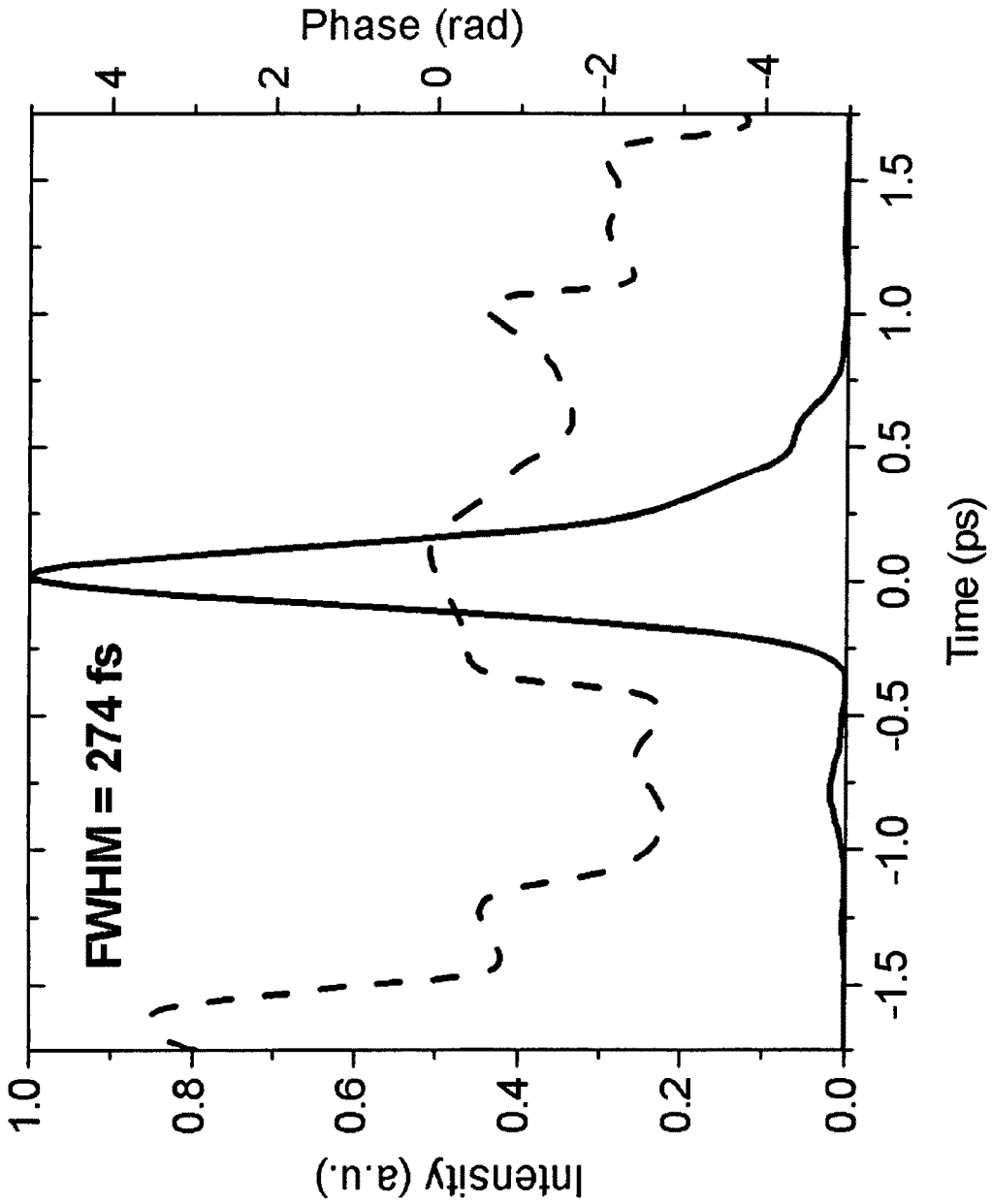
Phase (rad)
4
2
0
-2
-4
FWHM = 274 fs
Intensity (a.u.)
1.0
0.8
0.6
0.4
0.2
0.0
Time (ps)
-1.5
-1.0
-0.5
0.0
0.5
1.0
1.5

Figure 40

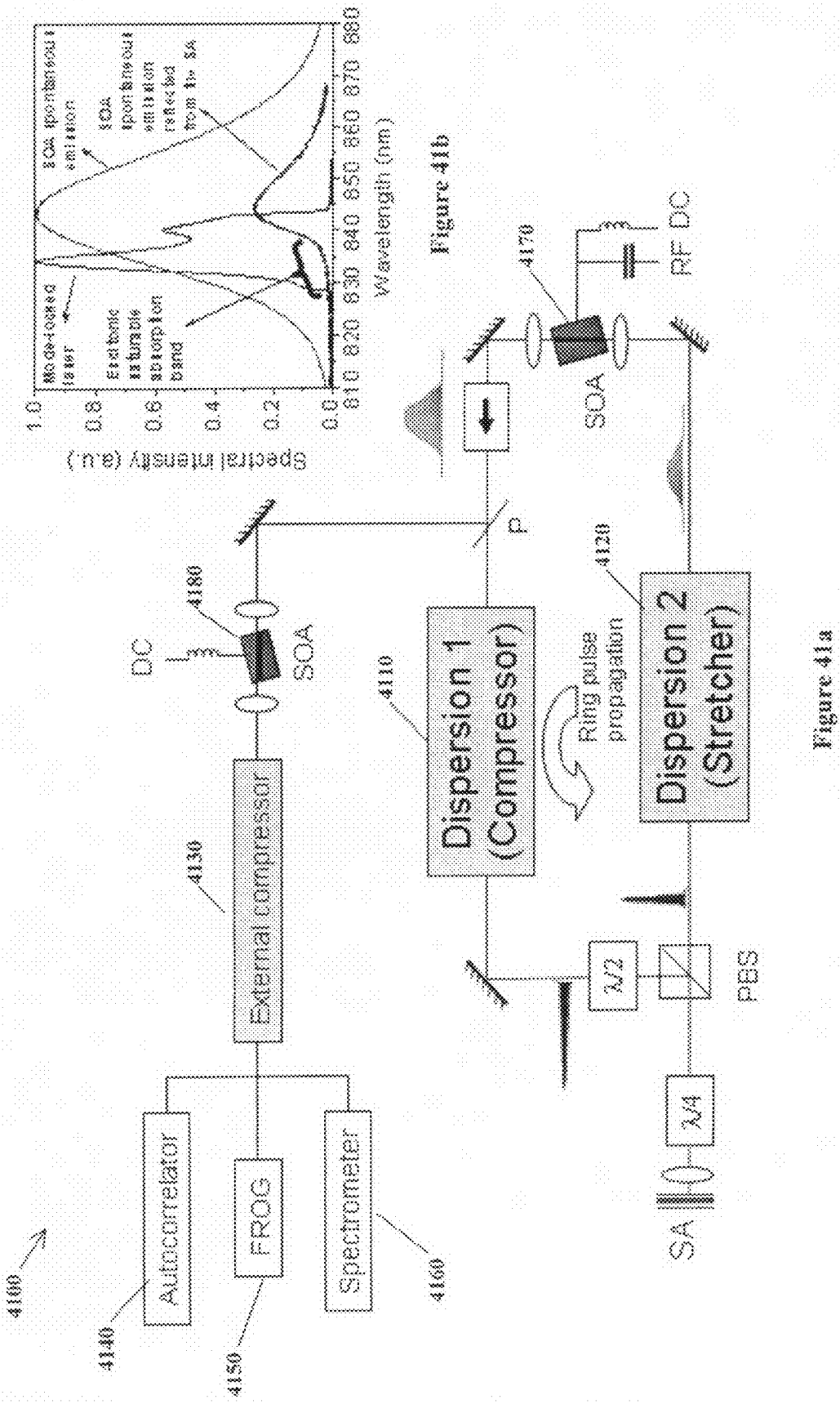

Figure 41a

Figure 41b

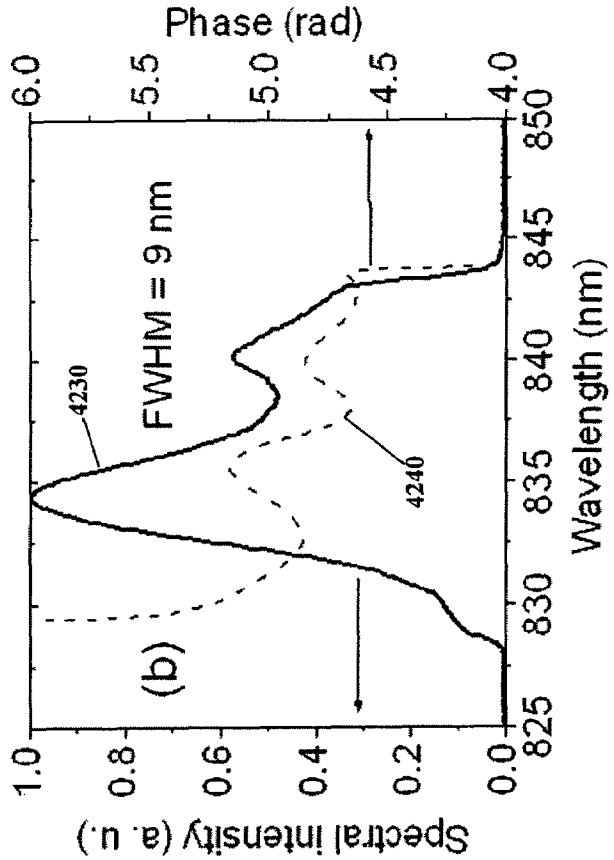

Figure 42b

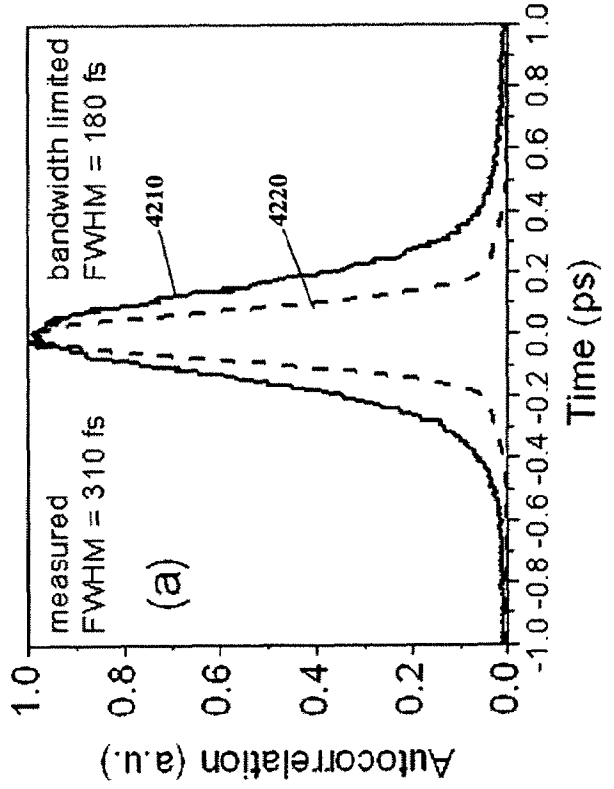

Figure 42a

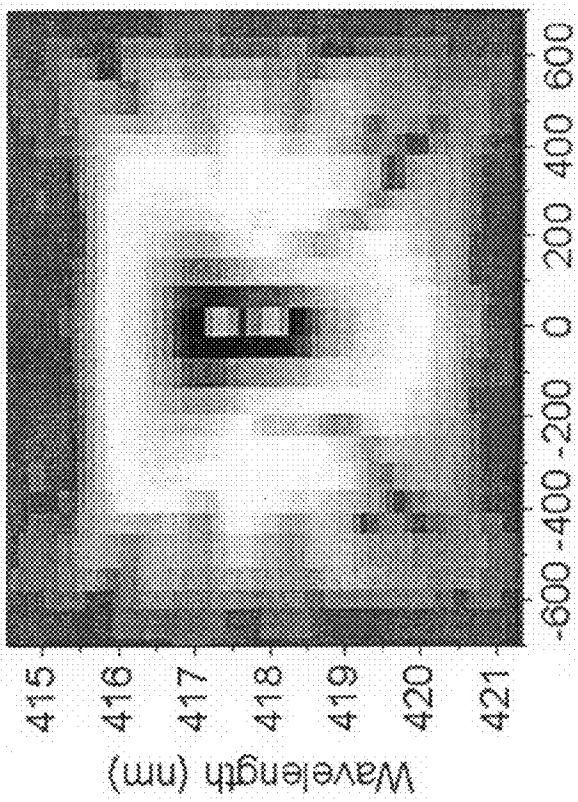

Figure 43b

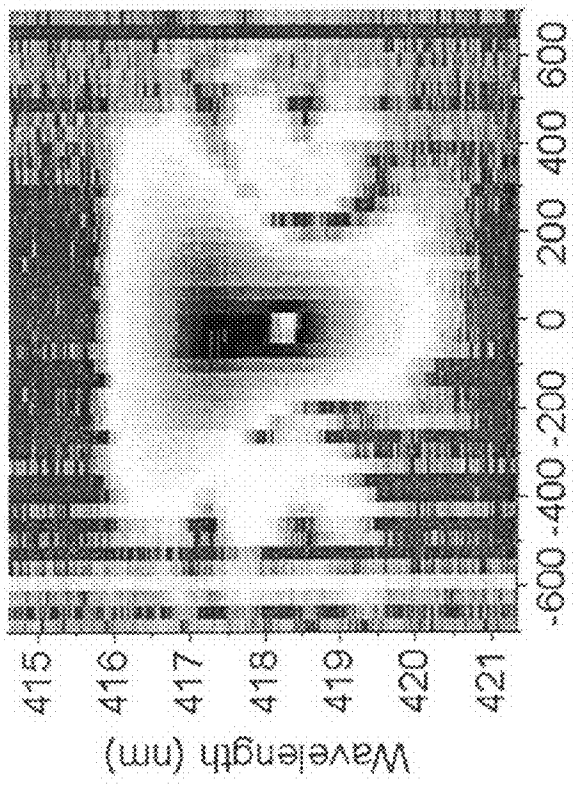

Figure 43a

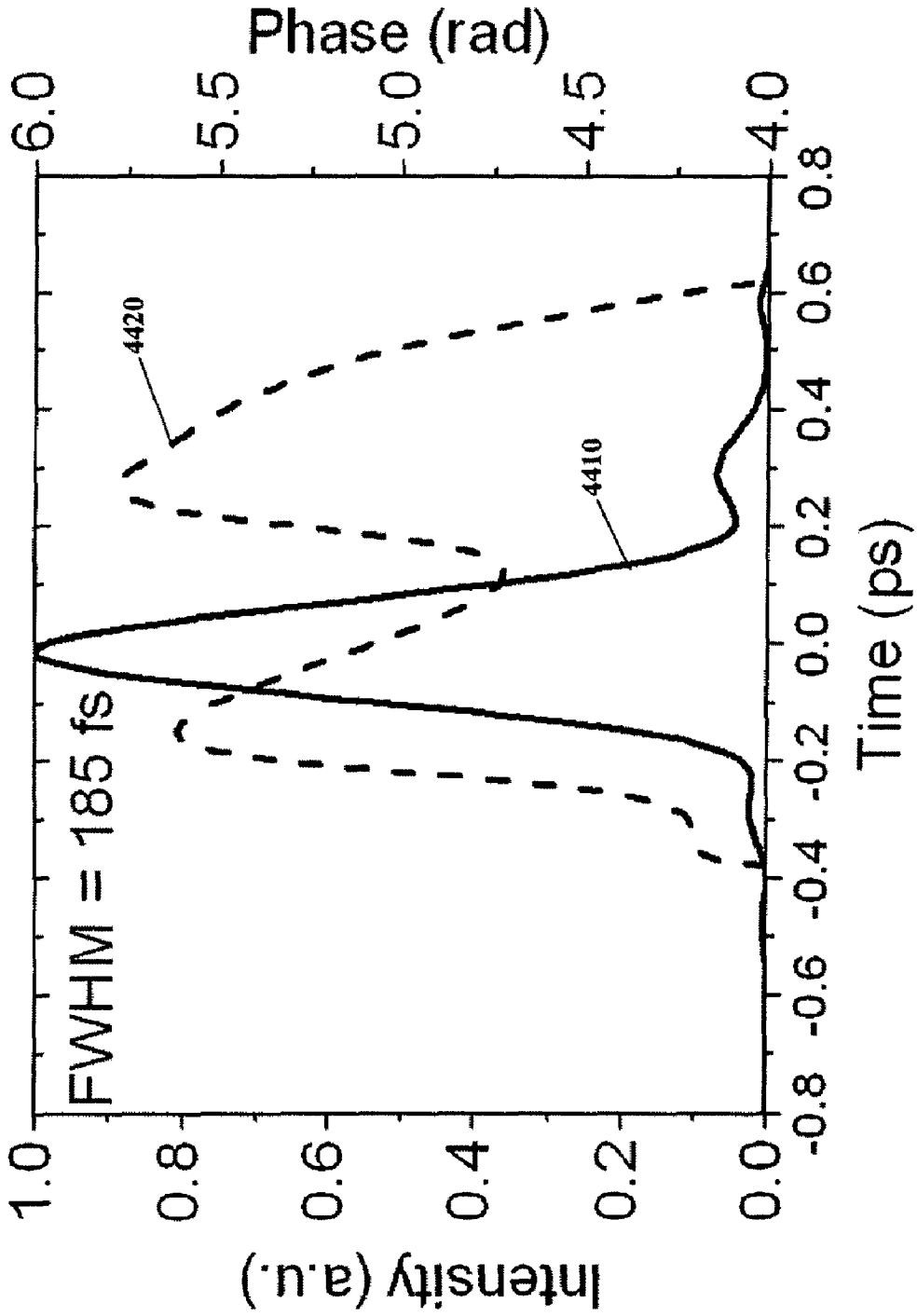
Phase (rad)
6.0
5.5
5.0
4.5
4.0
4420
4410
FWHM = 185 fs
Intensity (a.u.)
1.0
0.8
0.6
0.4
0.2
0.0
-0.8
-0.6
-0.4
-0.2
0.0
0.2
0.4
0.6
0.8
Time (ps)

Figure 44

EXTREME CHIRPED/STRETCHED PULSED AMPLIFICATION AND LASER

This is a Divisional of application Ser. No. 11/445,565 filed Jun. 2, 2006 which is a Divisional of application Ser. No. 10/828,965 filed Apr. 21, 2004, now U.S. Pat. No. 7,095,772 which claims priority of U.S. Provisional Application 60/472,383 filed May 21, 2003.

FIELD OF USE

This invention relates to lasers, in particular to methods, devices and systems for generating ultra-short optical pulses with very high power by stretching optical pulses to durations longer than the energy storage time of an optical amplifier, and for deployment of an extreme chirped pulse amplification (XCPA) effect in an laser oscillator and an external amplification.

BACKGROUND AND PRIOR ART

Semiconductor gain mediums have a short energy storage lifetime which makes energy extraction from the semiconductor gain medium less efficient compared with other gain mediums that have a longer energy storage lifetime. That is, a semiconductor optical amplifier is easily saturated and, after reaching the saturation regime, energy extraction from the semiconductor optical amplifier is dramatically decreased. It is well known that semiconductor optical amplifiers are not a proper optical amplifier for high power generation.

Previously, external cavity mode-locked semiconductor laser oscillators did not use dispersion management schemes that provide breathing mode operation. In non-breathing modes of operation, laser pulse time duration is similar at all cavity points. However, the preferable pulse duration, prior to a saturable absorber, is much shorter than pulse duration passing through the semiconductor gain media. Short pulses below ~1 ps. bleach the saturable absorber much easier, but such short pulses would initiate different ultra-fast dynamic processes in gain media which are detrimental for the laser operation—the gain would be decreased and the pulse would be strongly nonlinearly chirped. The nonlinear chirp is very difficult to compensate and generate in the end ultrashort pulses

SUMMARY OF THE INVENTION

A primary objective of the present invention is to provide methods, devices and systems for generating stretched, linearly chirped optical pulses with high power from the all-semiconductor laser oscillator that could be efficiently externally compressed to approximately 200 fs. This is achieved in the breathing mode operation of laser oscillator by stretching time duration of the pulses passing the gain media, to suppress self-phase modulation, and compressing it subsequently prior to the saturable absorber.

A secondary objective of the present invention is to provide methods, devices and systems for generating ultra-short optical pulses with very high power by increasing the temporal duration of the pulses passing the gain medium to be longer than the storage time of amplifying medium. If the time duration of the optical pulse is longer than the energy storage lifetime, then the energy extraction from semiconductor gain medium is not limited by the energy storage lifetime of the semiconductor optical amplifier but by continuous saturation power multiplied by the time duration of optical pulse. This is done by an extreme chirped pulse amplification technique using chirped fiber Bragg grating.

A third objective of the present invention is to provide methods, devices, and systems to deploy an extreme chirped pulse amplification (XCPA) effect in an laser oscillator and to generate extremely linearly chirped high-power pulses externally compressible to approximately 200 fs.

Preferred embodiment methods and systems of generating ultrashort optical pulses having increased optical power can include generating optical pulses from a source, such as a modelocked laser source, stretching duration of each of the optical pulses to be greater than energy storage time of an optical amplifier, amplifying the stretched optical pulse with the optical amplifier, and compressing the optical pulse, wherein optical power of the compressed optical pulse can be increased at least approximately 100 times.

The optical pulses can be linear chirped pulses. The mode locked laser source can be a gain-flattened mode-locked laser source, and the optical amplifier can be a semiconductor optical amplifier, such as a grating coupled surface emitting optical amplifier.

Preferred embodiments of an extreme chirped pulse amplifier (XCPA), can include methods, systems and devices for generating optical pulses, stretching temporal duration of the optical pulses to be greater than storage time of an amplifying medium, amplifying the stretched optical pulses, and compressing the stretched optical pulse, wherein higher power optical pulses are generated.

Additional preferred embodiment methods and systems of generating ultrashort optical pulses having increased optical power can include generating optical pulses with high optical energy and a linear chirp, stretching the duration of each optical pulse to be greater than the energy storage time of an optical amplifier, amplifying the stretched optical pulse with said optical amplifier, compressing the optical pulse, wherein the optical power of compressed optical pulse is increased.

The embodiments can include modulating the optical pulse whereby the optical pulse is further shortened, by using an active modulator such as a LiNbO3 modulator. Modulating can also include a passive modulator such as a multiple quantum well saturable absorber.

The embodiments can further rout the compressed optical pulse back to the generating step, and output coupling the compressed optical pulse by an fiber coupler.

Additional preferred embodiments of an extreme chirped pulse amplifier (XCPA) laser can include methods, systems and devices for generating optical pulses, stretching temporal duration of the optical pulses to be greater than storage time of an amplifying medium, compressing the stretched optical pulses and amplifying the compressed optical pulses, wherein higher power optical pulses are generated.

The optical pulses can be generated by a gain-flattened mode-locked laser source. Stretching can include a chirped fiber Bragg grating. Compressing can include a dual pass grating compressor.

The embodiments can include modulating the optical pulse wherein the pulse is further shortened, by using an active modulator such as a LiNbO3 modulator. The modulating can also include a passive modulator such as a multiple quantum well saturable absorber.

The optical pulses can be generated by a gain-flattened mode locked laser source, and the stretching and compressing can include a chirped fiber Bragg grating.

Further objects and advantages of this invention will be apparent from the following detailed description of the pres-

ently preferred embodiments which are illustrated schematically in the accompanying drawings.

BRIEF DESCRIPTION OF THE FIGURES

FIG. **1***a* shows a setup of a preferred embodiment of the extreme chirped pulsed amplifier invention.

FIG. **1***b* shows a detail of the optical circulator with arrows indicating the direction of optical pulse travel.

FIG. **2** is a chart showing the components used for extreme chirped pulse amplification (XCPA) and the advantage of each for the setup of FIG. **1***a*.

FIG. **3** is a preferred embodiment of the gain-flattened mode-locked laser (GFMLL) oscillator.

FIG. **4***a* shows the optical spectrum bandwidth of the GFMLL embodiment of FIG. **3** operating in active mode-lock at approximately a 200 MHz repetition rate.

FIG. **4***b* shows the mode-locked output pulse shape in time domain as measured by a fast photo-detector and digital sampling oscilloscope for FIG. **3**.

FIG. **5***a* shows the optical spectrum bandwidth of the GFMLL embodiment operating with a bandwidth from approximately 970 nm to approximately 980 nm.

FIG. **5***b* shows the corresponding mode-locked output pulse shape in time domain as measured by a fast photo-detector and digital sampling oscilloscope.

FIG. **6***a* shows the reflection bandwidth for a pair of chirped fiber Bragg grating (CFBG) used for stretching/compression of the optical pulse.

FIG. **6***b* shows the group delay for a pair of chirped fiber Bragg grating (CFBG) used for stretching/compression of the optical pulse.

FIG. **7***a* shows the reflected optical spectrum of the stretched optical pulse after the CFBG that has the positive dispersion **640** as shown in FIG. **6***b*.

FIG. **7***b* shows the streak camera image of the stretched pulse after the CFBG that has the positive dispersion **640** as shown in FIG. **6***b*.

FIG. **7***c* shows the reflected optical spectrum of the recompressed pulse after the CFBG that has the negative dispersion **630** as shown in FIG. **6***b*.

FIG. **7***d* shows the streak camera image of the recompressed pulse after the CFBG that has the negative dispersion **630** as shown in FIG. **6***b*.

FIG. **8***a* shows the streak camera image of the output optical pulse train of the GFMLL oscillator.

FIG. **8***b* shows the streak camera image of the stretched optical pulse.

FIG. **8***c* shows the streak camera image of the compressed optical pulse.

FIG. **9** shows the normalized optical power spectra at three different points in the extreme chirped pulsed amplifier (X-CPA) invention.

FIG. **10** shows a schematic representation of the GFMLL followed by the preamplifier and pulse picker stage.

FIG. **11***a* shows the digital sampling oscilloscope image of mode-locked output pulse train of the GFMLL oscillator that operates at 200 MHz.

FIG. **11***b* shows the streak camera image of stretched optical pulse train from the GFMLL oscillator.

FIG. **12***a* shows the digital sampling oscilloscope image of the mode-locked output pulse after the preamplifier and pulse picker stage in the time domain.

FIG. **12***b* shows the streak camera image of the output pulse after the preamplifier and pulse picker stage.

FIG. **13** is a schematic representation of the experimental setup to verify the concept of the X-CPA invention using a GFMLL oscillator, optical isolator, and amplifier.

FIG. **14** is a schematic representation of the experimental setup to verify the concept of the X-CPA invention using a GFMLL oscillator, optical isolator, preamplifier, optical isolator, fiber loop as a pulse stretcher, and amplifier.

FIG. **15***a* shows the optical power spectrum results of the GFMLL used as oscillator in the experimental setup of FIG. **14**.

FIG. **15***b* shows the digital sampling oscilloscope image of GFMLL used as oscillator in the experimental setup of FIGS. **13** and **14**.

FIG. **15***c* shows the streak camera image of the optical pulse before pulse stretching.

FIG. **15***d* shows the stream camera image of the optical pulse after pulse stretching using a fiber spool **1445** in FIG. **14**.

FIG. **16***a* shows output power vs. input power for an unstretched pulse.

FIG. **16***b* shows gain vs. output power for an unstretched pulse.

FIG. **17***a* shows output power vs. input power for a stretched pulse of approximately 3 ns. in time duration.

FIG. **17***b* shows gain vs. output power for a stretched pulse of approximately 3 ns. in time duration.

FIG. **18***a* is another schematic representation of the experimental setup to verify the concept of the X-CPA invention.

FIG. **18***b* shows the chart system parameters and throughputs of the schematic representation of FIG. **18***a*.

FIG. **19***a* shows the 100 ns. 10 kHz electrical pulse at the output of the second amplifier **1850**.

FIG. **19***b* shows the signals at the output of the 2nd amplifier, at the output of 2nd plus 1st amplifiers, and at the output of the amplified signal through 2nd and 1st amplifiers amplifier.

FIG. **19***c* shows the average power vs. peak current for the second amplifier.

FIG. **20***a* is a schematic representation of another embodiment of experimental setup to verify the concept of the X-CPA invention.

FIG. **20***b* is a chart showing the system parameters and throughputs of the schematic representation of FIG. **20***a*.

FIG. **20***c* shows the optical spectrum of the amplified signal and the ASE (Amplified Spontaneous Emission) noise of the schematic representation of FIG. **20***a*.

FIG. **21** is a simulation sequence flow chart for the preferred embodiment of the invention.

FIG. **22***a* shows the simulation results of a 1 nm transform limited (TL'd) pulse without pulse stretching, with 87.5 ps/nm/km CFBG and with 2000 ps/nm/km CFBG.

FIG. **22***b* shows the simulation results of a 5 nm transform limited (TL'd) pulse without pulse stretching, with 87.5 ps/nm/km CFBG and with 2000 ps/nm/km CFBG.

FIG. **23** shows a "Breathing Mode" Mode locked laser (MLL) embodiment with a modulator. The modulator used in FIG. **23** can be a multiple quantum well saturable absorber or a LiNbO3 modulator.

FIG. **24***a* shows an experimental set-up for dispersion managed semiconductor mode-locked σ-ring cavity laser.

FIG. **24***b* shows the experimental set-up for diagnostics measurement of spectra and autocorrelation.

FIG. **24***c* shows the set-up for the dispersion elements and external compressor.

FIG. **25** shows the spectral changes in the laser output after the SA when element **1** introduced dispersion is varied and element **2** introduced dispersion is constant.

FIG. **26** shows pulse second harmonic autocorrelation vs. introduced dispersions of the experimental set-up of FIG. **24***a*.

FIG. **27** shows pulse spectrum vs. introduced dispersions by element **1** and element **2** of the experimental set-up of FIG. **24***a*.

FIG. **28** shows the externally compressed autocorrelation and spectral FWHM vs. element **2** introduced dispersions.

FIG. **29***a* shows the experimental set-up of the hybridly mode-locked σ-cavity semiconductor laser with four outputs for pulse evolution characterization.

FIG. **29***b* shows the experimental set-up for diagnostics measurement of spectra and autocorrelation.

FIGS. **30***a*, **30***b*, **30***c*, **30***d* shows the optical spectra of the experimental set-up of FIG. **29***a*.

FIGS. **31***a*, **31***b*, **31***c*, **31***d* shows the cross-correlation traces from the experimental set-up of FIG. **29***a*.

FIG. **32** is a flow diagram representing the algorithm for dispersion-managed mode-locked ring laser simulations.

FIG. **33** is a table of the constants used in the simulations.

FIG. **34** shows the formation of the stretched pulse after the gain media from random noise input.

FIG. **35** shows the mode-locked spectrum build-up after the cavity gain element.

FIG. **36** shows the mode-locked spectrum build-up after the saturable absorber.

FIG. **37***a* shows the comparison of simulated and measured stretched pulse spectrum after the gain.

FIG. **37***b* shows the comparison of simulated and measured compressed pulse spectrum after the saturable absorber.

FIG. **37***c* shows the comparison of simulated and measured stretched pulse temporal intensity after the gain.

FIG. **37***d* shows the comparison of simulated and measured compressed pulse temporal intensity after the saturable absorber.

FIG. **38** shows the locking-up of stretched pulses after the gain media to the external-cavity injected Gaussian pulses.

FIG. **39** shows the comparison of the bandwidth-limited calculated and the measured autocorrelations of the externally compressed pulses after the gain media.

FIG. **40** shows the PICASO retrieved temporal intensity and phase of the externally compressed pulses after the gain media.

FIG. **41***a* shows an experimental setup of dispersion-managed breathing-mode semiconductor mode-locked σ-ring cavity laser with diagnostics.

FIG. **41***b* shows the spectra of the SOA spontaneous emission, the SA excitonic absorption band, and the mode-locked laser.

FIG. **42***a* shows the comparison of measured and calculated bandwidth limited pulse autocorrelation.

FIG. **42***b* shows the measured pulse spectrum with SGH-FROG retrieved spectral phase.

FIG. **43***a* shows the SHG-FROG experimentally measured trace.

FIG. **43***b* shows the SHG-FROG retrieved trace.

FIG. **44** shows the SHG-FROG retrieved pulse temporal intensity.

DESCRIPTION OF THE PREFERRED EMBODIMENTS

Before explaining the disclosed embodiments of the present invention in detail it is to be understood that the invention is not limited in its application to the details of the particular arrangements shown since the invention is capable of other embodiments. Also, the terminology used herein is for the purpose of description and not of limitation.

FIG. **1***a* shows a setup of a preferred embodiment of the extreme chirped pulsed amplifier (X-CPA) invention, **100**. Mode-locked laser **110** with semiconductor gain medium is used as an oscillator. The repetition rate of the oscillator is adjustable. Optical isolator (OI) **120**, **140** allows the optical pulse to travel in the direction of the arrow and blocks the optical pulse in the reverse direction. Preamplifier **130** is a semiconductor optical amplifier that (a) compensates for losses from the first optical isolator **120**, the optical circulator **150**, and the chirped Bragg grating **160**; (b) develops more power to saturate the amplifier **170**; and (c) adjusts the optical pulse repetition rate. Optical circulator (OCIR) **150**, **180** is a component that transmits an incoming pulse from port **1** to port **2** while transmitting a second incoming pulse from port **2** to port **3** as illustrated by the arrows in FIG. **1***b*. The first chirped fiber Bragg grating (CFBG) **160** is used to stretch the optical pulse and the second chirped fiber Bragg grating (CFBG) **190** is used to compress the optical pulse. Amplifier **170** is a semiconductor optical amplifier for high power generation.

By stretching the time duration of the optical pulse duration such that it is longer that the energy storage lifetime of the semiconductor gain medium, the energy extraction from the semiconductor gain medium is not limited by the energy storage lifetime of semiconductor optical amplifier but by continuous saturation power multiplied by the time duration of optical pulse. In the preferred embodiment, chirped fiber Bragg grating **160**, **190** provides dispersion of approximately 2000 ps/nm so that an approximate 8 nm pulse was stretched to approximately 16 ns. The recombination lifetime (energy storage lifetime) of the semiconductor gain medium of amplifier **170** can be less than approximately 1 ns.

FIG. **2** is a chart showing the preferred components used for chirped pulse amplification and the advantages as to their use for the setup of FIG. **1***a*.

GFMLL Oscillator

FIG. **3** is a preferred embodiment of the oscillator **300** for the X-CPA invention **100**. The oscillator is a gain-flattened mode-locked laser (GFMLL) where characteristics are such that (1) amplitude, phase, and optical spectrum bandwidth can be manipulated using a Fourier plane inside the cavity and (2) active, passive, and hybrid mode-locking techniques are possible.

The oscillator is comprised of the first high reflector (HR) **305** and second high reflector **330** that are mirrors that exhibit high reflectance at the operating wavelength of the oscillator. The band pass filter (BPF) **310** allows the optical spectrum bandwidth of the oscillator output to be changed. The gain flattening filter (GFF) **315** allows the amplitude of the optical spectrum to be modified. The first lens **320** and the diffraction grating (DG) **325** form the Fourier plane inside the cavity of oscillator **300**. The second lens **335** and the third lens **345** collimate the beam to and from the semiconductor optical amplifier (SOA) **340**. The aperture **350** provides for selection of the spatial beam profile. The output coupler **360** couples the mode-locked pulse train out from the oscillator. The fourth lens **355** and the fifth lens **365** provide for stabilization of the cavity.

FIG. **4***a* shows the optical spectrum bandwidth of the GFMLL oscillator **300** of FIG. **3** operating in active mode-lock at an approximately 200 MHz repetition rate. Optical bandwidth is approximately 11.4 nm in the range from approximately 961.8 to approximately 973.2 nm. FIG. **4***b* shows the mode-locked output pulse shape of the GFMLL

oscillator **300** in the time domain as measured by a fast photo-detector and a digital sampling oscilloscope.

FIG. **5***a* shows the bandwidth of the GFMLL oscillator **300** of FIG. **3** with the Fourier plane manipulated to produce optical characteristics different from that of the prior example. The optical bandwidth is adjusted to approximately 7.8 nm in the range from approximately 971.1 to approximately 978.9 nm with the optical power spectrum equalized to an average power of approximately 15.2 mW. Energy per pulse was approximately 45 pJ. The optical spectrum is adjusted to match the reflection bandwidth of the diffraction grating **325**. FIG. **5***b* shows the mode-locked output pulse shape of the GFMLL oscillator **300** in the time domain as measured by a fast photo-detector and a digital sampling oscilloscope. Pulse width is approximately 189 ps.

Active mode-locking for the GFMLL oscillator **300** is achieved by way of gain modulation. Spectrum modulation is achieved by way of the fourier plane inside the cavity. Homogeneous spectrum narrowing is prevented by using a gain flattening filter.

Stretcher and Compressor

FIGS. **6***a* and **6***b* show the reflectance spectrum of the chirped fiber Bragg grating (CFBG) **160**, **190** of FIG. **1** used for dispersion of the optical pulse. FIG. **6***a* shows the optical spectrum of the reflection **610** from the first chirped fiber Bragg grating **160** with a negative dispersion. FIG. **6***a* also shows the optical spectrum of the reflection **620** from the second chirped fiber Bragg grating **190** with a positive dispersion. The reflectance bandwidth for both the compressor CFBG **160** and the stretcher CFBG **190** is approximately 8 nm in the range from approximately 971 nm to approximately 978 nm and the spectrum exhibits a nice flat reflectance. FIG. **6***b* shows the group delays **630**, **640** of the two CFBG **160**, **190** used as a stretcher and a compressor to be approximately 2000 ps/nm each. This means an approximately 8 nm bandwidth optical pulse can be stretched to approximately 16 ns.

FIG. **7***a* shows the reflected optical spectrum for the stretcher CFBG **160** mapped onto the streak camera image FIG. **7***b* of the optical pulses from the stretcher CFBG **160**. FIG. **7***c* shows the reflected optical spectrum for the compressor CFBG **190** mapped onto the streak camera image FIG. **7***d* of the optical pulses for the compressor CFBG **190**. For both FIGS. **7***c* and **7***d*, the vertical axis of the streak camera image represents time and the horizontal axis of the streak camera image represents wavelength. In both images, each optical pulse has a bandwidth of approximately 8 nm and is stretched approximately 16 ns.

FIGS. **8***a* to **8***c* shows streak camera images of the optical pulse at three different points in the extreme chirped pulsed amplifier (X-CPA) invention, **100**. FIG. **8***a* shows the optical pulse train as output from the oscillator **110**, with an approximately 8 nm optical spectrum bandwidth and a pulse repetition rate of approximately 5 ns. FIG. **8***b* shows the optical pulse stretched to approximately 16 ns from the stretcher CBFG **160**. FIG. **8***c* shows the optical pulse compressed from the compressor CBFG **190**. For FIGS. **8***a* to **8***c*, the vertical axis of the streak camera image represents time and the horizontal axis of the streak camera image represents wavelength.

FIG. **9** shows the normalized optical power spectra at three different points in the extreme chirped pulsed amplifier (X-CPA) invention, **100**. The optical spectrum **910** is measured at the output of the preamplifier **130**, the optical spectrum **920** is measured at the output of the amplifier **170**, and the optical spectrum **930** is measured at the output of the compressor CBFG **190**. Optical power spectra are nearly flat in all instances.

Preamplifier and Pulse Selection

FIG. **10** shows a schematic representation of the Gain Flattened Mode-Locked Laser **300** followed by the preamplifier and pulse picker **1000**. The preamplifier/pulse picker stage is comprised of a first lens **1010**, a semiconductor optical amplifier (SOA) **1020**, and a second lens **1030**. Modulation **1050** of the SOA **1020** provides amplification and pulse selection of the optical pulse train **1040** from the GFMLL **300**.

FIG. **11***a* shows the mode-locked output pulse shape of the GFMLL oscillator **300** in the time domain as measured by a fast photo-detector and a digital sampling oscilloscope. The repetition rate of the oscillator is 200 MHz. FIG. **11***b* shows a streak camera image (20 ns time window) of the stretched pulse from the GFMLL oscillator **300**. FIG. **11***b* has been stretched in the vertical axis to show that optical pulses overlap so that there are approximately four pulses at the same moment as indicated by the horizontal line **1100**. Pulse overlap is indicative of inefficient energy sharing between pulses.

FIG. **12***a* shows the mode-locked output pulse shape after the preamplifier stage **1000** in the time domain as measured by a fast photo-detector and a digital sampling oscilloscope. The output pulse train **1060** of the preamplifier stage **1000** has been amplified and pulses selected so that the resulting frequency is 50 MHz. FIG. **12***b* shows a streak camera image (100 ns time window) of the stretched pulse from the preamplifier stage **1000**. Temporal pulse overlap has been eliminated by the pulse biased preamplifier stage **1000**.

Semiconductor Optical Amplifier

The semiconductor optical amplifier of the preamplifier stage **1000** and the amplifier **170** is an approximately 980 nm InGaAs Quantum Well structure that is an angled stripe inverse bow-tie gain guide amplifier. The angled stripe provides low reflectivity. The structure is a low loss that is good for high power generation and provides a good spatial mode profile. The amplifier provides large gain volume and adiabatic beam expansion.

The benefits of using an inverse bow-tie gain guided SOA as the optical gain element in a high-power external cavity semiconductor laser are further discussed in S. Gee et al., "High-Power Mode-Locked External Cavity Semiconductor Laser Using Inverse Bow-Tie Semiconductor Optical Amplifiers", *IEEE Journal of Selected Topics in Quantum Electronics*, Vol. 4, pp 209-215.

Concept Verification

FIGS. **13** and **14** are schematic representations of the experimental setup to verify the concept of the X-CPA invention using a semiconductor gain medium. FIG. **13** demonstrates the amount of gain saturation without pulse stretching and is comprised of GFMLL **1310**, optical isolator **1320**, and amplifier **1330**. Amplifier **1330** is further comprised of the first lens **1340**, the SOA **1350**, and the second lens **1360**.

FIG. **14** demonstrates the amount of gain saturation with pulse stretching and is comprised of GFMLL **1410**, first optical isolator **1415**, preamplifier **1420**, the second optical isolator **1440**, optical fiber as an optical pulse stretcher **1445**, and amplifier **1450**. The preamplifier **1420** is further comprised of the first lens **1425**, the first SOA **1430**, and the second lens **1435**. The amplifier **1450** is further comprised of the third lens **1455**, the second SOA **1460**, and the fourth lens **1465**.

FIGS. **15***a* through **15***d* show the experimental results of the gain saturation of the experimental setups of FIGS. **13** and **14**. FIG. **15***a* shows the optical power spectrum of the GFMLL **1410** with FWHM pulse width of approximately 11.4 nm and an average power of approximately 3 mW. FIG. **15***b* shows the mode-locked output pulse shape of the

GFMLL oscillator with pulse duration of approximately 96.4 ps. FIG. **15***c* is a streak camera image of the pulse at the output of the GFMLL **1410** showing no pulse stretching.

FIG. **15***d* is a streak camera image of the stretched pulse after fiber spool **1445** that provides pulse stretching. The pulse is stretched to approximately 2.96 ns and corresponds to approximately −64.9 ps/km/nm.

FIGS. **16***a*, **16***b*, **17***a*, and **17***b* show experimental measurements of gain saturation determined from the experimental setups of FIGS. **13** and **14**.

FIG. **16***a* shows output power vs. input power with an unstretched pulse of approximately 100 ps. The square data points **1610** represent data for an injected current of approximately 250 mA. The circular data points **1620** represent data for an injected current of approximately 500 mA. The triangular data points **1630** represent data for an injected current of approximately 750 mA. FIG. **16***b* shows gain vs. input power with an unstretched pulse of approximately 100 ps. in length. The square data points **1640** represent data for an injected current of approximately 250 mA. The circular data points **1650** represent data for an injected current of approximately 500 mA. The triangular data points **1660** represent data for an injected current of approximately 750 mA. FIG. **16***b* shows decreasing gain with output power indicating saturation.

FIG. **17***a* shows output power vs. input power with a stretched pulse of approximately 3 ns. The square data points **1710** represent data for an injected current of approximately 250 mA. The circular data points **1720** represent data for an injected current of approximately 500 mA. The triangular data points **1730** represent data for an injected current of approximately 750 mA. FIG. **17***b* shows gain vs. input power with a stretched pulse of approximately 3 ns. in length. The square data points **1740** represent data for an injected current of approximately 250 mA. The circular data points **1750** represent data for an injected current of approximately 500 mA. The triangular data points **1760** represent data for an injected current of approximately 750 mA. FIG. **17***b* shows no saturation behavior of the output power so that energy extraction through the XCPA will be improved.

X-CPA System Experimental Results

FIG. **18***a* shows a schematic view of the experimental set-up **1800** for the X-CPA invention. The GFMLL **1810** generates a 200 MHz mode-locked pulse fed to preamplifier **1815** that amplifies and selects pulses from the optical pulse train so that the output pulse rate is approximately 50 MHz. The optical pulse is stretched by way of the CFBG **1830** and sent to the amplifier **1845**. The optical pulse is further amplified by amplifier **1845** and sent to a second amplifier **1850**. The second amplifier **1850** is pulse biased with 100 ns electrical pulse at 10 kHz repetition rate in order to avoid a thermal management due to high current injection.

FIG. **18***b* shows the system throughputs at various points around the experimental setup **1800**. At the output of the GFMLL **1810**, the optical pulse has energy of approximately 44 pJ. with a pulse rate of approximately 200 MHz. The preamplifier **1815** provides an increase in pulse energy to approximately 296 pJ. with pulse rate of approximately 50 MHz. After first amplifier **1845**, optical pulse energy is approximately 504 pJ. with pulse rate of approximately 50 MHz. The optical pulse energy is further increase to approximately 11 nJ. and stretched to an approximately 100 ns pulse with approximately 10 kHz pulse rate by second amplifier **1850**.

FIG. **19***a* shows the approximately 100 ns electrical pulse at approximately 10 kHz pulse rate provided to the second amplifier **1850**. FIG. **19***b* shows the amplified spontaneous emission (ASE) signal **1910** from the first amplifier, the ASE signal **1920** for the first and second amplifiers, and the amplified signal **1930** from the whole system of FIG. **18***a* at the output of the second amplifier **1850**. In comparison with the ASE signal from the first and second amplifiers amplifier **1920**, **1930**, the dominant amplified signal **1910** due to injection is clearly seen.

FIG. **19***c* shows the average power **1950** and energy per pulse **1940** vs. peak current of the device used as second amplifier in the experimental setup **1800**. Looking at the amplified spontaneous emission power in quasi-continuous wave operation, at least 100 nJ. per pulse is obtainable from the experimental set-up **1800**.

FIG. **20***a* shows a schematic view of an experimental set-up **2000** for the X-CPA invention. FIG. **20***b* shows the operating parameters for the experimental set-up **2000** of FIG. **20***a*. The GFMLL oscillator **2010** generates a 200 MHz mode-locked pulse fed via a first faraday isolator **2015** to pulse-picker **2020** that selects pulses from the optical pulse train so that the output pulse rate is approximately 50 MHz and provides approximately 8.4 dB gain. The optical pulse is stretched by way of the CFBG **2030** and provided to the pre-amplifier **2035**, a RWG SOA, that provides approximately 10.1 dB gain. The optical pulse is passed through the second faraday isolator **2040** and further amplified by the first amplifier **2040** with approximate gain of 9.9 dB, passed through a third faraday isolator **2050** and provided to a second amplifier **2055**. The second amplifier **2050** is pulse biased with 100 ns electrical pulse at 10 kHz repetition rate in order to avoid a thermal management due to high current injection. Total gain through the system **2000** is approximately 33.3 dB.

FIG. **20***c* shows two optical spectrum curves of final amplifier before and after signal injection. When a signal is injected into final amplifier, the strong ASE suppression due to gain saturation is occurred.

Simulation Sequence

FIG. **21** is a preferred embodiment of the simulation sequence flow chart for the invention. FIG. **21** explains the effect of the X-CPA in terms of stretched pulse widths. The energy extraction efficiency between unstretched and stretched pulse is simulated using dynamic semiconductor laser rate equations.

For simulation, the oscillator was selected to have parameters of input energy from approximately 0.1 pJ to approximately 1 nJ and a transform-limited Gaussian input pulse with an approximately 1 nm to approximately 5 nm spectrum bandwidth. The amplifier was selected to have saturation energy of approximately 100 pJ, carrier lifetime of approximately 200 ps., line-width enhancement factor of approximately 3, and small signal gain of approximately 30 dB. CFBG constants of both approximately 87.5 ps/nm and approximately 2000 ps/nm dispersion, each with an approximately 1 nm and 5 nm optical spectrum bandwidth, were selected for the simulation.

FIGS. **22***a* and **22***b* are graphs of the simulation results (gain characteristics) of the invention. The simulation results show how stretching (the basic concept of X-CPA) influences energy extraction efficiency (i.e. extracted gain) in terms of stretched pulse width.

FIG. **22***a* shows the simulation results of an approximate 1 nm transform limited (TL'd) pulse with gain shown on the vertical axis and normalized saturation level Ein/Esat shown on the horizontal axis. The rectangular data points **2310** represent the unstretched pulse. The circular data points **2320** represent the stretched pulse using the CFBG with an approximately 87.5 ps/nm stretching/compression and

approximately 8 nm optical spectrum bandwidth resulting in a pulse length of approximately 87.5 ps. The triangular circular data points **2330** represent the stretched pulse using the CFBG with approximately 2000 ps/nm stretching/compression and an approximately 1 nm optical spectrum bandwidth resulting in a pulse length of approximately 2000 ps.

FIG. **22***b* shows the simulation results of a 5 nm transform limited (TL'd) pulse with gain shown on the vertical axis and normalized saturation level Ein/Esat shown on the horizontal axis. The rectangular data points **2240** represent the unstretched pulse. The circular data points **2250** represent the stretched pulse using the CFBG with an approximately 700 ps/nm stretching/compression and approximately 5 nm optical spectrum bandwidth resulting in a pulse length of approximately 437.5 ps. The triangular circular data points **2260** represent the stretched pulse using the CFBG with approximately 2000 ps/nm stretching/compression and an approximately 5 nm optical spectrum bandwidth resulting in a pulse length of approximately 10,000 ps.

The simulation results show the gain difference between a 1 nm and 5 nm transform-limited pulse laser with the CFBG of approximately 2000 ps/nm stretching/compression. The simulation results also show that the gain difference between amplification without and with the CFBG of approximately 2000 ps/nm stretching/compression and approximately 8 nm optical spectrum bandwidth is greater than approximately 15 dB with approximately 1 nJ input energy for an approximately 5 nm TL'd pulse.

Breathing MLL with Modulator

FIG. **23** shows a compact "Breathing Mode" Mode locked laser (MLL) embodiment **2300** with a modulator **2350**. The laser is comprised of fiber components such as the SOA **2310**, the output coupler **2320**, the first optical circulator **2330**, first CFBG (stretcher) **2380**, the modulator **2350**, the second optical circulator **2370**, and the second CFBG (compressor) **2340**.

Instead of free space bulk diffraction gratings as a pulse stretcher and a pulse compressor (FIG. **24**), two CFBGs are put inside cavity to make a laser compact; first CFBG **2380** is a stretcher and second CFBG **2340** is a compressor. The time duration of stretched pulse before SOA **2310** is much longer than energy storage time of SOA **2310**. Therefore nonlinearity i.e. self phase modulation which can distort an optical pulse can be reduced and at the same time optical pulse can extract more energy that stored energy inside SOA **2310**. After SOA **2310**, optical pulse is divided by output coupler **2320**. an optical pulse which remains inside cavity is compressed by a CFBG stretcher **2340** and then it goes though a modulator **2350** that has a short gating time. The modulator **2350** can be a passive MQW SA or LiNbO3 intensity modulator.

Dispersion-Managed Breathing Mode-Locked Semiconductor Ring Laser

FIGS. **24***a* to **24***c* show an experimental set-up **2400** for the dispersion managed breathing-mode σ-ring cavity diode laser. FIG. **24***a* shows the mode-locked semiconductor σ-ring cavity **2402**. FIG. **24***b* shows the set-up for diagnostics measurement of spectra and autocorrelations **2404**. FIG. **24***c* shows the setup **2450** used for dispersion element **1** (compressor) **2416**, dispersion element **2** (stretcher) **2420**, and the external compressor **2435**.

The salient feature is the incorporation of the compressor **2416** and stretcher **2420** in the sigma cavity. An optical isolator **2413**, such as a commercial product from Electro-Optics Technology with isolation >30 dB, permits light propagation only in the counterclockwise direction inside the cavity. Since the saturable absorber (SA) **2428** is designed for normal incidence, σ-shape ring propagation is managed with an optical circulator comprising half-wave plate **2418**, quarter-wave plate **2426**, and a polarizing beam-splitter (PBS) **2419**. FIG. **24***c* shows the external compressor **2435**, dispersion element **1**, **2416**, and dispersion element **2**, **2420** are standard dual pass grating compressors **2451**, **2454**, (we used commercial Spectrogon gratings with 1800 lines per mm), with internal telescopes, hence they can operate as pulse compressors or stretchers. The introduced dispersion amounts of those components were controlled by the relative position between gratings. Output ports **2414**, **2424** are after the gain medium **2410** and after the SA **2428**. Both intracavity diode **2410** and external cavity semiconductor optical amplifier (SOA) **2432** are angle-stripe, approximately 0.5 mm long SOAs. The chirped SA **2428** has multiple quantum wells with thickness of approximately 70/75/80 Å to sustain broad bandwidth saturable absorption. Passive mode locking is established using the SA **2428** and a dc-biased (approximately 190 mA) intracavity SOA **2410**. The sigma cavity laser outputs **2415**, **2425** are individually directed to a spectrometer **2430**, such as a commercial Jarell Ash equipped with a Reticon CCD camera, or to an external SOA **2432** to boost the power prior to the autocorrelator **2436**, such as a commercial Femtocrome FR-103.

The pulse train repetition rate is approximately 1.116 GHz, corresponding to the 31^{st} harmonic of the laser cavity. The pulse spectrum after the SA **2428** is recorded from output **2425** while keeping the introduced dispersion by element **2** **2420** constant and varying the dispersion introduced by element **1** **2416** and is shown in FIG. **25**. A fixed dispersion of approximately 4.57 ps/nm is introduced by element **2** **2420**. In each dispersion element, a 1 cm grating position variation corresponds to an introduced dispersion of approximately 0.83 ps/nm. There is an optimal grating position in element **1** **2416**, which introduces approximately −0.25 ps/nm additional dispersion than that introduced by element **2** **2420**. When such optimal dispersion is introduced, the obtained spectrum is the broadest and pulses are compressible to their shortest duration. The optimal total dispersion of approximately −0.25 ps/nm introduced by elements **1** **2416** and **2** **2420** compensates the dispersion of other cavity elements. Small variations in the total cavity dispersion cause dramatic changes in the spectral shape and width.

FIG. **26** displays measurements after the gain element **2410** from output **1** **2415** of the second harmonic intensity autocorrelation versus dispersion introduced by elements **1** **2416** and **2** **2420**. Data points are collected for movable grating position adjustments of approximately 1 cm yielding approximately 200 data points and the map is obtained by interpolation. On-diagonal map values occur for dispersions of equal magnitude and opposite sign in elements **1** **2416** and **2** **2420**. From the map we can see that when the laser operates in the regime near the diagonal region of the map, output pulses were shorter without coherent spikes. In contrast, noise bursts—temporally broad pulses with coherence spikes—were observed for off-diagonal map values.

FIG. **27** illustrates similar measurement after the SA **2428** from output **2** **2425** of spectral bandwidth (FWHM) versus dispersion in elements **1** **2416** and **2** **2420**. The bandwidth is slightly broader close to the map diagonal. The results along the diagonal of the map are summarized in FIG. **28**. Externally compressed pulse autocorrelation and bandwidth are plotted versus dispersion introduced by element **2** **2420**. A threshold value for the dispersion occurs at approximately −3.3 and approximately +3.3 ps/nm for dispersion elements **1** **2416** and **2** **2420**, respectively. Beyond this threshold, the

spectrum broadens more than twice, output pulses are externally compressible below approximately 1 ps and the laser is operating in breathing mode. The breathing mode means that with each cavity round-trip, the pulse is stretched when passing through the gain medium **2410** and compressed when incident on the SA **2428**.

FIGS. **29***a* and **29***b* show a cross-correlation measurement set-up. FIG. **29***a* shows a hybridly mode-locked σ-cavity laser **2902** with four outputs **2915**, **2922**, **2930**, **2932**, for pulse evolution characterization. FIG. **29***b* shows the set-up **2904** for measurements of spectra as well as autocorrelation and cross-correlation traces. The intracavity SOA **2910** was biased with approximately 92 mA of DC and a superimposed radio frequency (RF) signal modulated the gain at approximately 323 MHz. Introduced dispersions were approximately −5 ps/nm in the element **1** (compressor) **2916** and approximately +5 ps/nm in element **2** (stretcher) **2930**. As depicted in FIG. **29***b*, the signals from the four different cavity ports **2940** are split after the SOA amplifier **2943** with a 50/50 beam splitter **2946**. Half of the beam is guided through the delay line **2950** and then recombined with the other half which passes through the external compressor **2947**. The pulse from the cavity is combined with a compressed version of itself, and the autocorrelator **2960** signal reveals the two-pulse autocorrelation trace. The side pulse on the trace represents the cross-correlation of the two versions of the pulse. When the compressed version is much shorter than the original (in this case it is more than approximately 40 times shorter), the cross-correlation trace measures the temporal profile of original pulse intensity.

FIGS. **30***a*, **30***b*, **30***c*, **30***d* shows the optical power spectra from the four key points of the cavity—after the gain media (intracavity SOA) output **2915**, before the SA output **2930**, after the SA output **2932**, and before entering back to the gain media output **2922**. Spectra of the pulse propagating through the laser cavity are similar in shape, with the peak around the same wavelength.

FIGS. **31***a*, **31***b*, **31***c*, **31***d* shows the cross-correlation traces from the four laser cavity outputs. The stretched pulses exhibit an asymmetric temporal profile with a steep leading edge and a long decaying trailing edge. The stretched pulse traces FIG. **31***a* and FIG. **31***d* also contain an artifact from the autocorrelation. The dashed line depicts how the contributions from autocorrelation and the cross-correlation overlap. The cross-correlation traces from before and after the SA in FIG. **31***b* and FIG. **31***c* are similar to autocorrelation traces, since those are already short pulses in the cavity and were not externally compressible. The stretched pulse before and after the gain media is more than approximately 20 times broader than compressed one before and after the SA. This measured pulse duration change while propagating in the cavity demonstrates that laser operates in the breathing mode. The pulse energy after the cavity gain media is more than approximately 100 times higher than before the gain media as shown in FIG. **31***a* and FIG. **31***d*. This verifies that intracavity chirped pulse amplification was achieved.

Dispersion-Managed Breathing Mode-Locked Semiconductor Ring Laser Numerical Simulation

FIG. **32** is a flow diagram representing the algorithm to simulate the laser pulse formation from random noise input in the dispersion-managed breathing mode-locked semiconductor ring laser of FIG. **24***a*. Elements of the Split-Step Fourier algorithm are arranged in an order analogous to the semiconductor ring laser. The constants used in the simulations are listed in the table of FIG. **33**. A frequency filter with FWHM equal to approximately 7.6 nm accounts for the finite bandwidth of the SA and the semiconductor gain. A time filter with FWHM equal to approximately 131 ps. represents a RF modulation of the SOA as a gain element. The results from the simulations are scaled to the measured pulse energies after the cavity gain element energy is equal to approximately 33 pJ and after the SA energy is equal to 0.86 pJ. The pulse energy after the gain is approximately 1.64 times larger than the gain saturation energy and the pulse energy after the SA is approximately 2.8 times larger than the saturation energy of the SA.

The mode-locked stretched pulse formation from input random noise is shown in FIG. **34**. The steady-state pulse shape is formed after approximately 350 cavity round trips.

FIGS. **35** and **36** show the build-up of the mode-locked spectra after the cavity gain element and after the SA. The steady-state pulse spectral and temporal intensity after approximately 600 simulated cavity round trips are compared with the measured ones as shown in FIGS. **37***a*, **37***b*, **37***c* and **37***d*. The main part of the simulated stretch pulse fit well as compared to the experimentally measured pulse. The leading part of the cross-correlation trace of FIG. **37***c* contains an artifact from the middle autocorrelation trace of FIG. **31***a* which enhances the leading and trailing edge of the pulse measured by the two-pulse autocorrelation technique.

In FIG. **37***d* the steady-state simulated compressed pulse temporal intensity after the SA is compared with the corresponding pulse retrieved by the PICASO method. The pulse temporal intensity and phase are calculated by use of the PICASO algorithm from the measure spectrum and second-order intensity autocorrelation. Both pulses exhibit the same trend. The difference between the retrieved pulse by PICASO and the pulse obtained through simulation differs by approximately 150 fs. This difference may be due to additional dispersion encountered in the experimental setup prior to the intensity correlation measurements, minor inaccuracies in the PICASO algorithm, or the finite resolution of the temporal grid used in the simulation.

FIG. **38** shows simulation of lock-up of the dispersion-managed breathing-mode semiconductor mode-locked ring laser to externally injected Gaussian pulses. Lock-up is achieved after less than approximately 50 cavity round trips.

FIG. **39** shows a comparison of the measured and the Fourier limited calculated second-harmonic autocorrelation of externally compressed pulses from the experimental set-up of FIG. **29***a*. The set-up **2904** for measurements of spectra as well as autocorrelation and cross-correlation traces is used without the delay line **2950** in the diagnostics part. Linearly-chirped pulses from the laser output **2915** after the cavity gain media **2910** are compressed using a dual-grating external cavity compressor **2947**. The bandwidth-limited autocorrelation is calculated from the measured spectrum of the laser output after the gain element as in (a) of FIG. **30**. The calculated autocorrelation FWHM of approximately 404 fs. is only approximately 10% shorter than the measured FWHM of approximately 445 fs. From this, we can conclude that efficient intracavity linear chirping and amplification as well as external cavity amplification and compression are achieved.

FIG. **40** shows the pulse temporal intensity and phase retrieved by the PICASO algorithm. The pulses from the output after the gain medium are externally compressed to FWHM of approximately 274 fs. A measured average amplified power of approximately 6.25 mW after external compression at the repetition rate of approximately 323 MHz would correspond to pulse energy of approximately 19 pJ with peak power approximately 70 W and a focused intensity of approximately 1 GW/cm^2.

SHG-FROG Experimental Results

FIG. **41***a* shows an experimental setup of dispersion-managed breathing-mode semiconductor mode-locked σ-ring cavity laser with diagnostics. As in the embodiment of FIG. **24***a*, the salient feature of the laser cavity is the incorporation of dispersion element **1 4110** and dispersion element **2 4120**. The elements**1 4110** and **2 4120** as well as the external compressor **4130** are typical dual pass grating compressors with internal telescopes providing tunable positive or negative group velocity dispersion (GVD).

The laser output after the cavity gain element is externally amplified and characterized by a spectrometer **4160**, a second-harmonic intensity autocorrelator **4140**, and second-harmonic generation frequency-resolved optical grating (SHG-FROG) **4150**. Pulse retrieval is performed with commercial software such as Femtosoft Technologies utilizing a standard SHG-FROG set-up.

The SOAs **4170**, **4180** used have a gain peak that is red shifted with respect to the excitonic saturable absorption band. The mode-locked spectrum is located between the gain peak and excitonic absorption band as shown in FIG. **41***b*. In this wavelength configuration, for up-chirped pulses the red spectral part of the pulse is strongly amplified. Since for up-chirped pulses the red part of the pulse arrives first to the SOA **4170**, due to gain depletion the leading (red) part is strongly amplified in temporal domain. The combination of these temporal and spectral effects tends to amplify only the red portion of the pulse and therefore limits the mode-locked spectral width. The laser output spectrum was no broader than approximately 4 nm for the up-chirped pulses. For down-chirped pulses the amplification in the spectral and temporal domain can be balanced. The red part of the pulse is strongly amplified due to red shifted gain peak, but the blue part of the pulse is first incident to the SOA **4170** and is amplified more before the SOA **4170** gain depletes. It should be noted that up chirping would be preferable if the SOA **4170** gain peak is blue shifted with respect to the excitonic absorption peak.

FIGS. **42***a* and **42***b* show the measured laser output after external cavity amplification and compression. As displayed in FIG. **42***a*, the measured autocorrelation **4210** of FWHM equal to approximately 310 fs, is 1.7 times wider than the bandwidth limited autocorrelation **4220**, calculated from the measured spectrum shown in FIG. **42***b*. FIG. **42***b* additionally shows the broadened pulse spectrum **4230** of FWHM equal to approximately 9 nm using down chirping along with the corresponding SHG-FROG retrieved spectral phase **4240**.

FIG. **43***a* shows the SHG-FROG experimentally measured trace and FIG. **43***b* shows the SHG-FROG retrieved trace. This demonstrates that the retrieved trace recovers the salient features observed in the experimentally generated trace. The extracted temporal intensity profile along with corresponding phase plots are shown in FIG. **44**. The retrieved pulse FWHM is approximately 185 fs.

The invention encompasses a wide body of disciplines ranging from astrophysics to nuclear physics with applications ranging from communications to medical surgery.

The invention has applications in the medical sciences. The X-CPA laser becomes a very accurate scalpel in the performance of femtosecond precision surgery. Ultra-short pulsed lasers allow for non-thermal laser tissue interaction and small collateral tissue damage as compared to longer-pulsed lasers. Cutting by photo-disruption produces much less damage to surrounding tissues than photo-ablation. Intra-ocular micro-surgery can ablate or vaporize tissue without creating large "shock waves" that can damage surrounding healthy tissue.

The invention has application in surgery such as ophthalmic surgery, photo-refractive surgery, glaucoma treatment, and corneal refractive surgery to correct refractive problems such as nearsightedness and astigmatism. Surgical procedures such as laser channel cuts for intra-corneal ring segment (ICRS) implantation, femtosecond lamellar keratoplasty (FLK), and intrastromal vision correction, that rely on ultra-short pulsed lasers, are in development. Additionally, the invention can be used for photodynamic therapy of various carcinomas, for hard tissue ablation in dental procedures, and for multiple surgical procedures that have heretofore been performed with a surgical scalpel or a longer-pulsed laser.

The invention can be used for high-speed diagnostic applications such as multi-photon imaging, optical coherence tomography (OCT), and terahertz imaging. The invention can be used to measure optical-matter phenomena in condensed matter materials, to measure very fast events, processes, mechanisms, interactions, and the like.

Such applications are useful not only for medical diagnosis, but also in the study of chemical reactions at the atomic and molecular level.

The invention has applications in the material sciences. Ultra-short pulsed lasers can be used for material processing by way of non-thermal ablation and deposition of materials.

The invention has applications for commercial information networks, along with military and aerospace optical signal processing systems. In communications, the invention can be used as a high-speed transmitter of optical data in fiber optic networks.

In computers, the invention can be used as a transmitter of optical data, as high speed processors of optical data, and as high speed switches of optical data, and the like.

Additionally the invention can be used in the communication through free space.

While the invention has been described, disclosed, illustrated and shown in various terms of certain embodiments or modifications which it has presumed in practice, the scope of the invention is not intended to be, nor should it be deemed to be, limited thereby and such other modifications or embodiments as may be suggested by the teachings herein are particularly reserved especially as they fall within the breadth and scope of the claims here appended.

We claim:

1. A method of generating an-extreme chirped pulse amplification (XCPA), comprising the steps of:

generating optical pulses by a semiconductor mode-locked laser as an oscillator;

compressing the optical pulses by a first chirped fiber Bragg grating wherein optical power of the compressed optical pulses is increased at least approximately 100 times;

amplifying the compressed optical pulses by a semiconductor optical amplifier;

stretching the amplified optical pulses by a second chirped fiber Bragg grating, wherein the stretched amplified optical pulses have a duration longer than the storage time of the amplifying medium of the optical amplifies; and

outputting stretched optical pulses.

* * * * *